Flow measurements related to gas exchange applications

by

Fredrik Laurantzon

May 2012
Technical Reports from
Royal Institute of Technology
KTH Mechanics
SE-100 44 Stockholm, Sweden

Akademisk avhandling som med tillstånd av Kungliga Tekniska Högskolan i Stockholm framlägges till offentlig granskning för avläggande av teknologie doktorsexamen fredagen den 1 juni 2012 kl 10.15 i sal E2, Lindstedtsvägen 3, Kungliga Tekniska Högskolan, Stockholm.

Universitetsservice US–AB, Stockholm 2012

Fredrik Laurantzon 2012, **Flow measurements related to gas exchange applications**

CCGEx & Linné Flow Centre, KTH Mechanics, SE-100 44 Stockholm, Sweden

Abstract

This thesis deals with flow measuring techniques applied to steady and pulsating gas flows relevant to gas exchange systems for internal combustion engines. Gas flows in such environments are complex, i.e. they are inhomogeneous, three-dimensional, unsteady, non-isothermal and exhibit significant density changes. While a variety of flow metering devices are available and have been devised for such flow conditions, the performance of these flow meters is to a large extent undocumented when a strongly pulsatile motion is superposed on the already complex flow field. Nonetheless, gas flow meters are commonly applied in such environments, e.g. in the measurement of the air flow to the engine or the amount of exhaust gas recirculation. The aim of the present thesis is therefore to understand and assess, and if possible to improve the performance of various flow meters under highly pulsatile conditions as well as demonstrating the use of a new type of flow meter for measurements of the pulsating mass flow upstream and downstream the turbine of a turbocharger.

The thesis can be subdivided into three parts. The first one assesses the flow quality of a newly developed flow rig, designed for measurements of steady and pulsating air flow at flow rates and pulse frequencies typically found in the gas exchange system of cars and smaller trucks. Flow rates and pulsation frequencies achieved and measured range up to about 200 g/s and 80 Hz, respectively. The time-resolved mass flux and stagnation temperature under both steady and pulsating conditions were characterized by means of a combined hot/cold-wire probe which is part of a newly developed automated measurement module. This rig and measurement module were used to create a unique data base with well-defined boundary conditions to be used for the validation of numerical simulations, but in particular, to assess the performance of various flow meters.

In the second part a novel vortex flow meter that can measure the time-dependent flow rate using wavelet analysis has been invented, verified and extensively tested under various industrially relevant conditions. The newly developed technique was used to provide unique turbine maps under pulsatile conditions through time-resolved and simultaneous measurements of mass flow, temperature and pressure upstream and downstream the turbine. Results confirm that the quasi-steady assumption is invalid for the turbine considered as a whole.

In the third and last part of the thesis, two basic fundamental questions that arose during the course of hot/cold-wire measurements in the aforementioned high speed flows have been addressed, namely to assess which temperature a cold-wire measures or to which a hot-wire is exposed to in high speed

flows as well as whether the hot-wire measures the product of velocity and density or total density. Hot/cold-wire measurements in a nozzle have been performed to test various hypothesis and results show that the recovery temperature as well as the product of velocity and stagnation density are measured.

Descriptors: Flow meters, vortex flow meters, compressible flow, pulsating flow, hot-wire anemometry, cold-wire anemometry, time resolved measurements, wavelet analysis.

Preface

This doctoral thesis in fluid mechanics deals with flow measurement techniques applied on steady and pulsating compressible flows. It is mainly based on experimental work. The thesis is divided into two parts. Part I comprises an introduction to issues related to flow metering in gas exchange applications, together with some useful concepts, and also a summary of the main results. Part II consists of seven papers, where certain papers are altered from their respective original format, in order to comply with the format of the thesis main body. In Chap. 6 of Part I in the thesis, the respondent's contributions to all papers are stated.

May 2012, Stockholm
Fredrik Laurantzon

Contents

Part II. Papers

Part I

Overview and summary

CHAPTER 1

Introduction

This thesis deals with flow metering for both stationary and pulsating flows. Specifically, it is focused on measurements of gas flows where density changes can be significant, i.e. compressible flows. This work is motivated by the need to accurately measure mass flow rates of gas/air flows in internal combustion engines, both directly on the engine during normal operation, but also under laboratory conditions during simulations of full engines or various engine components.

1.1. Flow metering

A flow meter is an instrument for determining the flow rate of a fluid in some sort of conduit, for instance natural gas or oil in pipelines, domestic water supply, intake air to a combustion engine etc. The necessity of accurate flow rate measurement is as important today as it has been in the ancient history.

An early primitive, albeit useful flowmeter installation was made by the Roman engineers for the use in public aqueduct and piping systems. The measuring device in that case, can be seen as a primitive ancestor to the *orifice plate*. However, the practical Romans did not fully comprehend the theory behind the physics of the orifice plate. The Egyptians on the other hand, some 200 years prior to the Roman flowmeter, knew that the flow rate was dependent on the cross section area of the pipe A and the fluid velocity u, such that $Q = Au$. A more profound insight in the fundamental relationship between quantities, such as pressure, velocity and cross section area was not establish until about the 16^{th} century. For a more exhaustive elaboration regarding the developments in flow measurement from this time on, consult e.g. Cascetta (1995).

Nowadays, the costs that are controlled by flow meters, are worldwide estimated to be of the order of 10 000 billion US dollars annually, as discussed in the editorial of Flow Measurement and Instrumentation (1989). Moreover *Bosch Automotive* announced recently the production of their 100 millionth hot-film mass airflow sensor (designed to measure the engine's air intake). Thus the market for flow meters in various types of industries is quite large. It is therefore desirable for flow meters to have good performance in terms of accuracy, repeatability, and rangeability.

Flow meters can in principal be divided into four distinctive groups depending on how the flow rate is obtained. These are: *differential pressure flow meters* (e.g orifice plate, venturi, Pitot tube), *mechanical flow meters* (turbine flow meter, rotameter), *electronic flow meters* (electromagnetic flow meter) and *mass flow meters* (hot wire/hot-film, Coriolis flow meter). In common for all of these meters is that they are designed to measure the *bulk flow*, i.e. the volume or mass of fluid, flowing through some sort of flow conduit, per unit time (volume flow rate Q and mass flow rate $\dot{m}$ respectively).

1.2. Steady and pulsating flow

Steady flow is a type of flow which in general can be of *turbulent* nature with random fluctuations in the flow. However, the statistical moments for the velocity u, such as mean value U and root mean square value u_{rms} are independent of time, (for long enough time series) and the autocorrelation of the signal will for long time shifts tend to zero.

Pulsating flow on the other hand, is a specific type of *unsteady flow*, where a cyclic variation is superimposed on a constant (in time) flow. The statistical moments will for pulsating flow also be independent of time, but the autocorrelation will not go to zero, but show the pulsating component also for large time separations. A commonly used parameter to characterize the pulsating flow amplitude is $u_{\text{rms,pulse}}/u_b$, where $u_{\text{rms,pulse}}$ is the root-mean-square value of the pulsations and u_b is the bulk-mean velocity. For several flow meters, such as differential pressure flow meters and turbine flow meters, the metering error depends on this parameter.

1.3. Flow measurement in the gas exchange system

Due to gradually tougher emission legislation, the necessity to be able to accurate measure flow rate in the gas exchange system of internal combustion engines, such as intake air or exhaust gas recirculation (EGR) flows, becomes even more important. These stations in the internal combustion engine can be seen in Fig. 1.1, where a so called short route EGR system is illustrated. The signals from the flow meter devices are provided to the control system of the engine and this information is used to adjust the fuel delivery, either based by the amount of air or the combustion results. In this manner, the air/fuel ratio the engine is designed for can be maintained, thereby optimizing the engine performance and efficiency as well as catalytic efficiency.

However, several difficulties are associated with flow metering in this harsh environment: the gas is hot and contaminated, which put demands on the material of the device. The gas exchange system comprises pipe bends, valves, filters etc., such that the flow motion is swirling and the velocity profile is skewed. Furthermore, high amplitude pulsating flow at high frequency implies that the technique has to have inherent high frequency response and dynamic

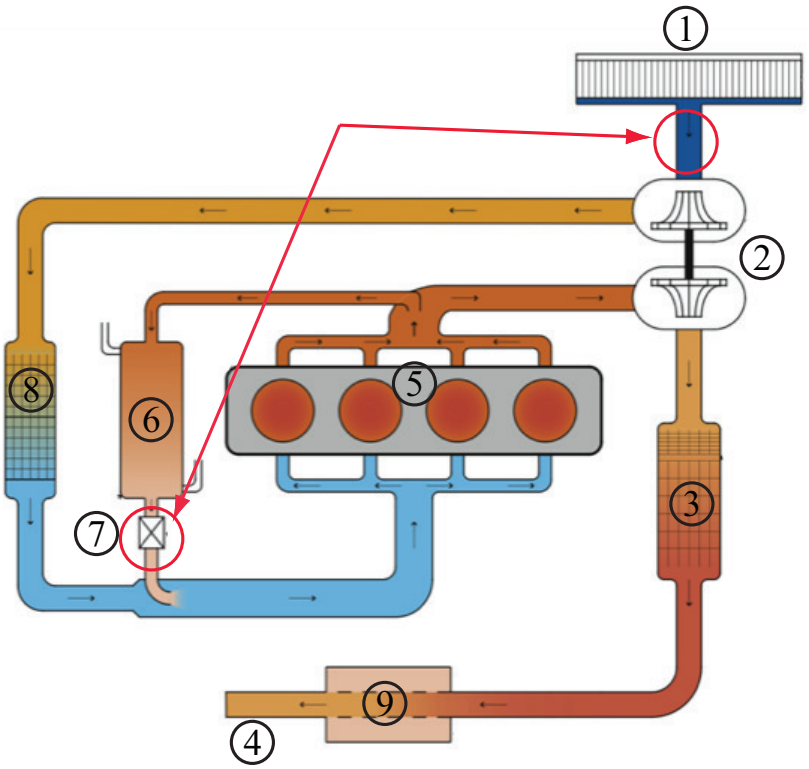

FIGURE 1.1. Short route EGR system, where stations suitable for flow measurements are indicated by red circles. (1) Air filter. (2) Turbocharger. (3) Catalytic converter. (4) Exhaust pipe. (5) Engine. (6) EGR cooler. (7) EGR valve. (8) Intercooler. (9) Muffler.

range. Hence, the flow conditions are non ideal and flow metering in this respect is a great challenge.

The objective of the present work is to evaluate and develop flow measuring methods, that can be used in the range of typical internal combustion engine gas exchange flows. For the present work we focus on pulsating flows up to 80 Hz pulse frequency and mass flow rates up to about 200 g/s, typical values for passenger car engines.

1.4. Thesis outline

The thesis is organized in the following way: Chapter 2 is an introduction to relevant gas dynamics concepts useful for understanding compressible flow related to flow metering, and also an introduction to pulsating flows. Chapter 3,

gives a short introduction to turbocharging, and discusses difficulties associated with the unsteady flow through the turbine. In Chapter 4 the experimental set-ups, both the flow facility and the measurement techniques that have been used are described and in Chapter 5 a summary and main conclusions of the appended papers are given. Chapter 6 gives an overview of the appended papers, where the author's contributions are stated. Finally, in Appendix A, a brief introduction to the wavelet transform is given.

CHAPTER 2

Basic theory

In this chapter, the fundamentals of thermo- and gas-dynamics for the analysis and understanding of flow behavior in stationary and pulsating (under quasi-steady conditions), compressible flow in various flow metering situations will be discussed.

2.1. Basic thermodynamics of gases

To analyze the phenomena in compressible flows the laws of thermodynamics is a necessary ingredient. The first law of thermodynamics reads

$$de = \delta q + \delta w, \tag{2.1}$$

where de is the change in internal energy when heat (δq) and/or work (δw) is added to the system. The second law of thermodynamics can be written

$$ds = \frac{\delta q}{T} + ds_{\text{irrev}}, \tag{2.2}$$

where s is the entropy and T the temperature. The quantity ds_{irrev} is always greater or equal to zero. Thus an alternative form of Eq. (2.2), would be

$$ds \geq \frac{\delta q}{T}. \tag{2.3}$$

It should be noted here that both e and s are state variables, i.e. the change in these variables from one start condition to an end condition, does not depend on how the change was made, it only depends on the conditions at the start and end states[1].

The state law for a perfect gas can be written

$$p = \rho RT, \tag{2.4}$$

where p is the pressure, ρ is the density and R the specific gas constant which for air has the value R =287 J/(kg K). Two other important quantities are the specific heats at constant pressure, c_p, and constant volume, c_v, which are related such that $R = c_p - c_v$ assuming that the values are constant. This is approximately true in the temperature range up to about 5-600 K when vibrational modes of the molecules are not yet excited (a so called calorically

[1]Here, the notation d is adopted for exact differentials, whereas δ is used for inexact differentials, i.e. for path-dependent quantities.

perfect gas). The ratio between the specific heats are usually written as $\gamma = c_p/c_v$ and for air (or any calorically perfect gas with two-atomic molecules) $\gamma = 1.40$.

In many processes, the change of state can be seen as isentropic, i.e. the changes occur adiabatically and reversibly. It can readily be deduced from the thermodynamic laws, Eqs. (2.1), (2.2) and (2.4), that if the flow process is isentropic, i.e. $ds = 0$, then the following relation is valid

$$\frac{p}{\rho^\gamma} = \text{const.} \tag{2.5}$$

Similar relations can also be obtained between the pressure, density or temperature by using the state law Eq. (2.4) to obtain

$$\frac{p}{p_{\text{ref}}} = \left(\frac{\rho}{\rho_{\text{ref}}}\right)^\gamma = \left(\frac{T}{T_{\text{ref}}}\right)^{\gamma/(\gamma-1)}, \tag{2.6}$$

where index "ref" refers to some reference condition. Note that these isentropic conditions are independent of the flow as long as it is reversible and adiabatic, i.e. there is no constraint that it should be e.g. stationary.

2.2. Gas dynamics fundamentals

2.2.1. *Conservation laws*

Compressible fluid flow is in principle governed by three fundamental physical conservation laws, namely, conservation of mass, momentum and energy. The perhaps most lucid description of these, is the integral formulation (see for example Anderson 2004), where we consider the conservation laws of the fluid within a fix, stationary control volume V.

Conservation of mass

$$\frac{\partial}{\partial t}\int_V \rho dV = \int_S -\rho \mathbf{u}\cdot d\mathbf{S} \tag{2.7}$$

Note from the above equation that the integrand on the right hand side is the mass flow $d\dot{m}$, into the control volume through the surface $d\mathbf{S}$, where in general $d\mathbf{S}$ is an infinitesimal surface element. However, if the flow variables are constant, the total mass flow through a cross section A, is simply

$$\dot{m} = \rho A u, \tag{2.8}$$

where u is orthogonal to the surface. Moreover from Eq. (2.8), two more quantities can be extracted, that are frequently occurring in fluid flow measurements. These are the *mass flux* and *volume flow*:

$$\dot{\mathcal{M}} = \rho u \tag{2.9}$$

$$Q = Au \tag{2.10}$$

respectively.

Conservation of momentum

$$\frac{\partial}{\partial t}\int_V \rho \mathbf{u} dV = \int_S \mathbf{u}(-\rho \mathbf{u}\cdot d\mathbf{S}) + \int_V \rho \mathbf{f} dV - \int_S p d\mathbf{S} + \mathbf{F}_{\text{visc}} \tag{2.11}$$

The term on the left hand side corresponds to the change in momentum inside the control volume per unit time, whereas the first term on the right hand side is the net influx of momentum into the control volume. The three other terms can be viewed as source terms for momentum, corresponding to changes due to body forces on the volume, pressure forces and viscous forces ($\mathbf{F}_{\text{visc}}$) acting on the surface of the control volume. Here $\mathbf{f}$ is a body force per unit mass.

Conservation of energy

$$\begin{aligned}\frac{\partial}{\partial t}\int_V \left[\rho\left(e+\frac{u^2}{2}\right)\right]dV &= \int_S \left(e+\frac{u^2}{2}\right)(-\rho \mathbf{u}\cdot d\mathbf{S}) - \int_S p\mathbf{u}\cdot d\mathbf{S} \\ &+ \int_V \rho(\mathbf{f}\cdot\mathbf{u})dV + \int_V \dot{q}\rho dV \\ &+ \dot{W}_{\text{shaft}} + \dot{W}_{\text{visc}}\end{aligned} \tag{2.12}$$

In the energy equation the left hand side expresses the changes of energy per unit time of the fluid inside the control volume where the energy is the sum of the inner (microscopic) energy (e) and the macroscopic kinetic energy ($\frac{1}{2}u^2$). The terms of the right hand side are respectively, net transport of energy into the control volume, work carried out by pressure forces, work carried out by body forces, heat transferred to the volume, the rate of work on the fluid in the volume by a rotating shaft and finally the rate of work by viscous stresses acting on the surface of the volume.

2.2.2. *One-dimensional flow*

By assuming that the flow is stationary and one-dimensional, i.e. the flow is in one direction inside a *stream tube*, there are no variations over the cross section and the cross section area (A) of the control volume is constant, the three conservation laws become

$$\rho_1 u_1 = \rho_2 u_2 \tag{2.13}$$

$$p_1 + \rho_1 u_1^2 = p_2 + \rho_2 u_2^2 \tag{2.14}$$

$$h_1 + \frac{1}{2}u_1^2 + \dot{q} = h_2 + \frac{1}{2}u_2^2 \tag{2.15}$$

where the enthalpy $h = c_p T$ has been introduced and indices 1 and 2 define the inflow and outflow of the stream tube. From the energy equation, Eq. (2.15), assuming adiabatic conditions ($\dot{q} = 0$) one may deduce the following expression for the stagnation temperature

$$\frac{T_0}{T} = 1 + \frac{\gamma - 1}{2} M^2 \tag{2.16}$$

where $M = u/a$ is the *Mach number* and $a = (\gamma RT)^{1/2}$ is the *speed of sound*. Note that T_0 is not constant for an unsteady flow.

2.2.3. *Streamline flow*

The Bernoulli's principle states that for a constant density fluid, in steady, frictionless flow, the stagnation pressure p_0 is constant along a streamline, and can be expressed as

$$p_0 = p + \frac{1}{2}\rho u^2 = \text{const.} \tag{2.17}$$

Here p is the *static pressure* and $\frac{1}{2}\rho u^2$ is the *dynamic pressure*. It is also possible to express the Bernoulli principle for compressible flow, which then takes the form

$$\frac{1}{2}u^2 + \int \frac{dp}{\rho} = \text{const.} \tag{2.18}$$

where the integral should be taken along the streamline. It is readily seen that this expression is equal to the incompressible form if ρ is a constant.

Using the isentropic relationship between T and p (Eq. 2.6) it is easily seen that in compressible flow the ratio between the stagnation and static pressures becomes

$$\frac{p_0}{p} = \left(1 + \frac{\gamma - 1}{2} M^2\right)^{\gamma/(\gamma-1)}. \tag{2.19}$$

The right hand side of Eq. (2.19) can be expanded through the binomial theorem such that

$$\begin{aligned} p_0 - p &= \frac{1}{2}\rho u^2 \left[1 + \frac{M^2}{4} + \frac{2-\gamma}{24} M^4 + \ldots\right] \\ &= \frac{1}{2}\rho u^2 f(M, \gamma), \end{aligned} \tag{2.20}$$

where the bracketed function is sometimes referred to as the *compressibility factor*, a factor that increases with increasing Mach number. At $M = 0$ the incompressible Bernoulli relation Eq. (2.17), is recovered.

2.2.4. *One-dimensional flow with friction*

In many flow systems it is necessary to take friction at the walls into account. In gas-dynamical flow problems it is usual to model the viscous forces in the fluid as a shear stress at the pipe wall, acting on the fluid. Usually this is expressed through a friction factor f which is defined as

$$f = \frac{\tau_w}{\frac{1}{2}\rho u^2}. \tag{2.21}$$

The friction factor f is a weak function of the Reynolds number $\mathrm{Re} = \rho u D/\mu$, where μ is the dynamic viscosity and D is a characteristic length. For smooth pipes the friction factor is usually taken as $f = 0.005$.

As a starting point one may assume that the flow is adiabatic and the simple theory assumes that all fluid properties solely vary in the pipe axis direction, and moreover a constant cross section area is assumed.

Since the flow is assumed to be adiabatic and stationary, it implies that $T_0 = \text{const}$. Using Eq. (2.16) twice for two locations along the pipe (see Fig. 2.1), we obtain

$$\frac{T_2}{T_1} = \frac{T_0/T_1}{T_0/T_2} = \frac{2 + (\gamma - 1)M_1^2}{2 + (\gamma - 1)M_2^2}. \tag{2.22}$$

Now, because the mass flux ρu, is constant for one-dimensional flow, and furthermore having in mind that $u = M\sqrt{\gamma RT}$, the above equation can be expressed in terms of the corresponding pressure ratio

$$\frac{p_2}{p_1} = \frac{M_1}{M_2}\sqrt{\frac{T_2}{T_1}} = \frac{M_1}{M_2}\sqrt{\frac{2 + (\gamma - 1)M_1^2}{2 + (\gamma - 1)M_2^2}}. \tag{2.23}$$

Let us assume that the flow at section 2 is sonic, i.e. $M_2 = 1$, the distance between section 1 and 2 is L and the pipe diameter is D, then (for a derivation

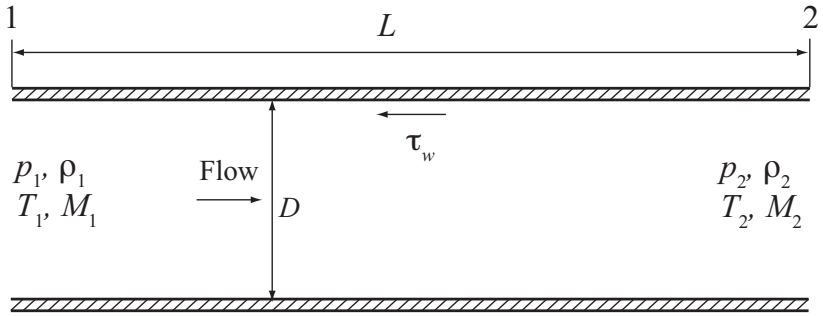

FIGURE 2.1. Pipe section with constant cross section area, for adiabatic one-dimensional flow. The friction is modeled as a shear stress τ_w acting on the fluid from the wall.

see e.g. Anderson 2004) it follows that the Mach number at section 1 is a function of the quantity $4fL/D$, viz.

$$\frac{4fL}{D} = \frac{1-M_1^2}{\gamma M_1^2} + \frac{\gamma+1}{2\gamma}\ln\left[\frac{(\gamma+1)M_1^2}{2+(\gamma-1)M_1^2}\right]. \tag{2.24}$$

This means that the Mach number M_1 can be determined if f, L and D are given, and from this all other ratios between the various flow quantities can be obtained.

2.2.5. *Quasi one-dimensional theory*

If all flow variables just vary with one spatial direction, say the x-direction, the flow is said to be one-dimensional. Furthermore, if the cross-section area A also varies with spatial direction x, i.e. $A = A(x)$ the flow is said to be quasi one-dimensional. The conservation equations for this case, where we assume that the cross-section areas of the stream tube are A_1 and A_2 at the inflow and outflow, respectively, become

$$\rho_1 u_1 A_1 = \rho_2 u_2 A_2 \tag{2.25}$$

$$p_1 A_1 + \rho_1 u_1^2 A_1 = p_2 A_2 + \rho_2 u_2^2 A_2 - \int_{S_{\text{lat}}} u(\rho \mathbf{u}\cdot d\mathbf{S}) \tag{2.26}$$

$$h_1 + \frac{1}{2}u_1^2 + \dot{q} = h_2 + \frac{1}{2}u_2^2. \tag{2.27}$$

The change in the mass conservation equation is readily seen, in the momentum conservation there will be a contribution from the pressure on the lateral area (S_{lat}) of the control volume, whereas the energy equation does not change with respect to the 1-D case.

In the following some basic quasi one-dimensional relations will be described.

The mass conservation equation Eq. (2.25), in quasi one-dimensional flow, shows that at two locations along a *nozzle* (see Fig. 2.2), one can relate the Mach numbers and cross section areas according to

$$\left(\frac{A_1}{A_2}\right)^2 = \left(\frac{M_2}{M_1}\right)^2 \left(\frac{1+\frac{\gamma-1}{2}M_1^2}{1+\frac{\gamma-1}{2}M_2^2}\right)^{(\gamma+1)/(\gamma-1)}, \tag{2.28}$$

where the flow between section 1 and 2 is assumed to be isentropic. The second parenthesis on the right hand side in the above relation can be expressed by means of the pressure ratio p_2/p_1 since

$$\frac{p_2}{p_1} = \frac{p_2/p_0}{p_1/p_0} = \left(\frac{1+\frac{\gamma-1}{2}M_1^2}{1+\frac{\gamma-1}{2}M_2^2}\right)^{\gamma/(\gamma-1)}. \tag{2.29}$$

Moreover, if M_2 is eliminated through Eq. (2.19) and using that $\frac{p_0}{p_2} = \frac{p_0}{p_1}\frac{p_1}{p_2}$, where $\frac{p_0}{p_1}$ can be expressed as a function of M_1 through Eq. (2.19), it is possible to express the Mach number at location 1 in terms of the area and pressure ratio alone

$$M_1^2 = \frac{2}{\gamma - 1}\left[1 - \left(\frac{p_2}{p_1}\right)^{(\gamma-1)/\gamma}\right]\left[\left(\frac{A_1}{A_2}\right)^2\left(\frac{p_2}{p_1}\right)^{-2/\gamma} - 1\right]^{-1}. \tag{2.30}$$

Now assume that we are studying the flow in a nozzle, such as the one in Fig. 2.2. If the pressure difference between the inlet and the outlet of the nozzle is gradually increased, the Mach number at the throat section of the nozzle, will ultimately reach unity. When this happens, the flow is said to be *choked*, and the mass flow rate will stay constant, regardless if the pressure difference is further increased. In fact, the mass flow rate essentially becomes a linear function of the stagnation pressure. If the the quantities at the throat at sonic conditions are denoted with an asterisk, one has $\dot{m} = \rho^* A^* a^*$ and hence

$$\begin{aligned} \dot{m} &= \frac{\rho^*}{\rho_0}\rho_0 A^* \frac{a^*}{a_0} a_0 \\ &= \frac{p_0 A^*}{\sqrt{RT_0}}\sqrt{\gamma}\frac{\rho^*}{\rho_0}\sqrt{\frac{T^*}{T_0}}. \end{aligned} \tag{2.31}$$

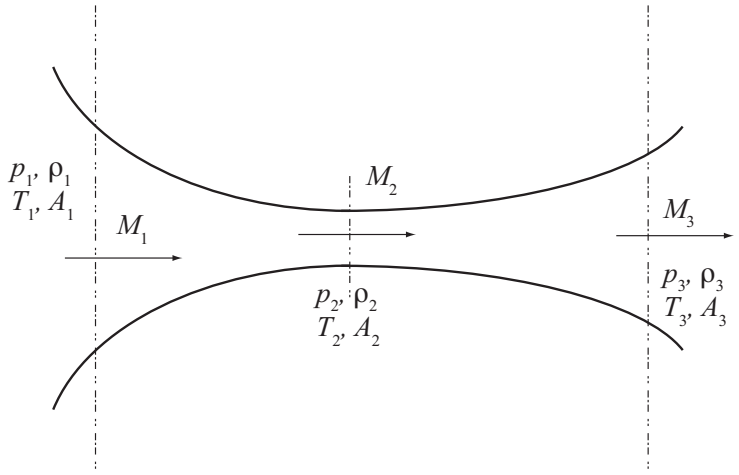

FIGURE 2.2. *Convergent-divergent nozzle.* For high enough pressure ratio p_1/p_3, the flow becomes choked, and at section 2 the sonic speed is obtained.

In the above relation, the ratios ρ^*/ρ_0 and T^*/T_0 are simply constants since they only depend on M, which is equal to one at the critical condition, i.e. if the flow is choked. Insertion of these constants in Eq. (2.31), results in the expression for the mass flow through a choked nozzle

$$\dot{m} = \frac{p_0 A^*}{\sqrt{RT_0}} \sqrt{\gamma \left(\frac{2}{\gamma+1}\right)^{(\gamma+1)/(\gamma-1)}}, \tag{2.32}$$

where the square root term for a gas with $\gamma = 1.40$ is equal to 0.685.

2.3. Unsteady flow

For unsteady flows, the left hand side of the conservation laws Eqs. (2.7), (2.11) and (2.12), i.e. the temporal derivative, is $\neq 0$, which complicates the equations considerably and to find general analytic solutions is difficult, hence numerical techniques have to be employed.

Pulsating flow is a specific kind of unsteady flow, where a regular cyclic variation in flow velocity superposed on an average flow rate, which will be described more detailed in the following section. Pulsating flow can sometimes be treated as quasi-steady, which means that flow rate varies continuously but slowly with time and is hence fully unsteady, but the inertia of the fluid and the forces causing it are negligible. For quasi-steady flow the steady flow equations are assumed to be valid at each instant of time.

2.3.1. *Pulsating flow*

Streamwise pulsating turbulent velocity can in general be written

$$u(r,\theta,t) = u_s(r,\theta) + u_a(r,\theta) f(\omega t + \Delta\phi) + u_T(r,\theta,t) \tag{2.33}$$

where r and θ is the radial and azimuthal coordinates respectively, u_s is the steady part, u_a the amplitude of the oscillation and u_T is the turbulent fluctuations. The pulsations are given by the angular velocity ω of the periodic function f and $\Delta\phi$ is the phase lag.

For simplicity, consider simple periodic harmonic flow with at a given radius and azimuthal coordinate, i.e.

$$u(t) = u_s + u_a sin(\omega t) \tag{2.34}$$

Depending on the order of magnitude of u_s and u_a four cases can be considered (Nabavi & Siddiqui 2010), see Fig. 2.3:

- Fig. 2.3(a) shows oscillating flow ($u_m = 0$), an example of this kind of flow, is the one in human respiratory system.
- In Fig. 2.3(b) $u_a >> u_s$, e.g. superposition of an acoustic standing wave and acoustic streaming.
- In Fig. 2.3(c) $u_a \sim u_s$, e.g. exhaust gas flow from internal combustion engines.
- In Fig. 2.3(d) $u_a << u_s$, e.g. blood flow in veins.

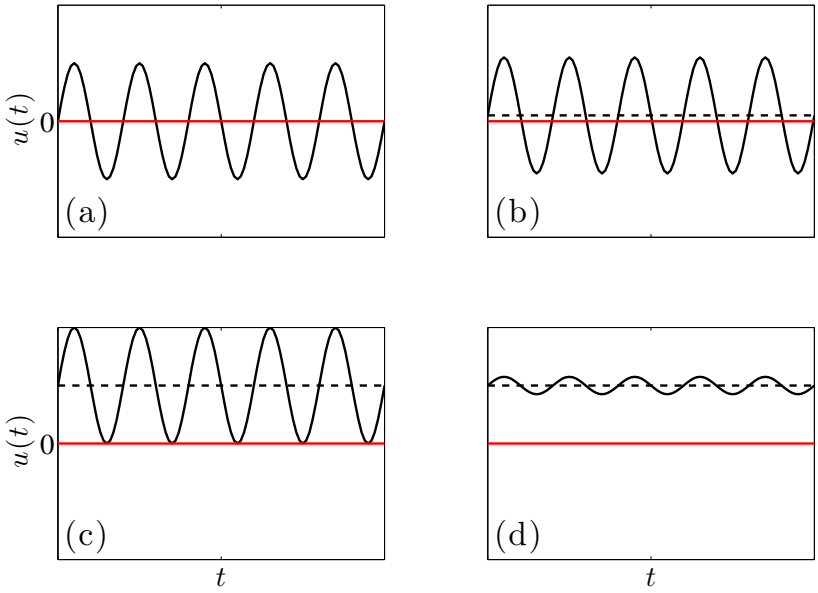

FIGURE 2.3. Different kind of pulsating flow. (a) Pure oscillation. (b) $u_a >> u_s$. (c)$u_a \sim u_s$. (d) $u_a << u_s$.

2.3.2. *Pulsating pipe flow*

An example where an analytical solution is feasible for unsteady flow, is the axi-symmetric, streamwise laminar flow in a pipe, given by the Navier-Stokes equation in cylindrical coordinates

$$\rho \frac{\partial u}{\partial t} = \mu \left(\frac{\partial^2 u}{\partial r^2} + \frac{1}{r} \frac{\partial u}{\partial r} \right) - \frac{\partial p}{\partial z}. \tag{2.35}$$

If the pressure gradient has a sinusoidal variation with time, it is possible to solve for the velocity field and the solution will be given in terms of Bessel functions. The fundamental properties of a pulsating flow is the frequency

of oscillations $f = \omega/2\pi$, and the velocity amplitude (Carpinlioglu & Gundogdu 2001), which can be expressed by means of dimensionless numbers. A non-dimensional number that can be derived from Eq. (2.35) is the so called Womersley number or frequency parameter defined as

$$\mathrm{Wo} = L\sqrt{\frac{\rho\omega}{\mu}} = \sqrt{2\pi\mathrm{ReSt}}, \tag{2.36}$$

where L is a characteristic length scale (e.g. the pipe radius), $\mathrm{Re} = \rho u L/\mu$ is the Reynolds number and $\mathrm{St} = fL/u$, is the Strouhal number. In laminar pulsating flow this number is controlling the flow (Ohmi *et al.* 1982), however for turbulent flow Wo is not longer a controlling parameter, because molecular viscosity decrease in importance (Shemer *et al.* 1985). It is also usual to describe the unsteady motion by means of the Strouhal number alone and/or some slight modification of it (cf. Costall *et al.* 2005; Hu & Lawless 2001). Many authors adopted the velocity amplitude ratio $\beta = u_a/u_m$ together with the frequency parameter Wo to be the controlling parameters (e.g. Uchida 1956; Carpinlioglu & Gundogdu 2001; Timité *et al.* 2010). At very low frequencies $\mathrm{Wo} < 1$, the flow can be viewed as quasi-steady and the velocity profile at any instant is similar to that of Poiseuille flow. For $\mathrm{Wo} >> 1$ inertia effects becomes important and the flow cannot follow the rapid changes in pressure, thus the profile tends to be flatter. For laminar flow the phase-lag between the pressure and velocity is 90°, whereas it varies for turbulent flows between $0 - 90°$ and decreases with increasing Re.

CHAPTER 3

Turbocharging

The air flow to the engine intake manifold can be either natural aspirated or forced induction. In the latter case air is compressed in some way (supercharging). The simplest way to achieve this is by means of a mechanical supercharger Fig. 3.1(a), where the compressor is driven directly from the crankshaft of the engine, thus taking power directly from the engine, which in turn lower the efficiency. A turbocharger Fig. 3.1(b) on the other hand, consists of a compressor driven by a turbine, where the turbine instead utilizes the energy in the hot exhaust gases, that otherwise would be wasted[1], to drive the compressor. In this fashion it is possible to increase the power output for a given engine size or to maintain the same power output with a smaller engine (so called downsizing), thus the power to weight ratio is increased.

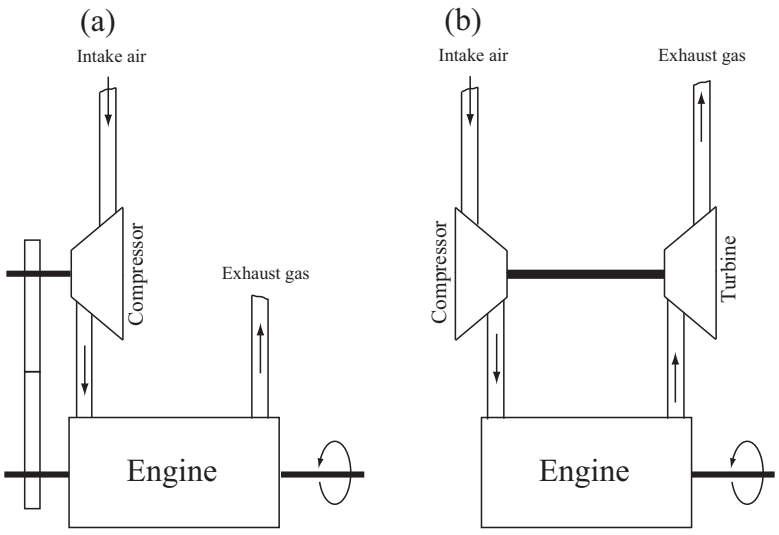

FIGURE 3.1. Supercharging concepts. (a) Mechanical supercharging. (b) Turbo(super)charging.

[1]Roughly 30-40% of the heat released from the fuel during combustion is found in the exhaust gas.

3.1. Energy conversion

The power that can be delivered from a internal combustion engine can be written (see Baines 2005)

$$P = \eta_f Q_f \dot{m}_f, \tag{3.1}$$

where η_f is the fuel conversion efficiency, Q_f is the specific energy for the fuel and $\dot{m}_f$ is the fuel mass flow. The amount of air an engine can induct is limited by flow obstructions (causing pressure drop), such as, filters, manifolds, valves etc. The effectiveness of the induction process can be described by the volumetric efficiency η_{vol}. For a four stroke engine the mass flow rate of air $\dot{m}_a$ can be expressed by means of the volumetric efficiency as

$$\dot{m}_a = \eta_{vol} \rho_a V \frac{N}{2}, \tag{3.2}$$

where ρ_a is the density of the air, V is the swept volume of the cylinder and N is the engine speed. Hence the power output can be expressed by means of the mass flow rate combining the two above equations as

$$P = \eta_f Q_f \dot{m}_a \frac{\dot{m}_f}{\dot{m}_a} = \eta_f Q_f \eta_{vol} \rho_a V \frac{N}{2} (F/A), \tag{3.3}$$

where (F/A) is the fuel/air ratio. All the quantities above are for a given engine more or less fixed, except the density of the air. Thus, by compressing the inlet air, the amount of combustible air is increasing, which in turn increases the power output.

The work transfer in a turbocharger is based on an interaction between a moving fluid and rotating blades attached to a shaft. The work produced by the turbine can be obtained from the energy equation Eq. (2.12) applied to the turbine, such that

$$\dot{Q} - \dot{W}_{\text{shaft}} = \dot{m} \left[\left(h + \frac{u^2}{2} \right)_2 - \left(h + \frac{u^2}{2} \right)_1 \right], \tag{3.4}$$

where $\dot{Q}$ is the heat transfer into the control volume, $\dot{W}$ is the shaft work rate out of the control volume, $\dot{m} = \dot{m}_a + \dot{m}_f$, and index 1 and 2 represent inflow and outflow respectively. The energy conversion is not completely adiabatic but $\dot{Q}$ in the above equation is usually negligible[2] in comparison to the other variables (Heywood 1988). Thus we get

$$-\dot{W}_{\text{shaft}} = \dot{m}(h_{02} - h_{01}) \tag{3.5}$$

which states that the work output is given by the change in stagnation enthalpy.

[2]This is especially true for normal and high load.

3.2. Turbocharger performance

The global performance characteristics[3] for a turbine (and compressor) can be expressed in terms of dimensionless numbers for easier comparison between different inlet conditions, in terms of pressure and temperature, but also different designs and sizes of the turbochargers (see e.g. Heywood 1988). The most important dependent variables are the mass flow rate $\dot{m}$, the efficiency η and the temperature difference over the device ΔT_0. The independent variables are inlet stagnation pressure p_{01} outlet pressure/stagnation pressure p_2, inlet temperature T_{01}, speed N, a characteristic length D, gas properties R and γ and viscosity μ. Hence

$$\dot{m}, \eta, \Delta T_0 = f(p_{01}, p_2, T_{01}, N, D, R, \gamma, \mu). \tag{3.6}$$

By dimensional analysis, such as Buckingham's pi theorem it is possible to reduce these 11 variables to a set of 7 non-dimensional variables instead

$$\frac{\dot{m}\sqrt{RT_{01}}}{p_{01}D^2}, \eta, \frac{\Delta T_0}{T_{01}} = \phi\left(\frac{ND}{\sqrt{RT_{01}}}, \frac{p_{01}}{p_2}, \frac{\dot{m}}{\mu D}, \gamma\right). \tag{3.7}$$

The quantity $\sqrt{RT_{01}}$ is associated with the speed of sound, and the non-dimensional mass flow rate and rotational speed, can be seen as flow Mach number and speed Mach number, respectively. It is common practice to drop quantities that are constant for a given gas and turbocharger, i.e. D, R and γ, furthermore the Reynolds number $\dot{m}/\mu D$, is usually high and variations do not influence the performance significantly and is also omitted. Hence, we are left with

$$\frac{\dot{m}\sqrt{T_{01}}}{p_{01}}, \eta, \frac{\Delta T_0}{T_{01}} = \phi\left(\frac{N}{\sqrt{T_{01}}}, \frac{p_{01}}{p_2}\right). \tag{3.8}$$

The quasi non-dimensional mass flow and speed in the above function is usually referred to as "corrected mass flow" and "corrected speed". The stagnation-pressure and temperature in the corrected variables are sometimes normalized with some reference state, such that the fundamental unit for the variable is recovered (see Baines 2005). The drawback when using corrected variables is that the performance maps (as will be described in the next section) will be dependent upon the size and design of the turbocharger as well as the gas.

3.2.1. *Performance maps*

Turbocharger performance is usually expressed by means of so called performance maps, i.e. turbine maps and compressor maps. In a turbine map it is conventional to plot the corrected mass flow $\dot{m}\sqrt{T_{01}/p_{01}}$ against the expansion

[3]The performance depends also on the boundary conditions to the turbo charger, such as e.g. the flow field.

ratio p_{01}/p_2 along lines of constant corrected speed $N/\sqrt{T_{01}}$, where also contours of efficiency are superposed[4]. Similar plots are used for the compressor, but with the flow rate as the independent variable. An example of an turbine map can be seen in Fig. 3.2. These are obtained from steady state measurements in a flow rig. The data is then inter- and extrapolated, prior to use in 1-D engine simulation software[5]. The engine simulation code then uses the turbine and compressor sub models to determine the mass flow rate and efficiency outputs for a given rotor speed and pressure ratio at every time step during the simulation (Winkler 2011). For this use it is assumed that the flow through the turbine is quasi-steady, which means that inertial and compressible effects are negligible. However, as has been shown by many authors, the flow through the turbine can not be treated as quasi-steady if the turbine is considered as a whole (cf. Baines 2010; Marelli & Capobianco 2011, see also Paper 3). An example of an unsteady turbine map is shown in Fig. 3.3, where the so called hysteresis curve is recognized. This implies that for a given expansion ratio, the

[4]It is common to define quantities at the turbine inlet and outlet as total-to-static, since the kinetic energy is essentially wasted.

[5]The 1-D computational techniques are used for optimization of turbocharger systems. The benefit is short computational time as compared to computational fluid dynamics (CFD), but with engineering accuracy of the output (Rehnberg 2011).

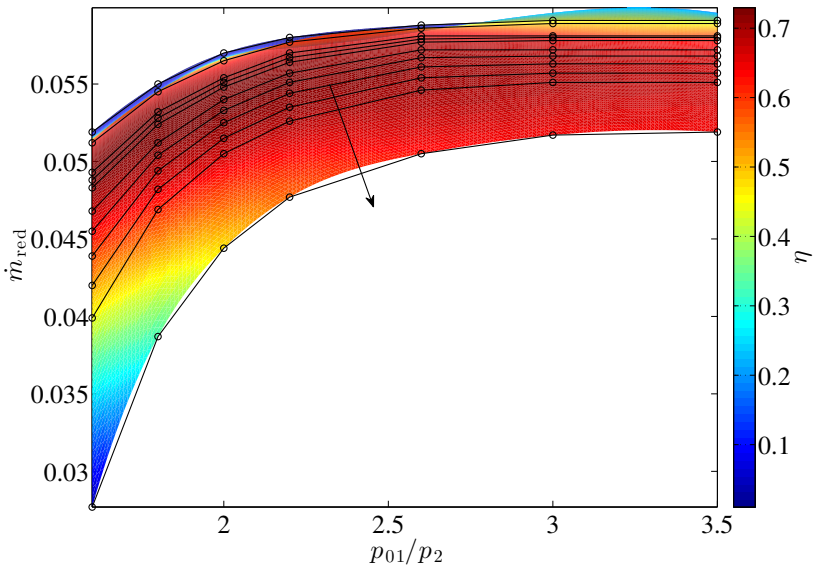

FIGURE 3.2. Turbine map for steady flow. The reduced mass flow rate is shown as function of the expansion ratio, with the efficiency shown as a contour. The lines represent constant rotational speed, increasing in the direction of the arrow.

mass flow rate can differ depending on whether the flow is in an acceleration- or deceleration phase, in contrast to the steady case where the flow rate is a single valued function of the expansion ratio. The efficiency is also affected by the pulsations, for instance it has been shown that pulsating flow causes a reduction in efficiency, referring to the cycle averaged level (Marelli & Capobianco 2011), although small amplitude high frequency pulsations actually can increase the efficiency (Copeland *et al.* 2011).

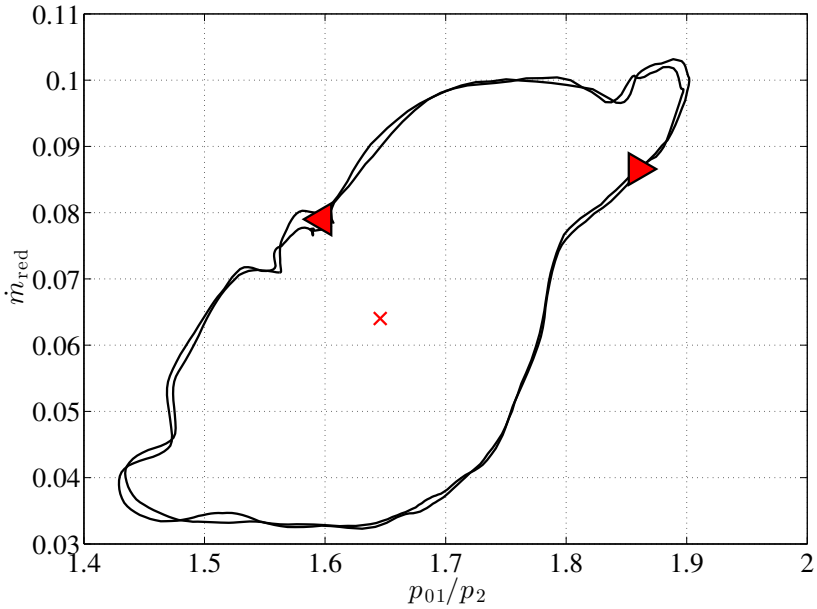

FIGURE 3.3. Turbine map for unsteady flow, showing the reduced mass flow rate as function of expansion ratio. The pulsation frequency (f_p) is 60 Hz and mean flow rate is 105 g/s. The x-mark shows the mean *reduced mass flow rate* and the arrows show the hysteresis loop path, which is clockwise. (Data from Paper 3).

CHAPTER 4

Experimental techniques and set-ups

The experiments have been carried out at the CICERO laboratory of *KTH CCGEx* in a new flow rig (also described in Paper 1), designed to produce both stationary and pulsating flow to simulate the exhaust flow range typical for internal combustion engines for cars and medium sized trucks. In this chapter, the flow facility and its relevant hardware are described together with the installation of different measurement equipment.

4.1. Flow facility

4.1.1. *Compressors and piping system*

Pressurized air to the laboratory is provided by means of two *Ingersoll Rand* screw compressors (*Nirvana 75* and *SSR ML75*), which together deliver a maximum flow rate of 0.5 kg/s at 5 bar (gauge pressure). The compressors are coupled through a pipe system to a filter and dryer, in order to give clean and dry air to the flow rig. This part of the flow facility is placed in a rock shelter and a piping system of a length of about 30 m brings the air to the laboratory. Before entering the system flow meter, the pipe is divided into two branches just downstream an electrically controlled valve (see Fig. 1). One of the branches is a bypass piping, which is used at low mass flow rates in order to maintain a stable flow, since the stability of the regulating valve as well as the compressors is better above a certain low mass flow rate. The other branch is the main piping to flow rigs in the laboratory. The flow rate into the test rig is measured by means of a mass flow meter of hot-film type (*ABB Thermal Mass Flowmeter FMT500-IG*). It is located downstream of a 10 m long and 100 mm in diameter, straight pipe section. Approximately two meters downstream the mass flow meter, the main pipe is in turn divided into two branches, where it is possible to chose one or the other by manual valves. One of the branches is used with an orifice plate meter to validate the calibration of the ABB thermal mass flow meter. The other pipe connects to a heater for which the power can be regulated up to 18 kW, if there is an interest or need to heat the flow before going to the measurement object. The approximate temperature increase can be estimated from

$$\Delta T = \frac{\dot{Q}}{\dot{m} c_p}, \tag{4.1}$$

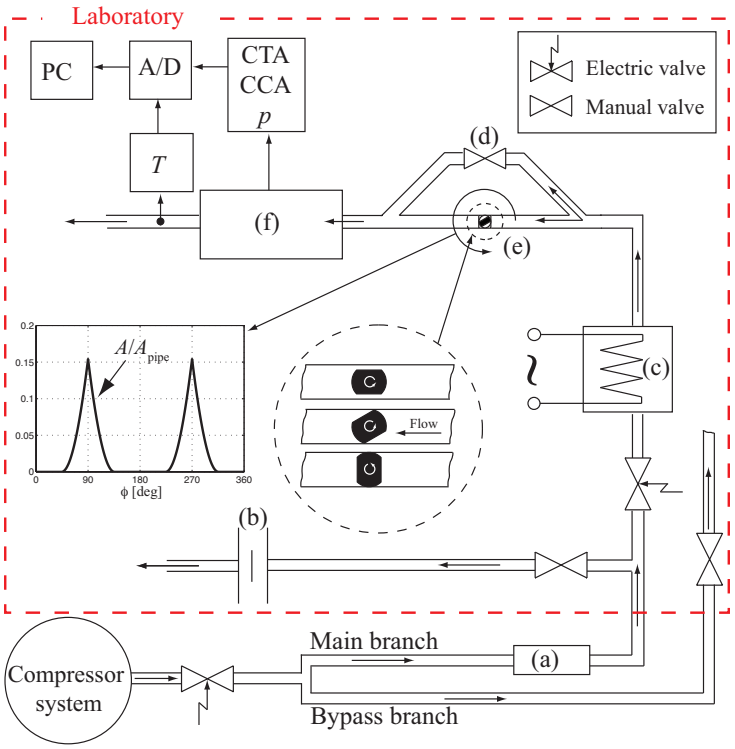

FIGURE 4.1. A schematic of the flow rig. a) Thermal mass flow meter (ABB), b) Orifice plate, c) Electric heater, d) Bypass branch, e) Pulse generator, f) Flow measurement device.

which for 0.2 kg/s gives a maximum temperature increase of about 90 °C. This feature is needed when running turbines, since otherwise the temperature of the gas in the turbine may easily fall below the freezing point of the moisture in the air. In Paper 5, some flow measurement techniques are evaluated under both steady and pulsating flow, these are located at (f) in Fig. 1.

4.1.2. *Pulse generator*

A pulse generator is used to create a pulsating flow that can be used in various experiments simulating exhaust engine flows. The pulse generator consists of a rotating ball, where two symmetrically located segments has been removed. The ball is tightly fitted in the pipe system, thereby the valve opens and closes twice a revolution. The ball is rotated by an AC motor, which is operated through a frequency controlled power unit, and can be rotated with frequencies up to 50 Hz, hence giving a pulse frequency up to 100 Hz. Fig. 4.2 shows the projected open valve area on a plane orthogonal to the pipe axis, as function

of the angle of rotation. It is possible to add a steady flow to the pulsating flow, through a pipe branch that by-passes the pulse valve. The by-pass branch emanates $4D$ upstream the pulse valve and reconnects $4D$ downstream of it. The amount of air through the by-pass valve can be regulated by a manual valve. Downstream the rotating valve the pulse module has a pipe with a length of 320 mm, which ends immediately downstream the by-pass reconnection.

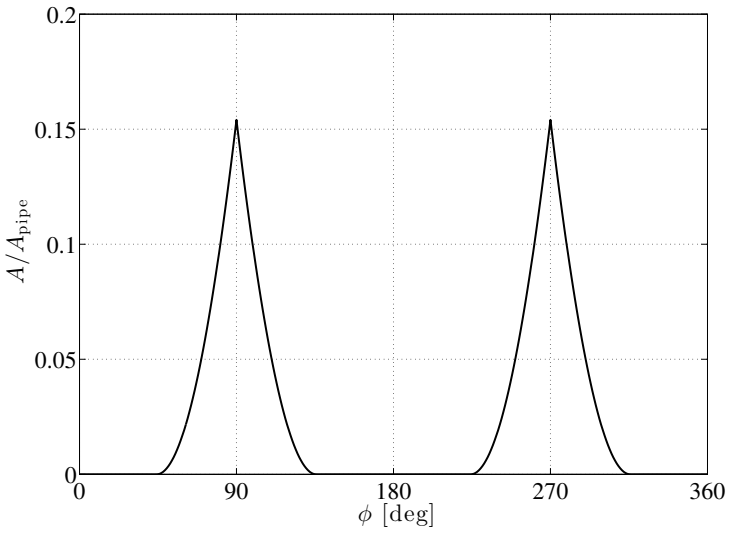

FIGURE 4.2. The projected open valve area.

4.1.3. *Turbocharger*

A turbocharger for passenger cars (*Garrett GT17 NS*), was used in the experiments. For the experimental setup and instrumentation, see Paper 3. The turbine was located at position (f) in Fig. 1, i.e. at the same position as the flow meters as described in Paper 5. A photo of the turbocharger with its connecting pipes can be seen in Fig. 4.3.

At higher flow rates the heater, (c) in Fig. 1 was employed to avoid freezing of the moist downstream the turbine as mentioned previously. In order to obtain different expansion ratios for the same flow rate in the turbine, it is possible to choke the flow by means of an electric valve, located downstream the compressor. This can be used to produce a steady turbine map, as shown in Chap. 3.

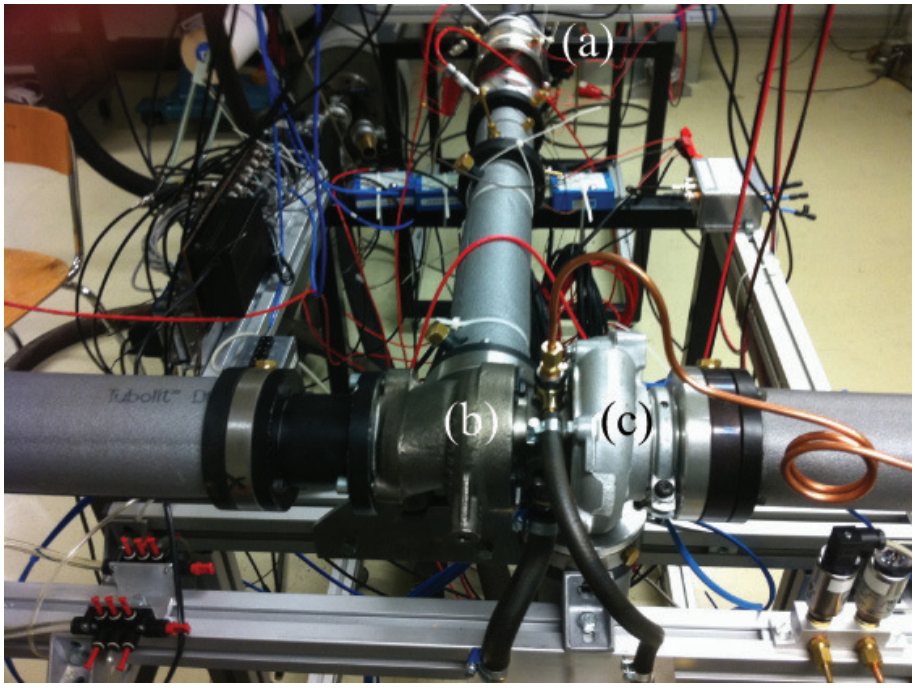

FIGURE 4.3. Photo of the turbocharger with connection pipes. a) Instrumentation just downstream the pulse generator ((e) in Fig. 1). b) Turbine. c) Compressor.

4.2. Mass flow measurement module

In order to determine the pulsating flow coming from the pulse valve, a mass flow measurement module has been developed, that makes it possible to determine the instantaneous flow rate during the pulsating cycle by traversing a probe module over the cross section of the pipe. The probe module consists of a hot-wire and a cold-wire sensor in order to measure the instantaneous mass flux (ρu) and stagnation, or rather recovery, temperature. For calibration purposes of the hot-wire there are two total head probes in parallel to measure the stagnation pressure at the probe module position, whereas the spatial mean static pressure is measured through four inter-connected pressure taps at the wall.

Since the mass flow measurement module is thoroughly described in Paper 1, merely some additional aspects of the meter will be mentioned in this section.

An important insight from Paper 1, is that the mass flow profile is close to a top-hat during pulsating conditions. The phenomenon that the velocity

profile tends to be of plug flow character in pulsating flow, has been reported previously (see e.g. Håkansson & Delsing 1994).

4.2.1. *The hot-wire probe and calibration procedure*

The hot-wire probe itself is a welded tungsten wire with diameter $d = 5\mu$m and length $L = 1$ mm, hence giving an L/d ratio of 200. The hot-wire was operated by means of a *DISA 55M01* main frame with a *55M10* standard *constant temperature anemometry* (CTA) channel.

The hot-wire is calibrated using King's Law

$$E^2 = A + B(\rho u)^n, \tag{4.2}$$

where the exponent n should be equal to 0.5 for an infinite long cylinder ($L/D \to \infty$) at 2-D steady flow, and A equal to the voltage squared at zero velocity (usually denoted by E_0) and B is a constant. Here all three constants are used in a fitting process to the calibration data and a typical calibration curve can be seen in Fig. 4.4.

4.2.2. *Temperature sensitivity*

The output from a hot-wire anemometer depends both on the mass flux and the temperature difference between the wire and the surrounding gas. If the temperature (T) of the gas during measurements differs from that of the calibration (T_{ref}), the output voltage E needs to be temperature compensated. A simple (and effective) relation for this is

$$E_{\text{comp}}^2 = E^2 \left(\frac{T_{\text{w}} - T_{\text{ref}}}{T_{\text{w}} - T} \right), \tag{4.3}$$

where T_{w} is the wire temperature and E_{comp} the compensated voltage (see e.g. Bruun 1995, p. 215).

If the hot wire is used in a pulsating flow the stagnation temperature will change during the pulse cycle, despite the fact that the flow is adiabatic. This means that the instantaneous hot-wire signal needs to be compensated for the changing stagnation temperature. Because the instantaneous temperature felt by the hot-wire is readily measured by means of the cold-wire exposed to the same local flow, this temperature can be directly used for the temperature compensation of the hot-wire readings.

The resistance of the hot wire is, as mentioned in the previous chapter, a function of the temperature of the hot wire according to

$$R(T_{\text{w}}) = R(T_{\text{ref}})[1 + \alpha_{\text{ref}}(T_{\text{w}} - T_{\text{ref}})]. \tag{4.4}$$

One parameter of importance dealing with hot-wire anemometry, is the overheat ratio of the wire

$$a_{\text{w}} \equiv \frac{R_{\text{w}} - R_{\text{f}}}{R_{\text{f}}}. \tag{4.5}$$

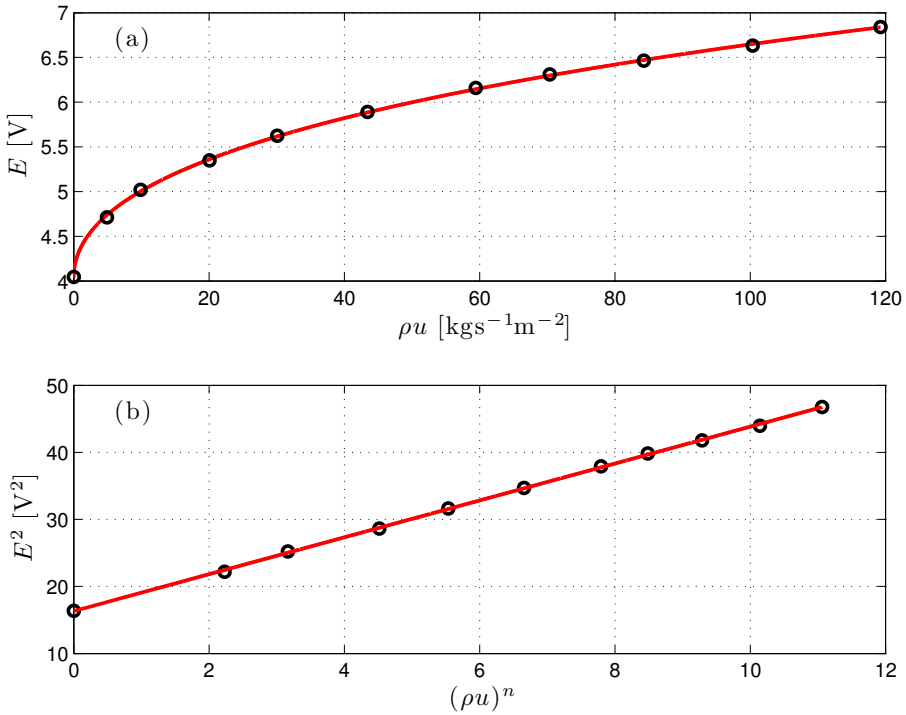

FIGURE 4.4. Hot wire calibration curve. Circles are measured calibration points, solid line is a fitted Kings law expression to the data, see Eq. (4.2). (a) E vs. ρu, b) E^2 vs. $(\rho u)^n$, for the fitted n. Here the fitting gave an exponent equal to $n = 0.50$, however n was found to vary in the range $0.42 - 0.52$ for different sensors.

This parameter is chosen by the user in advance. A high value of a_w results in high mass flux sensitivity and low temperature sensitivity, and vice versa (see Sec. 4.2.4).

If the fluid temperature varies during measurements, the output voltage signal can be compensated by combining Eqs. (4.4) and (4.5), for Eq. (6) to become

$$E^2_\mathrm{comp} = \frac{E^2}{[1 - \alpha_\mathrm{ref}(T - T_\mathrm{ref})/a_\mathrm{w}]}, \tag{4.6}$$

which can be used on the instantaneous hot-wire signal assuming the cold-wire

is sensing the temperature relevant for the heat transfer[1]. An example with this correction employed, can be seen in Fig. 4.5. These measurement are done with the nozzle as described in Laurantzon *et al.* (2010), Paper 6.

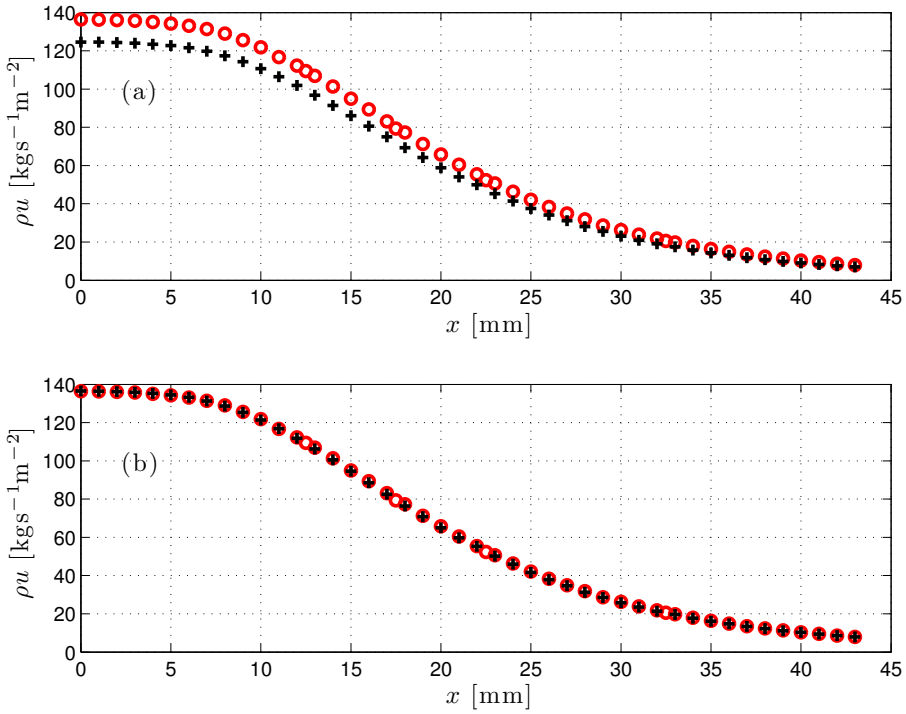

FIGURE 4.5. Mass-flux measurements along a nozzle. The nozzle exit is at x = 0 mm and has a diameter of 10 mm. At x = 45 mm, the nozzle diameter is 57 mm. The calibration temperature for the hot-wire measurements were 18 °C. Measurements were made at 18 °C (○) and at 31.5 °C (+). (a) Output from hot-wire measurement without temperature compensation. (b) The same data, but with compensation according to Eq. (4.6), applied to the 31.5 °C measurements.

[1]It should be mentioned that the value of α, in general must be found by means of calibration, since the value provided from the supplier is for pure untreated wires, and the value can differ considerable depending on how it was mounted to the prongs (Dijk & Nieuwstadt (2004)).

4.2.3. *Cold-wire for temperature measurements*

If the resistance wire instead is operated in *constant current anemometry* (CCA) mode it can be used for mass flux/velocity measurements, but is nowadays mainly used for the measurement of temperature fluctuations.

The CCA output was for the calibration and measurement obtained by means of an *AN*–1003 hot-wire anemometry system (AA labs). The output from the cold-wire will in contrast to the output from the hot-wire, be a linear function of the temperature, which can be explained as follows; if the current through the wire is held constant[2], the wire voltage E_w will be proportional to the wire resistance R_w. If we again consider Eq. (4.4), we see that $R_\mathrm{w} \sim T_\mathrm{w}$, and it therefore follows that

$$E_\mathrm{w} \sim T_\mathrm{w}, \tag{4.7}$$

for CCA. This linear dependence can be observed in Fig. (4.6), which is a typical calibration curve for a cold-wire.

During the calibration, it is of importance to ensure that the response from the cold wire is only due to temperature fluctuations. To accomplish this, T is kept constant and u is varied, which ideally ought to give a constant cold-wire output. Furthermore, the current in CCA is set by the user and should be

[2]A value of 0.5 mA for I was used for a wire of $d = 5\mu$m, however I can be adjusted to comply with the desired temperature resolution and velocity sensitivity.

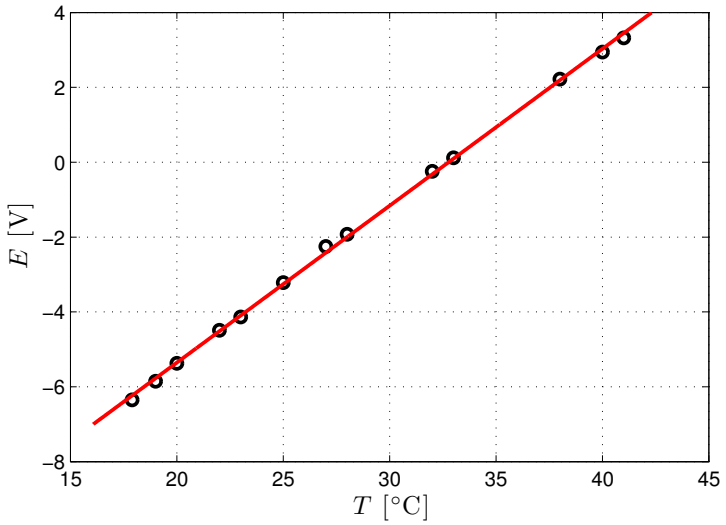

FIGURE 4.6. Cold wire calibration curve. Circles are measured points, solid line is a straight line fit to the calibration data.

sufficiently high to get good enough temperature resolution, but on the other hand small enough, in order to be able to neglect velocity fluctuations (see the equations in Sec. 4.2.4, or Örlü (2006) for a more detailed discussion regarding CCA).

4.2.4. *Velocity and temperature sensitivity for CTA and CCA*

In this section a summary of velocity and temperature sensitivities are gathered for the CTA and the CCA modes as a complement to the discussion in the previous section. The results and notations in this section are mainly adopted from Bruun (1995).

The anemometer voltage E can be related to the fluctuations in mass flux and temperature, ρu and θ respectively as

$$E = S_{\rho u}\rho u + S_\theta \theta, \tag{4.8}$$

where $S_{\rho u} = \partial E/\partial(\rho u)$ and $S_\theta = \partial E/\partial\theta$. The sensitivities in velocity and temperature fluctuations for the CTA and CCA mode, are:

$$S_{\rho u}^{CTA} = \frac{nB(\rho u)^{n-1}}{2}\left[\frac{R_\mathrm{w}(T_\mathrm{w}-T_\mathrm{f})}{A+B(\rho u)^n}\right]^{1/2} \tag{4.9}$$

$$S_\theta^{CTA} = -\frac{1}{2}\left[\frac{R_\mathrm{w}(A+B(\rho u)^n)}{T_\mathrm{w}-T_\mathrm{f}}\right]^{1/2} \tag{4.10}$$

$$S_{\rho u}^{CCA} = -\frac{nB(\rho u)^{n-1}I^3R_\mathrm{w}^2}{R_\mathrm{f}(A+B(\rho u)^n)^2} \tag{4.11}$$

$$S_\theta^{CCA} = \frac{\alpha I R_\mathrm{w} R_\mathrm{ref}}{R_\mathrm{f}}. \tag{4.12}$$

Forming the ratio of velocity to temperature sensitivity, Eqs. (4.9) and (4.10) respectively, one has

$$\frac{S_{\rho u}^{CTA}}{S_\theta^{CTA}} = -\frac{nB}{(\rho u)^{1-n}}\left[\frac{T_\mathrm{w}-T_\mathrm{f}}{A+B(\rho u)^n}\right]. \tag{4.13}$$

From the above ratio we can see that, as stated before; high mass flux sensitivity is obtained when applying a high overheat ratio ($a_\mathrm{w} \sim T_\mathrm{w} - T_\mathrm{f}$). Moreover, a higher mass flux implies higher temperature sensitivity. Thus, at higher speeds it becomes even more important to measure the temperature accurately.

4.3. LDV measurement technique

During the measurements with various flow meters it was observed that some of the results showed a strange behavior and a suspicion arose that back flow was occurring during the pulsating cycle. In order to investigate this, *laser Doppler velocimetry* (LDV) measurements that have the possibility to also measure back flow, were performed.

The main part of the LDV measurements were made with a single velocity component *DANTEC FlowLite* system together with a BSA 60 processor. The emitting light source is a 10 mW He-Ne laser with a wave length of 632.8 nm. The emitted laser beams are converged to a measuring volume after passing a lens with focal length of 400 mm.

The seeding particles (*Shell Odina oil 27*), were injected just downstream the pulse valve through a specially constructed pipe section. An optical sensor provided a trigger signal, sensing a given valve ball angle. This signal was in turn fed to the LDV processor, thus providing means to divide the velocity measurements into phase bins during the revolution of the pulse valve. For an exhaustive description of the technique, see Tropea *et al.* (2007), and for a typical application see Rocklage-Marliani *et al.* (2003).

4.4. Estimation of uncertainties

The aim with the present work is to perform accurate measurements in pulsating gas flows. The uncertainties in a long measurement chain (e.g. for the hot-wire measurements starting with the calibration of the pressure transducers to the deduction of the mean mass flux from the hot-wire), is at first glance not completely obvious. This section will attempt to assess typical uncertainties in the measurement techniques employed. Typically, the total uncertainty is the combination of the systematic (bias) and stochastic (precision) errors, which are usually treated seperately. However, in the experimental campaigns none of the variables are correlated, i.e. measured with the same sensor, therefore the uncertainty is treated with its global value.

The uncertainty for a quantity, for instance the Mach number, which for isentropic flow is given by $M = M(p_0, p)$, can be estimated by the propagation of errors formula (see e.g. Tropea *et al.* 2007). For stochastic errors one has

$$\sigma_M^2 = \left|\frac{\partial M}{\partial p_0}\right|^2 \sigma_{p_0}^2 + \left|\frac{\partial M}{\partial p}\right|^2 \sigma_p^2, \tag{4.14}$$

where σ denotes the standard deviation. For simplicity, consider the binomial expansion of the isentropic relation Eq. (2.19) and neglecting higher order terms

$$\frac{p_0}{p} = \left(1 + \frac{\gamma}{2} M^2\right) + \mathcal{O}(M^4), \tag{4.15}$$

or

$$M^2 = \frac{2}{\gamma}\left(\frac{p_0}{p} - 1\right), \tag{4.16}$$

hence

$$\begin{aligned} \frac{\partial M}{\partial p_0} &= \frac{1}{\gamma M p} \\ \frac{\partial M}{\partial p} &= -\frac{p_0}{\gamma M p^2}. \end{aligned} \tag{4.17}$$

If the two above relations are put in Eq. (4.14), one obtains

$$\sigma_M^2 = \frac{1}{\gamma^2}\left(\frac{p_0}{p}\right)^2 \left(\frac{\sigma_{p_0}^2}{p_0^2} + \frac{\sigma_p^2}{p^2}\right) = \frac{1}{\gamma^2}\left(\frac{p_0}{p}\right)^2 \left(\varepsilon_{p_0}^2 + \varepsilon_p^2\right), \tag{4.18}$$

where ε denotes the relative error. For the mass flux uncertainty, using the result in Eq. (4.18) and the definition Eq. (4.14) applied instead on the mass flux, noting that $\rho u = pM\sqrt{\gamma/RT}$, one obtains

$$\sigma_{\rho u}^2 = \rho u \sqrt{\varepsilon_p^2 + \varepsilon_M^2 + \frac{1}{4}\varepsilon_T^2}, \tag{4.19}$$

where $\varepsilon_M = \sigma_M / M$.

An estimation of the relative expanded uncertainty in a measurement chain, with the relative uncertainties $\varepsilon_1, \varepsilon_2, \varepsilon_3 \ldots$, can be obtained by

$$\varepsilon_{tot} = \sqrt{\varepsilon_1^2 + \varepsilon_2^2 + \varepsilon_3^2 + \ldots}. \tag{4.20}$$

Starting with the errors related to the measurement with CTA, the two major contributions to the uncertainty of the derived mass flux of the hot-wire is the mass flux determination by means of the pressure transducer and the thermocouple as well as the fitting of the data. The different sources of uncertainty for both CTA and also for the system reference flow meter, are listed in Table 1. Phenomena that have insignificant[3] uncertainties relative to those listed in Table 1 are not taken into consideration[4], examples of those are:

- A/D conversion
- Position of hot-wire relative to pressure transducers
- Atmospheric pressure
- Humidity

An estimation of the uncertainties of the derived mass flux obtained with the hot-wire, based on the calibration and the curve fitting, gives an uncertainty of about 2.3%. Together with the phenomena not accounted for, the uncertainty is closer to around 3%, which is a typical uncertainty for the derived velocity in CTA (Jorgenson 2004). The reference mass flow meter (ABB) is calibrated by the manufacturer, following ISO-standards. However, because the sensitivity of the meter typically decreases with time due to contamination, regular calibrations of the meter were performed by means of an orifice plate. Such a calibration can be seen in Fig. 4.7 (taken from Paper 4), where a previous fit for the ABB meter is compared with the orifice plate. As evident, the uncertainty is high at low flow rates ($\dot{m} \leq 25$ g/s), but becomes around ±1% at flow rates $\dot{m} \geq 40$ g/s. The uncertainties in Table 1 have been computed for a nominal flow rate above 40 g/s.

[3]Many small errors can of course make a perceptual contribution to the total error.
[4]A thorough elaboration of the uncertainty estimation related to CTA measurements can be found in Jorgenson (2004).

Source of uncertainty	Quantities	Uncertainty (±%)
	CTA	
Transducer	Stagnation pressure p_0	0.5
Transducer	Static pressure p	1
Thermocouple	Stagnation temperature T_0	0.4
Calibration	$\rho u = f(p_0, p, T)$	**2.2**
Curve fitting	E vs. ρu	**0.5**
Resulting error		**2.3**
	Reference flow rate	
Orifice plate	$\dot{m} = f(\Delta p, T, \mathrm{Re})$	**1**
Curve fitting	E_{ABB} vs. $\dot{m}_{OP}$	**1.5**
Resulting error		**1.8**

TABLE 1. Relative uncertainty. The values for transducers and thermocouples are taken from the manufacturers data and are typical values. The calibration uncertainty for the mass flux is calculated with Eq. (4.19), and the resulting errors are calculated with Eq. (4.20) and are based on the bold numbers.

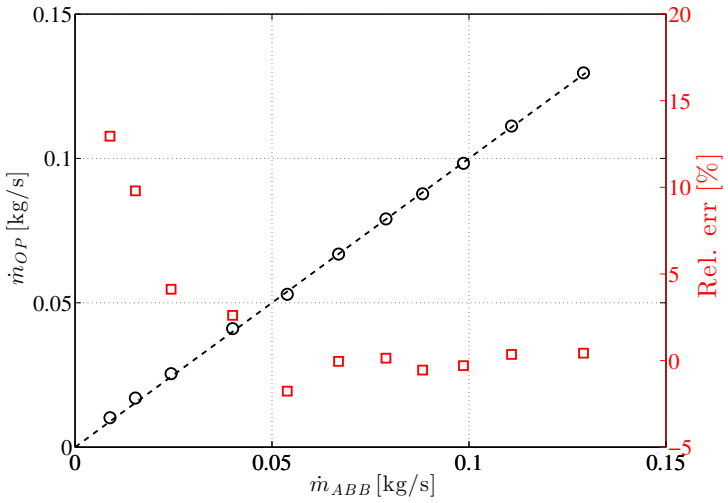

FIGURE 4.7. Calibration of ABB mass flow meter with orifice plate as reference. Measured values (ABB): ○. Relative error: □. The flow rate estimated with the ABB flow meter is based on a previous calibration of the output E_{ABB} against the orifice plate.

CHAPTER 5

Summary, conclusions and outlook

In this chapter, a short summary of the appended papers will be given as highlights, as well as some suggestions for future work.

5.1. A flow facility for the characterization of pulsatile flows

- A unique and versatile flow rig for the study of pulsatile flows relevant for internal combustion engines is described.
- The rig includes a flow measurement module with an automated traversing system to be able to measure the phase-averaged pulsating flow field.
- Time resolved mass flux and temperature can be measured via hot- and cold-wire anemometry.
- The rig provides the possibility to create a unique experimental database with well defined boundary conditions to be used for validation of numerical simulations.

5.2. Time-resolved measurements with a vortex flowmeter in a pulsating turbulent flow using wavelet analysis

- A novel analysis method to obtain the instantaneous flow rate in pulsating flows from a hot-wire placed in the wake of a vortex shedder has been developed.
- The frequency modulated signal is evaluated by means of wavelet transform to obtain a time resolved frequency, and via the Strouhal number, a time resolved velocity.
- Laser Doppler velocimetry and hot-wire measurements validate the accuracy in pulsating flows for the vortex flow meter.

For an introduction to the wavelet transform and its features see Appendix A.

5.3. Experimental analysis of turbocharger interaction with a pulsatile flow through time-resolved flow measurements upstream and downstream the turbine

- Time resolved measurements of velocity, temperature, and pressure, both upstream and downstream a turbine are performed in the facility described in Paper 1.

- The vortex flow meter as introduced in Paper 2 is employed in a complex flow application with success.
- The flow rate variations downstream the turbine are damped by more than a factor of two as compared to the upstream side, but the pulse-shape is preserved to a high degree.
- The variables in the turbine map are phase shifted by means of cross correlation to further assess the quasi-steadiness validity and the study confirms that the quasi-steady assumption is invalid for the turbine considered as a whole.

5.4. Vortex shedding flow meters: accuracy assessment and extension towards industrial configurations

- Measurements are performed on a vortex shedder in pipe flow both in a fully developed pipe flow as well as in a complex, industrial like pipe flow in order to assess the accuracy of the Strouhal-Reynolds number relation.
- The detection of the shedding frequency was performed both in the wake of the cylinder (hot-wire) and on the vortex shedder (imbedded microphone).
- A robust technique based on the detection of pressure fluctuations by means of a microphone attached to the vortex shedder, a hollow circular cylinder, showed promising results. This can be used in harsh environments such as in gas exchange systems of internal combustion engines.

5.5. Response of common flow meters to unsteady flow

- The performance of common flow meters (that are usually used for steady flow measurements) were investigated in pulsating compressible flow. These are: Venturi, hot-film, Pitot tube, turbine and vortex flow meters.
- The performance for all meters are quite acceptable for pulsating frequencies, as long as flow reversal does not occur, although the turbine shows the well known overestimation of flow rate at the lowest frequencies. The hot-film overestimates the flow rate considerably when back flow occurs, due to its inability to discriminate the flow direction.
- LDV measurements are performed to assess the amount of back flow. A simulation of the lag of the hot film is applied on the LDV signal (viewed as an input) and explains the qualitatively behaviour of the hot-film signal (viewed as an output).

5.6. Review on the sensed temperature in cold-wire and hot-wire anemometry

- This is a review that aims to describe what effective temperature is sensed using thermal anemometry.
- Experiments performed in a divergent nozzle with a cold-wire confirm previous results that the wire senses the recovery temperature. The measurement data also agree well with the theoretical recovery temperature, based on a laminar recovery factor equal to the square root of the Prandtl number.

5.7. What does the hot-wire measure?

- The paper discusses two hypotheses; (*i*) if the hot-wire is sensitive to the product of stagnation density and the velocity, i.e. $\rho_0 u$ or the mass flux ρu (or actually Re according to the prevailing theory); (*ii*) if the decreasing heat flux with decreasing Mach number can be explained by the Prandtl-Glauert rule.
- The experiments are performed with the same nozzle as the one described in Paper 6. The results indicate that the heat transfer from the hot-wire is sensitive to $\rho_0 u$ rather than ρu and that the Prandtl-Glauert transformation may be used to normalize the heat transfer results.

5.8. Suggestions for future work

As in all scientific work, the studies made in this thesis lead to new questions and possibilities for developments and future studies. In the following three future directions are suggested, (*a*) the development of the vortex flow meter to a useful tool for industrial applications, (*b*) continuation of the work on turbine performance under pulsating flow and (*c*) further studies of heat transfer from hot-wires under compressible flow conditions and especially the effect of the Mach number.

(*a*) *The vortex flow meter*

The present development of the vortex flow meter technique described in Paper 2, shows promise to be useful in flows related to internal combustion engines, but there are at least three different aspects that have to be further investigated. (*i*) the design, with the microphone as described in Paper 4, has to be optimized in order to obtain increased signal quality. This may be achieved by means of measuring the pressure fluctuations at two different locations on opposite side of the cylinder. By correlating the two signals it may be possible to exclude the acoustic noise, (*ii*) in order to be able to use the device in real time applications, some simplification in the signal analysis has to be done in order to expedite the computations, (*iii*) the technique as is cannot be used to detect flow reversals. Solutions to this problem should be pursued, one

possibility would be to measure the pressure at the stagnation line.

(*b*) *Turbine measurements*

With the present laboratory facilities, described in Paper 1, the first combined, simultaneous time resolved flow (velocity), temperature and pressure measurements upstream and downstream a turbine have been demonstrated in Paper 3. This naturally leads to a continuation where the turbine characteristics under different flow conditions are mapped and compared to both 1-D simulation codes as well as full 3-D CFD calculations. It would also be of interest to investigate how different types of pulse shapes affect the turbine characteristics. This can be done by modifying the rotating valve of the pulse generator. Similar measurements should also be performed for the compressor under various operating conditions.

(*c*) *Hot-wire response in compressible flow*

The use of hot-wire anemometry in compressible flows at subsonic Mach numbers were discussed in Paper 7 (and also partly in Paper 6). The decrease in heat transfer with increasing Mach number was investigated. A hypothesis was stated that relates this result to a decrease in the gradients normal to the flow direction when the Mach number is increased. This is known from the Prandtl-Glauert transformation and by using this rule to scale the heat transfer a result that was almost independent of Mach number was obtained. Experiments to further investigate this hypothesis need to be done, and the result provided in Paper 7 that the hot wire seems to be sensitive to $\rho_0 u$ rather than ρu should be further substantiated.

CHAPTER 6

Papers and authors contributions

Paper 1

A flow facility for the characterization of pulsatile flows
F. Laurantzon (FL), N. Tillmark (NT) , R. Örlü (RÖ) & P. H. Alfredsson (HAL).
Accepted in Flow Meas. Instrum.

The experimental set-up was designed by FL and NT. The experiments was carried out by FL under supervision of HAL and NT. The writing was done jointly, by FL, RÖ, HAL and NT. The work is accepted for publication in *Flow Measurement and Instrumentation.*

Paper 2

Time-resolved measurements with a vortex flowmeter in a pulsating turbulent flow using wavelet analysis
F. Laurantzon (FL), R. Örlü (RÖ), A. Segalini (AS) & P. H. Alfredsson (HAL).
Meas. Sci. Tech. **21** (2010)

The experimental set-up was designed by HAL and FL. The experiments were performed by FL, under supervision of HAL. The wavelet analysis code was provided by AS. The paper was written by RÖ with contributions from FL and input from AS and HAL. The work was published in *Measurement Science and Technology.*

Paper 3

Experimental analysis of turbocharger interaction with a pulsatile flow through time-resolved flow measurements upstream and downstream the turbine
F. Laurantzon (FL), R. Örlü (RÖ), A. Segalini (AS), N. Tillmark (NT) & P. H. Alfredsson (HAL).
10th International Conference on Turbochargers and Turbocharging

The experimental set-up was designed by FL. The experiments were performed by FL, under supervision of HAL and NT. Data evaluation was done by FL, RÖ and AS. The writing was done jointly, by FL, RÖ, AS, HAL and NT. The

work will be presented at the *10th International Conference on Turbochargers and Turbocharging*, London, May, 2012.

Paper 4

Vortex shedding flow meters: accuracy assessment and extension towards industrial configurations
F. Laurantzon (FL), A. Segalini (AS), S. Reifarth (SR), R. Örlü (RÖ), & P. H. Alfredsson (HAL).
Submitted

The experiments were performed by FL and SR. The data analysis was done by FL and AS. The report was written by AS, FL and SR, with input from RÖ and HAL. The paper is submitted for publication.

Paper 5

Response of common flow meters to unsteady flow
F. Laurantzon (FL), R. Örlü (RÖ), Nils Tillmark (NT) & P. H. Alfredsson (HAL).
Technical report

The experiments were performed by FL. The data analysis was done by FL, RÖ and HAL. The report was written by FL and HAL with input from RÖ and NT. This work is in its present form a technical report but planned to be revised and submitted for publication.

Paper 6

Review on the sensed temperature in cold-wire and hot-wire anemometry
F. Laurantzon (FL), A. Kalpakli (AK), R. Örlü (RÖ), & P. H. Alfredsson (HAL).
Technical report

The experiments were performed by AK and RÖ. The data analysis was done by FL. The report was written by AK and RÖ with input from FL and HAL. The work is a technical report.

Paper 7

What does the hot-wire measure?
F. Laurantzon (FL), Nils Tillmark (NT) & P. H. Alfredsson (HAL).
Technical report

The experiments were performed by FL. The data analysis was done by FL and HAL. The report was written by FL, NT and HAL. The work is a technical report.

Acknowledgements

This work was financially supported by the CCGEx competence centre through the Swedish Energy Agency (STEM), Swedish vehicle industry and KTH, which is greatly acknowledged. I would especially like to thank Dr. Johan Wallesten at Volvo, for providing the venturi and Dr. Björn Lindgren at Scania, for providing the hot-film.

The Erik Petersohn foundation is acknowledged for funding a major part of my conference expenses.

Moreover, I would like to express my appreciation to my supervisor Prof. Henrik Alfredsson, for fruitful discussions and massive support during this work, as well as introducing me to Italy among other things. My second supervisor Dr. Nils Tillmark is also greatly acknowledged for helping me out whenever I needed consultancy in all kinds of matters. Dr. Ramis Örlü for his never-ending enthusiasm and for helping me with everything from hot-wire issues to the accommodation of chocolate. Dr. Antonio Segalini is acknowledged for his transfer of knowledge and being a great support during the last part of my PhD studies. Prof. Laszlo Fuchs for reading and giving valuable feedback on both my licentiate and doctoral theses.

Special thanks go to the toolmakers Kim Karlström and Göran Rådberg, for skillful and express manufacturing of experimental equipment.

Thanks also to my dear colleagues for creating a really nice workplace, you know who you are!

Last but not least, I would like to thank my dear Alexandra and little Charlie for their support and love.

APPENDIX A

Introduction to wavelet transform

Spectral signal analysis with e.g. the fast Fourier transform (FFT) only contains time averaged information, and therefore hides transient and location specific features from the signal. Time-frequency signal analysis, such as the short time Fourier transform (STFT), Wigner-Ville transform and wavelet transform, on the other hand, provides simultaneous information about the signal in both frequency and time. Hence it is possible to find local spectral properties.

Wavelet transform is a time-frequency signal analysis method that has gained popularity during recent years by researchers and engineers to analyze complex signals, such as transients and other non-stationary signals[1]. The benefit with the wavelet transform is that it has variable frequency resolution, which implies that local scale-dependent spectral analysis is possible, in contrast to e.g. short time Fourier transform (STFT), where the resolution is fixed. There are essentially two types of wavelet transforms: the continuous wavelet transform (CWT) and the discrete wavelet transform (DWT), in this appendix the former will be presented. Which transform that is appropriate to use depends on the requirements: as the CWT contains information that is redundant if merely reconstruction of the original signal is concerned, the discrete wavelet transform can be used to provide a significant reduction of computation time, but at the expense of the information.

It shall be emphasized that this appendix is mainly based on concepts and notation from Tropea *et al.* (2007, ch. 22) and Addison (2005).

A.1. The continuous wavelet transform

A wavelet $\psi(t)$, is a function with zero mean and finite energy. The continuos wavelet transform of a signal $u(t)$, is a convolution between the signal and the wavelet, viz.

$$\tilde{u}(a,\tau) = \int_{-\infty}^{\infty} \left[u(t) \frac{1}{\sqrt{a}} \psi^* \left(\frac{t-\tau}{a} \right) \right] dt, \tag{A.1}$$

where the asterisk denotes complex conjugation, a is the dilation/scale parameter, τ is the time/location parameter and $\tilde{u}$ is the so called wavelet coefficient.

[1] Examples of the application in fluid mechanics is to detect turbulent structures or extract coherent structures form a velocity field.

The integral compares the local shape of the signal with the shape of the wavelet and can therefore be viewed as a correlation between $u(t)$ and $\psi(t)$, shifted with τ and dilated with a. The time shift gives the window middle-point, while the dilation factor defines the width of the observed part of the signal. The spectral components in the signal are inversely proportional to the scale a, i.e. $f = \chi/a$, where the proportionality constant χ depends on the chosen wavelet function. The contribution to the signal energy at the specific a scale and τ location is given by the two-dimensional wavelet energy density function known as the scalogram

$$E(a,t) = |\tilde{u}(a,t)|^2. \tag{A.2}$$

Thus, the higher resemblance between $u(t)$ and $\psi[(t-\tau)/a]$, the more contribution to the signal energy.

Since a convolution corresponds to a multiplication in Fourier space, it is convenient to implement the operation as a multiplication between a Fourier transform of the signal and the pre-calculated Fourier transform of the wavelet function. Hence Eq. (A.1) can equivalently be expressed as the inverse Fourier transform of this multiplication

$$\tilde{u}(a,t) = \sqrt{a}\int_{-\infty}^{\infty}[e^{2i\pi\omega t}\hat{\psi}^*(a\omega)\hat{u}(\omega)]d\omega, \tag{A.3}$$

where the Fourier transform of a function e.g. the wavelet $\psi(t)$ is defined as

$$\hat{\psi}(\omega) = \int_{-\infty}^{\infty}\psi(t)e^{-2i\pi\omega t}dt, \tag{A.4}$$

and its inverse

$$\psi(t) = \int_{-\infty}^{\infty}\hat{\psi}(\omega)e^{2i\pi\omega t}d\omega. \tag{A.5}$$

In this way, a fast Fourier transform (FFT) algorithm can be employed in practice to speed up the computation of the wavelet transform.

There are a vast number of wavelet functions two choose from and the two most commonly employed are the (real-valued) Mexican hat wavelet and the (complex-valued) Morlet wavelet.

The Mexican hat is the second derivative[2] of the Gaussian function:

$$F_a(t) = \frac{1}{a\sqrt{2\pi}}e^{-t^2/2a^2}, \tag{A.6}$$

giving

$$\psi_{MH}(a,t) = \left(\frac{t^2}{a^2}-1\right)\frac{1}{a^2}F_a(t), \tag{A.7}$$

[2]Usually the negative of the second derivative is used.

whereas the Morlet wavelet is a combination of a sine and a Gaussian envelope, given by

$$\psi_M(t) = e^{2i\pi t} e^{-2\pi^2 t^2/z_0^2}, \tag{A.8}$$

where z_0/π is the width of the envelope and hence z_0 controls the number of oscillations in the wave packet. Instead of the usual dilation parameter a, the inverse is used $\omega = 1/a$, where ω is obtained from the Fourier transform. These two wavelet functions can be seen in Fig. A.1, together with their respective Fourier spectra. The trade-off between them is that the Morlet wavelet has narrow spectral extent but wide time domain extent, while the vice versa applies for the Mexican-hat wavelet. In other words, the Morlet wavelet is suitable for signals with a sequence of maxima and minima, whereas the Mexican hat wavelet is suitable for sudden transient events. In Figs. A.2 and A.3, the respective transforms is applied on two different test signals a frequency modulated sine and a cosine with an abrupt change of frequency, respectively.

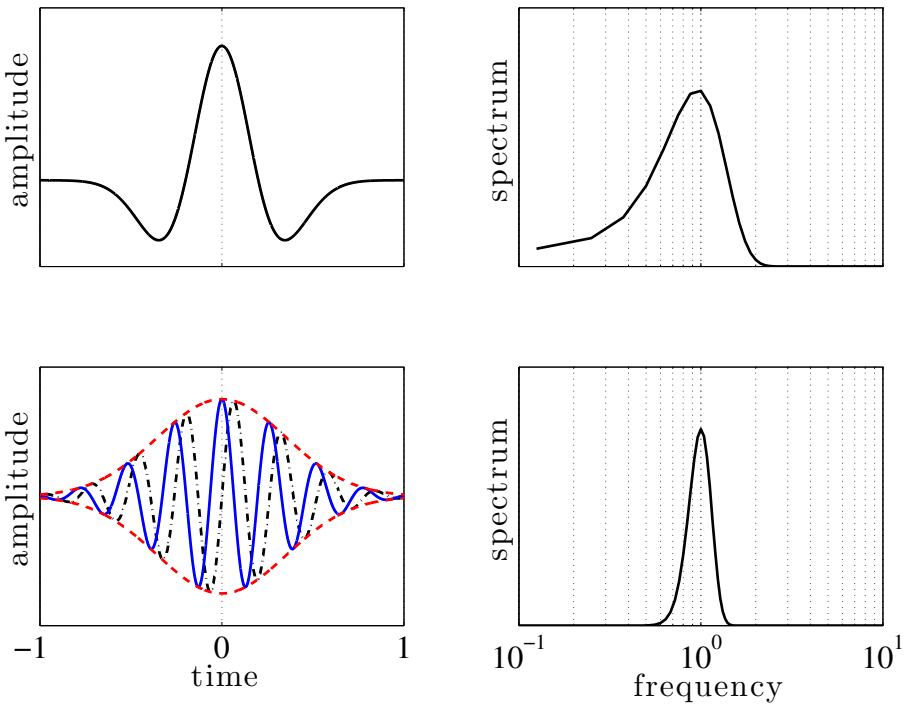

FIGURE A.1. The Mexican hat wavelet (upper left) and its spectra (upper right). The Morlet wavelet (lower left) with real part (solid), imaginary part (dot-dashed) and its absolute value/envelope (dashed), together with its spectra (lower right).

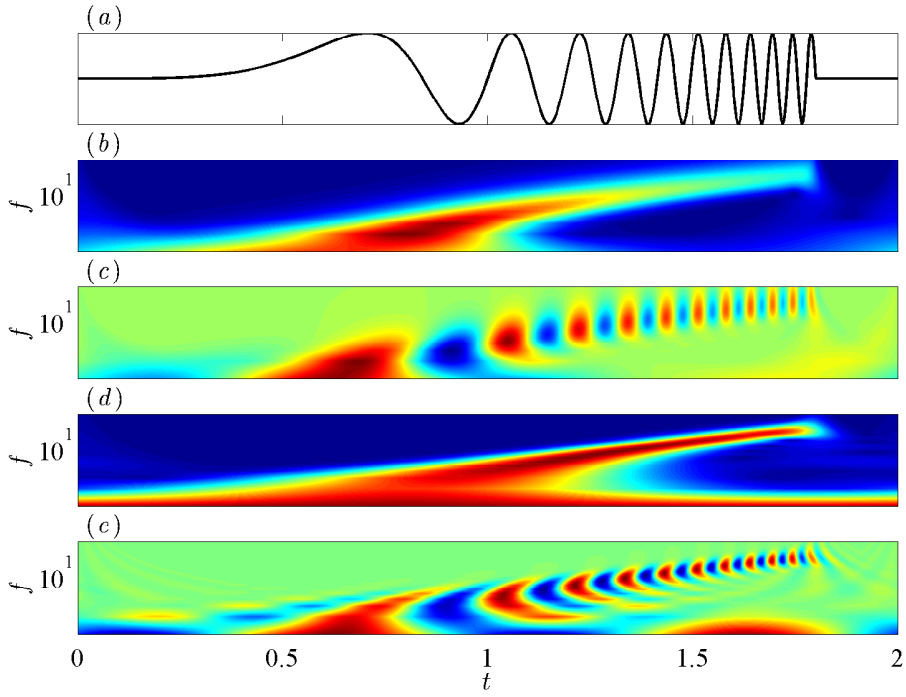

FIGURE A.2. Wavelet transforms. (a) A frequnecy modulated sine as test signal. (b) Mexican hat: scalogram. (c) Mexican hat: real part. (d) Morlet: scalogram. (e) Morlet: real part.

Here the features of the respective transform can be recognized, specifically in the scalograms, viz., the Mexican hat is able to limit the sudden change of frequency in Fig. A.3(b) to a narrow location, whereas the location is smeared out for the Morlet wavelet. On the contrary, the Morlet wavelet shows a more narrowly determined frequency, for both cases.

Finally, for many applications there is a large amount of redundant information obtained from the continuous wavelet transform $\tilde{u}(a,t)$. This can be reduced if one only consider local maxima and minima of the transform

$$\frac{d[E(a,t)/a]}{da} = 0. \tag{A.9}$$

These so called wavelet ridges are used to find instantaneous frequencies and amplitudes of the signal.

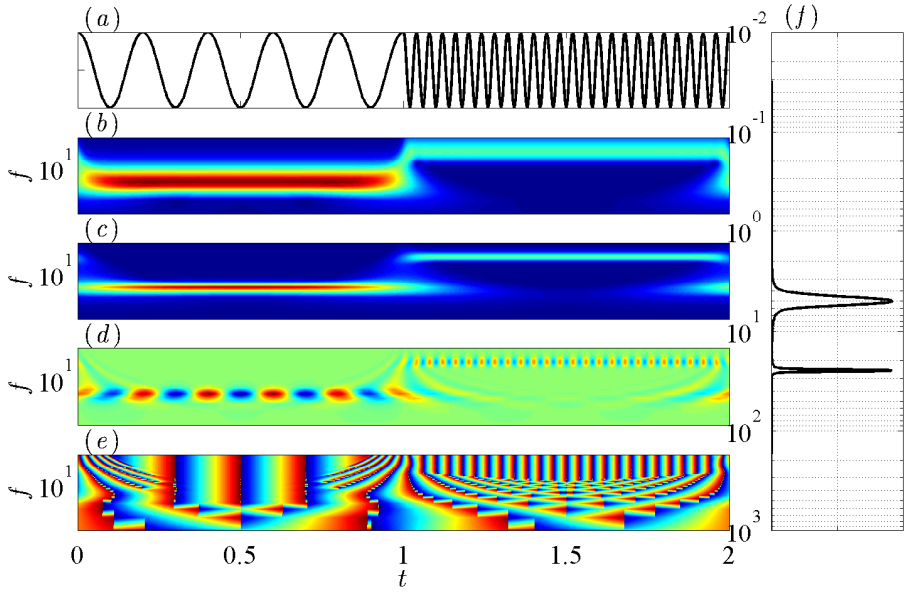

FIGURE A.3. Wavelet transforms. (a) A cosine with abrupt change in frequency. (b) Mexican hat: scalogram. (c) Morlet: scalogram. (d) Morlet: real part (e) Morlet: phase. (e) Power spectral density for the signal.

References

Addison, P. S. 2005 Wavelet transforms and the ECG: a review. *Physiol. Meas.* **26**, R155–R199.

Anderson, J. D. 2004 Modern compressible flow: with historical perspective. McGraw-Hill.

Baines, N. C. 2005 Fundamentals of Turbocharging. *Concepts ETI, Inc.*

Baines, N. C. 2010 Turbocharger turbine pulse flow performance and modelling – 25 years on. *9th Int. Conf. on Turbocharging and Turbochargers* pp. 347–362.

Bruun, H. H. 1995 Hot-wire anemometry: principles and signal analysis. *Oxford University Press Inc.*

Carpinlioglu, M. O. & Gundogdu, M. Y. 2001 A critical review on pulsatile pipe flow studies directing towards future research topics. *Flow. Meas. Instrum.* **12**, 163–174.

Cascetta, F. 1995 Short history of the flowmetering. *Isa T.* **34**, 229–243.

Copeland, C. D., Martinez-Botas, R. F. & Seiler, M. 2011 Comparison between steady and unsteady double-entry turbine performance using the quasi-steady assumption. *J. Turbomach.* **133**, 031001.

Costall, A., Szymko, S., Martinez-Botas, R. F., Filsinger, D. & Ninkovic, D. 2005 Assessment of unsteady behaviour in turbocharger turbines. *ASME Turbo Expo 2006* **6**, 1023–1038.

Dijk, A. & Nieuwstadt, F. 2004 The calibration of (multi-) hot-wire probes. 1. Temperature calibration. *Exp. Fluids* **36**, 540–549.

Håkansson, E. & Delsing, J. 1994 Effects of pulsating flow on an ultrasonic gas flowmeter. *Flow. Meas. Instrum.* **5**, 93–101.

Heywood, J. B. 1988 *Internal Combustion Engine Fundamentals* . McGraw-Hill.

Hu, X. & Lawless, P. B. 2001 Predictions of on-engine efficiency for the eadial turbine of a pulse turbocharged engine. *SAE Technical Paper 2001-01-1238*.

Jorgenson, F. E. 2004 *How to measure turbulence with hot-wire anemometers*. Dantec Dynamics.

Laurantzon, F., Kalpakli, A., Örlü, R. & Alfredsson, P. H. 2010 Review on the sensed temperature in cold-wire and hot-wire anemometry. *Tech. Rep. KTH Mechanics*.

Marelli, S. & Capobianco, M. 2011 Steady and pulsating flow efficiency of a

waste-gated turbocharger radial flow turbine for automotive application. *Energy* **36**, 459–465.

Nabavi, M. & Siddiqui, K. 2010 A critical review on advanced velocity measurement techniques in pulsating flows. *Meas. Sci. Technol.* **21**, 042002.

Ohmi, M., Iguchi, M. & Urahata, I. 1982 Flow patterns and frictional losses in an oscillating pipe flow. *Bulletin of JSME* **25**, 536–543.

Örlü, R. 2006 Experimental study of passive scalar mixing in swirling jet flows. *Lic. thesis, KTH Mechanics*.

Rehnberg, U. 2011 Analysis of shortcomings with 1-D engine calculations by means of 3-D computations on components. *PhD thesis, KTH Machine Design*.

Rocklage-Marliani, G., Schmidts, M. & Vasanta Ram, V. 2003 Three-dimensional laser-Doppler velocimeter measurements in swirling turbulent pipe flow. *Flow Turb. Combust.* **70**, 43–67.

Sanderson, M. 1989 Editorial. *Flow. Meas. Instrum.* **1**, 3–4.

Shemer, L., Wygnanski, I. & Kit, E. 1985 Pulsating flow in a pipe. *J. Fluid Mech.* **153**, 313–337.

Timité, B., Castelain, C. & Peerhossaini, H. 2010 Pulsatile viscous flow in a curved pipe: Effects of pulsation on the development of secondary flow. *Int. J Heat Fluid Fl.* **31**, 879–896.

Tropea, C., Yarin, A. L. & Foss, J. F. 2007 Springer Handbook of Experimental Fluid Mechanics. *Springer*.

Uchida, S. 1956 The pulsating viscous flow superposed on the steady laminar motion of incompressible fluid in a circular pipe. *Z Angew Math Phys* **7**, 403–422.

Winkler, N. 2011 Reduced models for flows in IC-engines. *PhD thesis, KTH Machine Design*.

Part II

Papers

1

Paper 1

A flow facility for the characterization of pulsatile flows

By F. Laurantzon[1,2], N. Tillmark[1,2], R. Örlü[1,2] and P. H. Alfredsson[1,2]

[1] CCGEx, KTH Mechanics, Royal Institute of Technology, SE-100 44 Stockholm, Sweden

[2] Linné Flow Centre, KTH Mechanics, Royal Institute of Technology, SE-100 44 Stockholm, Sweden

Accepted in *Flow. Meas. Inst.*

In this paper a new flow facility for studies of pulsating flows is described. The pulsating flow is generated by means of a rotating valve and the flow is quantified through a newly developed flow measurement module accurately measuring the phase averaged flow distribution. The measuring probe of the module consists of a hot/cold-wire pair that enables both the mass flux and recovery temperature to be measured simultaneously. Calibrations of both the hot and cold wire are done in-situ in steady flow by means of a Pitot tube and a thermocouple. Moreover, the phase averaged flow distribution can be obtained by an automatic traverse of the measuring probe across the pipe cross section in both the radial and azimuthal directions. In the paper we exemplify and describe the flow properties, using the new flow measurement module, both in steady and pulsating flow.

1. Introduction and background

Pulsating flow is a specific type of unsteady flow, which frequently occurs in many technical applications but also in nature. An example of the former are intake and exhaust flows of internal combustion engines Capobianco *et al.* (1989); Marelli & Capobianco (2011), whereas an example of the latter is blood flow in arteries and veins Paul *et al.* (2009). The study of pulsating pipe flow is important since in contrast to steady pipe flow where the theory is well-defined, the study of turbulent pulsatile pipe flows remains a very active and industrially relevant research field Carpinlioglu & Gundogdu (2001*a*). In this kind of flow an oscillating flow component is superimposed on a steady flow. The flow behaviour is strongly dependent on the frequency of the pulsations, which can be expressed in terms of the so called Womersley number defined as $Wo = R\sqrt{\rho\omega/\mu}$, where R is the pipe radius, ω the angular frequency of the

pulsations and μ the dynamic viscosity of the fluid. For $Wo = \mathcal{O}(1)$ the flow field can be viewed mainly as quasi-steady, whereas for high values of Wo the flow is strongly influenced by the pulsations.

The streamwise turbulent velocity field of a pulsating flow through a pipe can in general be described as

$$u(r,\theta,t) = u_s(r,\theta) + u_a(r,\theta)f(\omega t + \Delta\phi) + \\ + u_T(r,\theta,t). \tag{1}$$

Here r is the radial and θ the azimuthal coordinate defined with the origin of the coordinate system in the centre of the pipe, u_s the steady part, u_a the amplitude of the oscillating part and u_T describes the random turbulent fluctuations. The pulsations are given by the angular frequency (ω) of the periodic function $f(\omega t)$ and $\Delta\phi$ is the phase lag that may vary with both r and θ. The means of both the pulsations and the turbulent fluctuations are equal to zero. In analogy with steady turbulent flow, measurements of the statistical moments such as mean u_m (the first moment) and root mean square u_{rms} (square root of the second moment) of the velocity, are independent of time, for sufficiently long time series (see for instance Bendat & Piersol (1986) and Landahl & Mollo-Christensen (1992)). For instance $u_m = u_s$ and $u_{rms} = \sqrt{u_a^2\,\overline{f^2} + \overline{u_T^2}}$ if the pulsations and turbulence are uncorrelated (overbar denotes time average). The difference between a steady and a pulsating flow is, however, clearly observed if the autocorrelation is considered, which for a pulsating flow is periodic, whereas for a steady turbulent flow it decays exponentially towards zero. Following the notion in Sonnenberger *et al.* (2000), we are dealing with a periodic random process, for which the phase mean value (phase average) of e.g. the velocity in Eq. (1) is determined in the following way

$$U(r,\theta,\tau) = \lim_{N\to\infty} \frac{1}{N} \sum_{n=1}^{N} u(r,\theta,\tau + n\tau_0), \tag{2}$$

where $\tau_0 = 2\pi/\omega$ is the period and τ (or rather $\omega\tau$) is the phase for which $0 < \tau < \tau_0$, and N is the number of periods used in the averaging process.

Advantages	Drawbacks
High frequency response	Intrusive technique
High spatial resolution	Sensitive to dirt contamination
Wide dynamic range	Sensitive to temperature fluctuations
Inexpensive	Fragile
	Needs calibration

TABLE 1. Advantages and drawbacks with the HWA technique.

The aim with the present paper is to investigate and characterize pulses in a newly developed flow facility. While similar rigs exist (see for instance Marelli & Capobianco (2011); Carpinlioglu & Gundogdu (2001*b*); Szymko & Martinez-Botas (2005)), the present rig is used to simulate engine exhaust flows, and especially the inflow to the turbine of turbochargers, under well controlled conditions. The novelty of the facility–compared to previous rigs– is an integrated automatic measurement module that enables phase-resolved and simultaneous measurements under industrially relevant conditions of the mass flux and recovery temperature over the entire cross-section by means of hot/cold-wire anemometry. Typical pulsation frequencies of the exhaust flow for a four-cylinder engine are of the order of 40–80 Hz with mass flow rates up to and above 200 g/s in pipes with a cross section of the order of 10–20 cm^2. Corresponding Womersley numbers are of the order of 50 or higher, so there is a strong influence of the pulsations on the flow behaviour. Peak velocities at the turbine inlet during the pulsations may reach several hundred meter per second, and such a flow will experience both compressibility effects as well as unsteady temperature variations of the gas. While time resolved measurements have been made in previous studies in pulsating pipe flow, simultaneous time resolved measurements of mass flux and temperature, have to the authors knowledge not previously been reported.

Due to the complexity of pulsating flows care must be taken when choosing the measurement technique Mottram (1992). A number of techniques exists for flow measurements, but pulsatile flow conditions are known to bias the reading from many of these devices, e.g. the Coriolis mass flowmeter Vetter & Notzon (1994), the vortex flowmeter Hebrard *et al.* (1992) and the ultrasonic flow meter Håkansson & Delsing (1994), see also references in Grenier (1991), regarding the effect of the pulsations on these techniques. The choice of an appropriate technique becomes even more important if one is attempting to make time resolved measurements, see for instance Doblhoff-Dier *et al.* (2010). Quantities of interest are flow velocity or rather mass flux, temperature and pressure, but also density and instantaneous mass flow rate. A method to deduce the time-resolved mass flow from a vortex flow meter has recently been presented in Laurantzon *et al.* (2010*b*). To be able to do time resolved point-wise measurements of the mass flux, hot-wire anemometry (HWA) is a suitable choice since it actually senses the mass flux ρu rather than the velocity u Bruun (1995); Durst *et al.* (2008) and also because its high dynamic range and frequency response Nabavi & Siddiqui (2010). On the other hand, since the hot-wire cannot sense the direction of the flow, large errors may be obtained when estimating the mass flux, if flow reversals occur. This is commonly the case in pulsating flow, and it has been debated whether hot-wire anemometry is a suitable choice for pulsating flow measurement when pulsation amplitudes and frequencies are high Berson *et al.* (2010). Time resolved temperature

measurements can be obtained with cold-wire anemometry, but the frequency response is quite much lower than for hot-wire anemometry.

The remainder of the paper is organized as follows: Section 2 gives a theoretical background to hot and cold wire anemometry, with some emphasis on the temperature correction that has to be employed under high amplitude pulsations. In section 3, a brief description of the flow facility itself is given as well as a more detailed description of the flow measurement module. Results obtained by using the flow measurement module are shown in section 4, both typical pulsation traces and probability density distributions for mass flow rate and temperature, as well as examples of their spatial distribution over the pipe cross section.

2. Theory review

The flow measurement module developed for the characterization of the pulsating flow utilizes hot-wire anemometry which is a widely used flow measurement technique in fluid mechanics research laboratories. It is a rather simple technique, with high frequency response and good spatial resolution. Other advantages and also drawbacks associated with the technique are summarized in Table 1.

2.1. *Basics of HWA and CWA*

For constant temperature anemometry (CTA), the relation between the anemometer output voltage E and the non-dimensionalized flow quantity, the Reynolds number Re, can be written Abdel-Rahman *et al.* (1987)

$$\frac{E^2}{R_w(T_w - T_a)} = A' + B' Re^n, \tag{3}$$

where T_w and T_a are the wire temperature and the ambient temperature, respectively. For a given T_w (3) can be rewritten

$$E^2 = A(T_a) + B(T_a)(\rho u)^n, \tag{4}$$

where ρ is the fluid density and u the fluid velocity, see e.g. (Bruun 1995, ch. 2). Eq. 8 implies that the anemometer output in CTA mode is related to to the mass flux, but also to the gas temperature. The temperature sensitivity must be taken into consideration if measurements are performed in non-isothermal flow, such as high speed pulsating flows for which the total temperature is not constant.

Cold-wire anemometry (CWA) can be used for temperature measurements, in which case a low, constant current, is provided to the wire (so called Constant Current Anemometry, CCA), see e.g. (Bruun 1995, ch. 7). The output of the system will change with the resistance of the wire, since the resistance depends linearly on the temperature (at least for temperatures in the range up to 250°C).

This can be expressed as

$$R = R_{\mathrm{ref}}[1 + \alpha(T - T_{\mathrm{ref}})], \tag{5}$$

where α is the temperature coefficient of resistivity and R_{ref} is the resistance at the reference temperature T_{ref}.

2.2. *Temperature correction*

Several temperature correction methods for the CTA output voltage have been suggested, and the most commonly used is the one proposed by Kanevce & Oka (1973)

$$E_{\mathrm{c}} = E\left(\frac{T_{\mathrm{w}} - T_{\mathrm{ref}}}{T_{\mathrm{w}} - T_r}\right)^n. \tag{6}$$

The exponent n is 0.5, T_{w} is the wire temperature determined from the wire resistance, T_{ref} is the temperature at which the calibration was performed and T_r is the air temperature sensed by the sensor during the measurements. E_c is the hot-wire response obtained for the same velocity under isothermal ($T = T_{\mathrm{ref}}$) conditions, while E is the measured response from the anemometer output. Hence Eq. (6) provides the anemometer signal which would have been measured if the fluid around the hot-wire would have had the same temperature T_{ref} as during its calibration, whereas in reality it had temperature T. The temperature sensed by the hot-wire (T_r) is usually referred to as the recovery temperature. The recovery or adiabatic wall temperature is lower than the stagnation temperature and is the temperature of an adiabatic wall in a gas, see also Laurantzon *et al.* (2010*a*). Equation (6) relies on that the temperature change is small enough for fluid properties to be considered constant but the relation breaks down at larger changes Hultmark & Smits (2010); Benjamin & Roberts (2002). A slight change in n has been proposed ($n = 0.55$), which improves the results at high temperature offsets, 600 K $< T <$ 800 K, see Dijk & Nieuwstadt (2004). This may be of significance for pulsating flows, where temperature fluctuations can be substantial.

In order to determine the temperature sensed by the hot-wire sensor in an unsteady flow the cold-wire technique can be employed, which senses a temperature close to the recovery temperature Fingerson & Freymuth (1983), see also references in Laurantzon *et al.* (2010*a*). The recovery temperature is higher than the static temperature but lower than the total temperature and can be determined from

$$\frac{T_r}{T} = 1 + r\frac{\gamma - 1}{2}M^2, \tag{7}$$

where T is the static temperature, γ the ratio of specific heats, r the recovery factor and M the Mach number. For laminar flow around a body the recovery factor can be shown to be $r = \sqrt{\mathrm{Pr}}$ where Pr is the Prandtl number. The

Prandtl number is the ratio of momentum diffusivity to thermal diffusivity and is defined as

$$\mathrm{Pr} = \frac{c_p \mu}{k} \tag{8}$$

where c_p is the specific heat at constant pressure and k is the coefficient of thermal conduction of the gas. For air $\mathrm{Pr} \approx 0.72$ and this means that $r \approx 0.85$. Eq. (7) together with the energy equation for a compressible adiabatic flow (Eq. (7) with $r = 1$) give the following relation for r:

$$r = \frac{T_r - T}{T_0 - T}\,. \tag{9}$$

Another way to define the recovery temperature is through the so called recovery ratio

$$\eta = \frac{T_r}{T_0}\,. \tag{10}$$

For subsonic flows this factor is close to or greater than 0.98.

By using similar probe geometries for the cold and hot-wire sensors the temperature measured by the cold wire can be used to compensate the hot-wire output in order to obtain E_c in eq. (6). One should however bear in mind that the frequency response, due to thermal lag Berson *et al.* (2010); Olczyk (2008), of the cold wire is much less, usually limited to frequencies below 1 kHz, than for the hot-wire.

3. Experimental set-up and instrumentation

3.1. *Flow facility*

A new flow rig has been developed at KTH CCGEx within the CICERO laboratory, for both steady and pulsating flows. The aim is to accurately measure the flow quantities in order to be able to fully characterize the in- and out coming flow in various combustion engine components, such as turbines, pipe bends, flow restrictions etc.

Compressed air, at a maximum flow rate of 0.5 kg/s at 6 bar, is supplied to the laboratory from two *Ingersoll Rand* screw compressors (*Nirvana 75* and *SSR ML75*). The compressors are placed in a rock shelter 30 m from the laboratory together with a dryer and filter unit and connected to the laboratory by a 100 mm pipe. The system is schematically depicted in Fig. 1

The pipe system is divided into two branches just downstream of an electrically controlled pressure-regulating valve. One of the branches is a bypass line used in order to provide a stable flow at low mass flow rates, since the stability of the regulating valve and the compressors is improved above a certain mass flow rate. The other branch is the main pipe to the laboratory and the mass flow rate is measured by a high precision mass flow hot-film meter (*ABB Thermal Mass Flowmeter FMT500-IG*). The flow meter is located downstream of a 10 m long, 100 mm diameter, straight pipe section. Approximately two

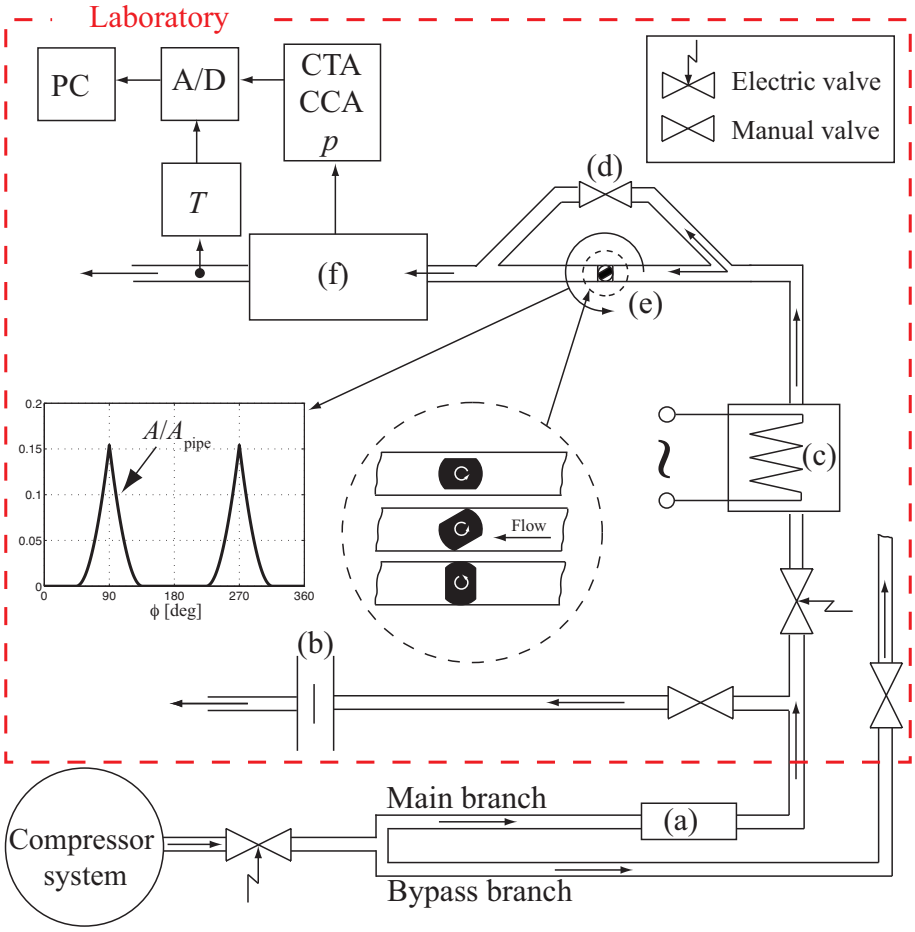

FIGURE 1. A schematic of the flow rig. (a) Thermal mass flow meter (ABB), (b) orifice plate, (c) electric heater, (d) by-pass branch, (e) pulse generator, (f) hot-wire/cold-wire unit.

metres downstream of the mass flow meter, the main pipe branches into two pipes, each controlled by manual valves. One of the branches has an orifice plate meter to calibrate the ABB meter and the other pipe, the main line, connects to a variable electric heater with a maximum power of 18 kW. The heater has a feed back loop to ensure a constant preset output temperature and used in order to calibrate the cold wire. This feature is also needed when running a turbocharger unit (which can be connected downstream of item (f) in Fig. 1), to prevent the turbine outlet air from falling below the dew point.

3.2. *Pulse generator*

The flow facility includes a pulse generator with the aim to mimic the pulses obtained from exhaust valves in internal combustion engines. The pulse generator, a rotating valve, consists of a ball, planed on two opposite sides along the axis of rotation tightly fitted into a circular pipe (see the close-up in Fig. 1). A frequency controlled AC motor rotates the ball causing the valve to open twice per revolution. The rotation frequency is limited to 50 Hz, hence giving a maximum pulse frequency of 100 Hz. The pulse frequency variation was found to be less than ± 0.5% for all cases performed. The insert in Fig. 1 also shows the projected open valve area on a plane orthogonal to the pipe axis, as a function of the angle of rotation. The pulse amplitude is modulated through a valve-controlled bypass line connected in parallel with the pulse valve.

3.3. *Mass flux measurement module*

An automated mass flow measurement module has been developed in order to characterize the flow pulses that develop downstream of the pulse generator (see Fig. 2). The device is based on hot-wire anemometry and cold-wire technique, for mass flow determination and temperature measurements, respectively.

The sensing elements of the probes are two tungsten wires with a diameter $d = 5$ μm that are welded between two prongs for each sensor. The length of the hot-wire is $L = 1$ mm, hence giving an L/d ratio of 200, whereas the cold-wire sensor is longer, namely 3 mm to reduce the effect of heat conduction to/from the prongs.

The hot-wire was operated by means of a *DISA 55M01* main frame with a *55M10* standard (CTA) channel. The hot-wire is calibrated *in-situ* against two Pitot tubes located on either side of the hot-wire sensor and a ring of four static pressure taps around the periphery of the pipe section. The benefit with *in-situ* calibration is that disturbances related to the probe and pipe geometry, will be the same for both calibration and experiments Bruun (1995); Perry (1982). The calibration is performed in steady flow and the flow rate is regulated with a valve upstream of the heater. Due to the high frequency response of the hot-wires, the pulsatile velocity signal can be fully resolved. A standard square wave test (see e.g. (Bruun 1995, ch. 2)) for the used hot-wire probes resulted in a frequency response of around 15 kHz. During calibration the stagnation pressure, static pressure and stagnation temperature are measured to obtain the velocity u and the density ρ, and consequently the mass flux ρu.

For pulsating flow also the stagnation temperature varies due to the alternating compression and expansion waves generated by the pulse generator. Therefore the probe head includes a cold-wire sensor next to the hot-wire, measuring the recovery temperature (see Fig. 3). The cold-wire is run in CCA mode by means of an *AN*–1003 hot-wire anemometry system (AA labs). The frequency response of the cold-wire in the present work is about 100 Hz. The

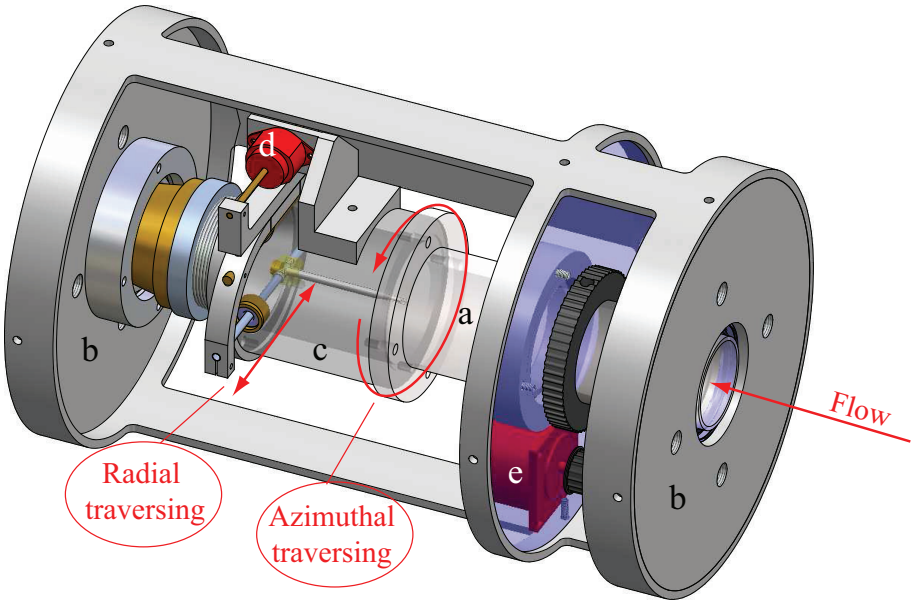

FIGURE 2. Schematic of the mass-flux measurement module (without cover). a) pipe, b) mounting flanges, c) mass flux measurement module, d) radial traversing mechanism with steppermotor, e) azimuthal traversing mechanism with steppermotor (in this figure without the belt between the gears)

.

cold-wire is calibrated in steady flow against a thermocouple just downstream of the measurement module. The mass flux probe is mounted in a slightly larger section of the pipe with the sensing part localized in the cross section where the diameter abruptly increases from 50 mm to 72 mm so that the probe can measure close to the wall.

The probe head of the measurement module is automatically traversed through the pipe along both the radial and the azimuthal directions through LabVIEW controlled stepper motors. All signals are sampled by a LabVIEW cRIO 16-bits A/D module and phase-locked with the position of the rotating valve. Typically the sampling is done at 7 radial and 12 azimuthal positions and a typical sampling time is 20 seconds at each position. Including the traversing time a full mapping of the cross section takes less than an hour. The phase averaged mass flux is determined by integrating the mass fluxes over the cross section. The flow profile without pulsation is determined the same way.

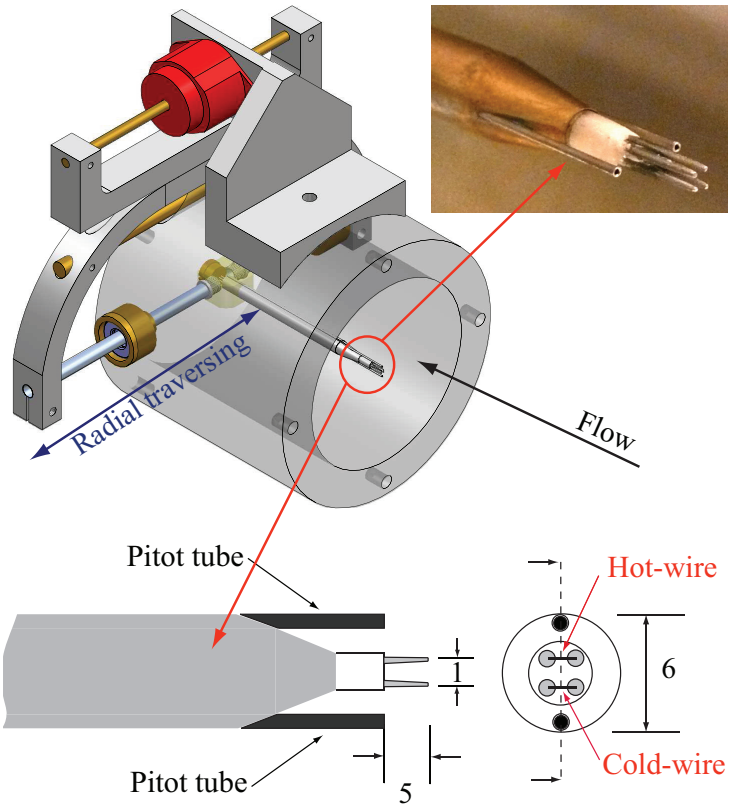

FIGURE 3. The hot-wire/cold-wire measuring probe (item c in Fig. 2). The probe tip is enlarged in a photo, and an illustration shows the relevant dimensions.

In order to have a time resolved pressure recording, a fast response *Kistler* pressure transducer is flush mounted at the pipe wall $7D$ upstream of the measurement module.

The mass flux (ρu) calibration typically covers the range $0-100$ kgs^{-1}m^{-2}, and the calibration curve used is the standard Kings law fit ((8)) where the constants A, B and n are determined through a calibration procedure using a least square fit. A typical calibration curve comprises 10 calibration points, where also the voltage at zero velocity is used. As pointed out by Dijk & Nieuwstadt (2004), the use of a literature value of the coefficient of thermal resistivity α, is not recommended since it can substantially deviate from the actual value. This fact was regarded in the hot-wire calibration procedure, where two measurement series were performed at different ambient temperatures, one

at low (~ 15° C) and one at high (~ 40° C) temperature. In Fig. 4(a) the uncompensated calibration curves are shown for the two different temperatures. The curve can be made to collapse by applying temperature compensation in the following way: If we first define the overheat ratio of the wire a_w, which is chosen by the user and is a fixed quantity defined through

$$a_w = \frac{R_w - R_{\text{ref}}}{R_{\text{ref}}} = \alpha(T_w - T_{\text{ref}}), \tag{11}$$

and apply this definition in Eq. (6), we obtain

$$E_c = E\left[1 - \frac{\alpha}{a_w}(T - T_{\text{ref}})\right]^{-1/2}. \tag{12}$$

Thus for a given set of output voltages E at two different temperatures, the only variable in the above equation is α which can be adjusted to minimize the norm between the two output vectors E_c for the low and the high temperatures respectively. This collapse of data can be seen in Fig. 4(b). Moreover the

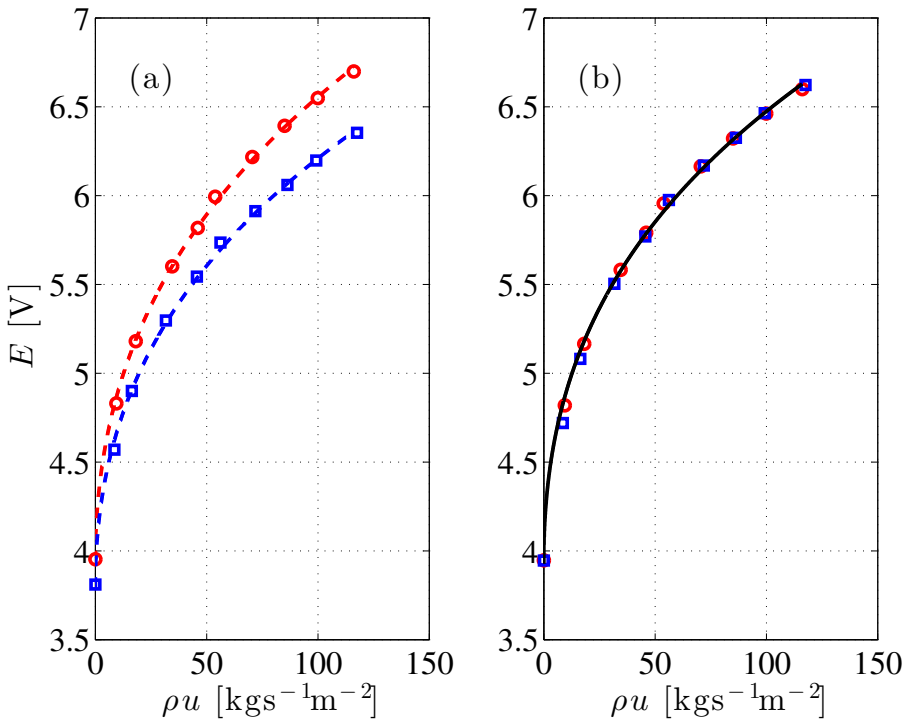

FIGURE 4. Calibration curve for the hot-wire. (a) Uncompensated, (b) temperature compensated. ◯ : T = 15°C, □ : T = 40°C.

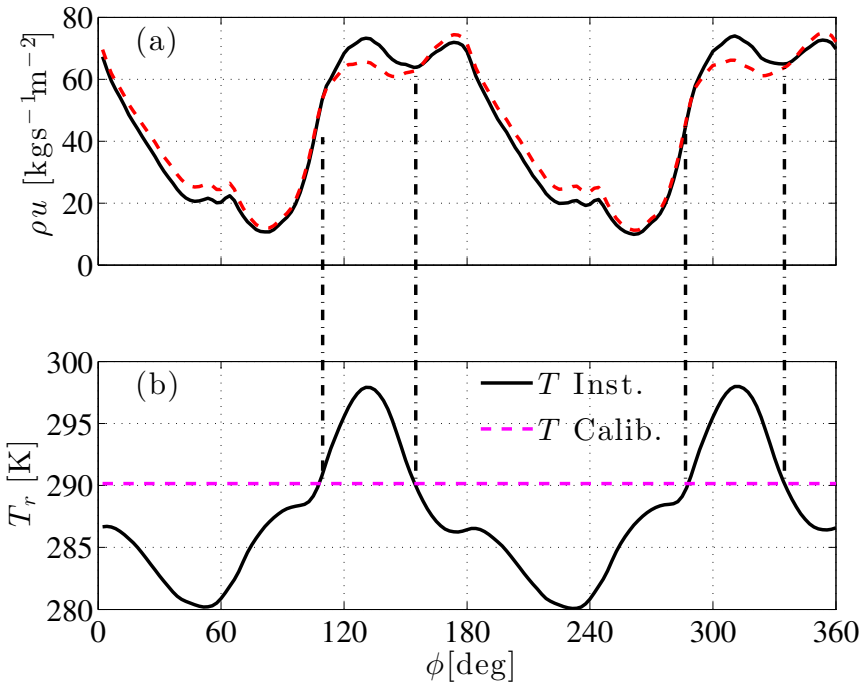

FIGURE 5. Phase averaged data at $\dot{m}$ = 80 g/s and f_p = 60 Hz. (a) Mass flux with temperature compensation (solid line) and without (dashed line). (b) Temperature with calibration temperature shown. Vertical lines are for visual aid and separates the regions of temperature higher and lower than the calibration temperature.

exponent n became equal to 0.49 in the fit, which is close to the theoretical value (n = 0.5), originally deduced by King King (1914).

As mentioned, the temperature variations during pulsations can be large and hence the measured mass flux must be compensated for this in each instant of time. Each sampled value from the CTA during the measurement was compensated by means of the simultaneously measured temperature signal obtained with the CCA, according to Eq. (6). This is illustrated in Fig. 5. As can be seen, when the temperature during the period is higher than the calibration temperature the mass flux is underestimated and is consequently compensated to a higher value, and vice versa.

4. Results

In this section, some experimental results will be demonstrated. Several flow rate/frequency combinations have been tested, but here we mainly show results for the case with a flow rate of 80 g/s and a pulse frequency of 60 Hz. The bypass valve was adjusted and was slightly open to create a steady flow component to avoid possible reverse flow.

4.1. *Time signals and radial distribution*

In Fig. 6 the time signals (i.e. the instant variation of a quantity in time) for the flow quantities mass flux $\widetilde{\rho u}$ (tilde denotes normalization with the bulk mass flux), the temperature measured with the cold-wire (T_r) and the pressure p, are plotted together with their respective phase average. The measurements of the mass flux and temperature are made at the centerline of the pipe. As previously mentioned, the static pressure is measured about 7 D upstream of the hot/cold-wire sensors and the time-lag that this distance gives rise to, is however compensated for in the plots (by correlating the time signals of the temperature and the pressure to find the time lag).

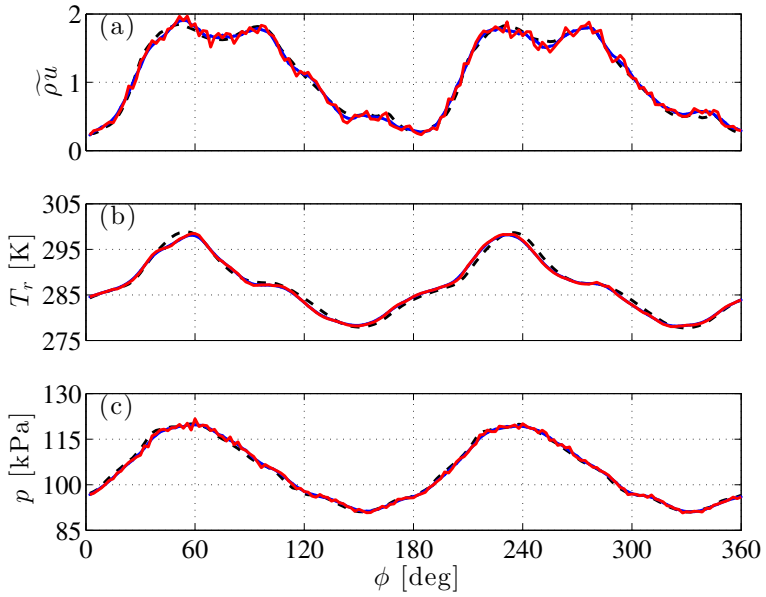

FIGURE 6. Time signal (solid line), phase average (dashed line) of (a) Normalized mass flux, (b) temperature, (c) static pressure. For $\dot{m}$ = 80 g/s and f_p = 60 Hz. The time signal for all quantities is taken from an arbitrary cycle during the pulsation measurements.

A schematic way to present the distribution of data is by means of the probability density function (pdf). In Fig. 7 the pdf for both steady and pulsating flow is shown. As can be seen, the pdf for the steady case resembles the Gaussian bell curve, whereas the pdf for the pulsating flow resembles a superposition of two signals, one sinusoidal and one Gaussian. As an orientation, in the four following plots the pdf for both the mass flux and temperature will be given at one azimuthal coordinate along the pipe cross section, shown as a contour. In other words, the horizontal axis in Fig. 7 will be the vertical in the plots, the horizontal axis will be the radial position and the pdf for each radial position will be represented by the contour.

In Fig. 8 and Fig. 9 the radial distribution of $\widetilde{\rho u}$ is shown both for steady and pulsating flow for the same mean mass flow rate. Here the measurement probe was traversed in the radial direction across the pipe cross section. The fluctuations around the mean are presented by the probability density function (pdf) normalized with its maximum value, together with the time average $\overline{\rho u}$ and the rms value both normalized with the bulk mass flux. For the steady

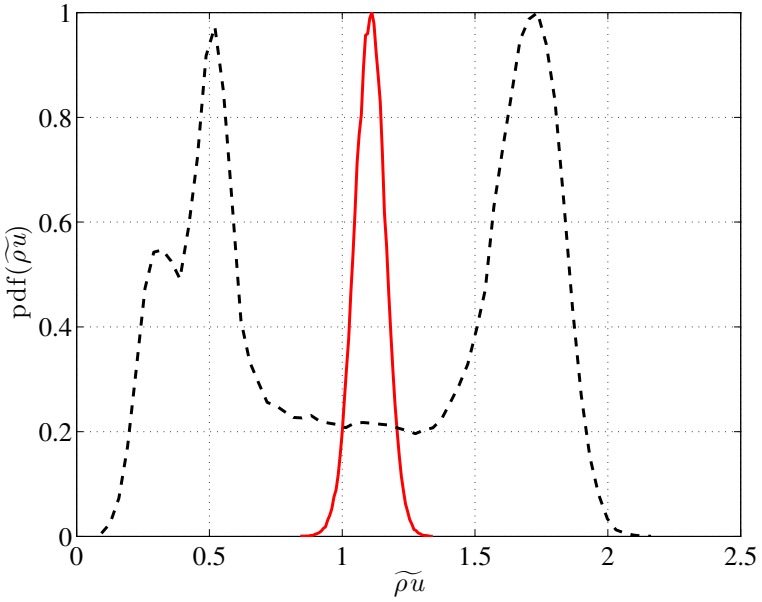

FIGURE 7. The pdf for the normalized mass flux for steady (solid line) and pulsating (dashed line), measured at the centerline, where the PDF is scaled by its maximum value. The reason the steady distribution shows a mean value slightly above the bulk flow rate is due to that the measurement is performed at the centerline.

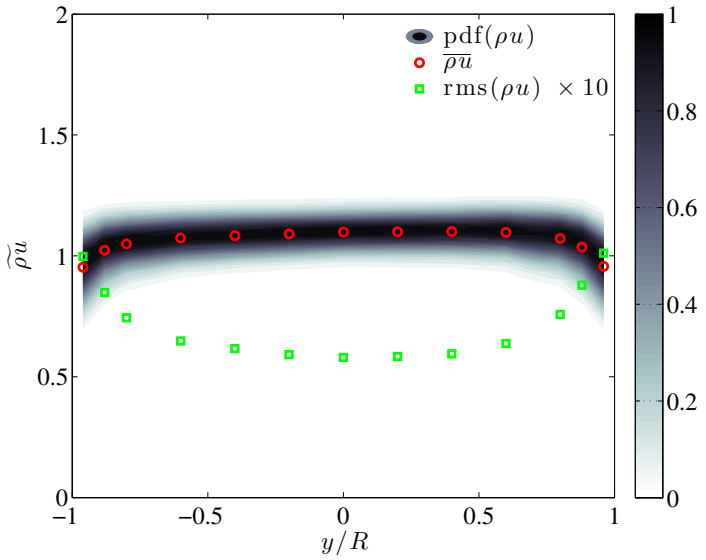

FIGURE 8. Normalized mean and rms of the mass flux (×10) at $\dot{m}$ = 80 g/s, steady flow.

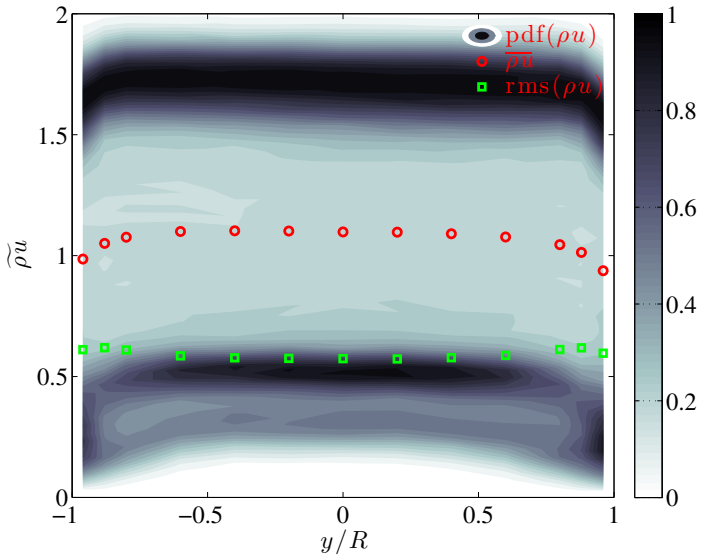

FIGURE 9. Normalized mean and rms of the mass flux at $\dot{m}$ = 80 g/s and f_p = 60 Hz.

case the profile looks as expected with a relatively flat distribution over most of the pipe diameter. The rms of the mass flux fluctuations is about 6% on the centreline and increases towards the pipe walls and reaches a value of about 10% at the point closest to the wall. One should note that for this case the mean velocity is about 35 m/s so one would not expect any compressibility effects. The behaviour is hence expected to be the same as for incompressible pipe flow, however the development length downstream of the pulse generator is too short to obtain fully developed pipe flow and therefore the rms is slightly higher here. For the pulsating case the picture is as expected quite different. The mean distribution is still close to that of the steady case, whereas the pdf shows two peaks, one at high and one at low values, similar to what one would expect for a sinusoidal signal. The rms value is about 60% across the full measured region.

A similar comparison was done for the measured temperature distributions (Figs. 10 and 11). The pdf is obtained from the measurements with the cold-wire probe, which is plotted together with its average temperature. In addition the mean of the thermocouple signal is plotted in the figures. The thermocouple measurements are made at the pipe center about $7D$ downstream of the cold-wire probe location. For the steady case one would expect agreement to a high degree since the cold-wire was calibrated with the thermocouple, however, since the standard deviation between the measured temperature and the fitted function from the calibration was below ± 0.1 K, the difference between the averages in Fig. 10 is within the measurement accuracy. The pulsating case in Fig. 11 shows a widespread pdf, with 3 peaks, one each at the two extremes and one approximately at the mean value. Here we can see that the averaging by the thermocouple overestimates the mean value by between 1 and 2 degrees. Since the cold-wire has a frequency response of about 100 Hz, it will not be able to capture the turbulent temperature fluctuations, that can be of the order of 10 kHz. Nevertheless it can resolve the temperature variations due to the pulsations, i.e. 60 Hz, on which the turbulent temperature fluctuations are superimposed. The obtained pdf can therefore be assumed to be representative for the actual temperature field, because the flow is dominated by the large time and length scales of the pulsatile motion.

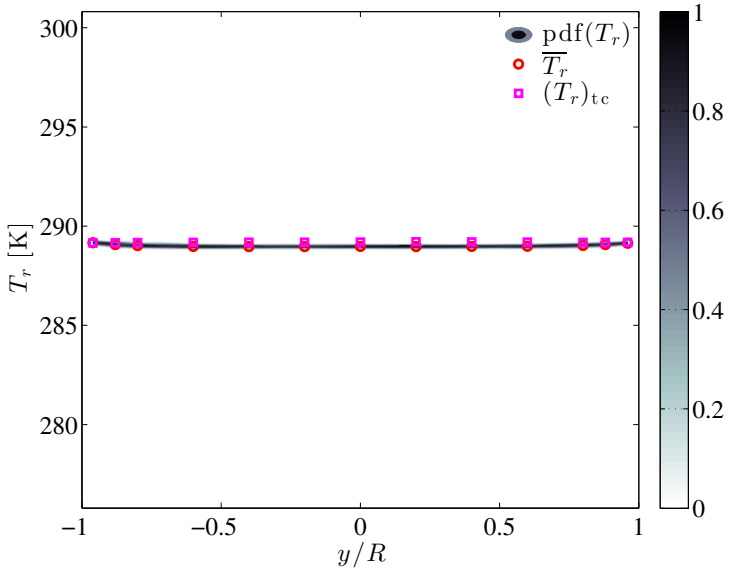

FIGURE 10. Temperature at $\dot{m}$ = 80 g/s, steady flow.

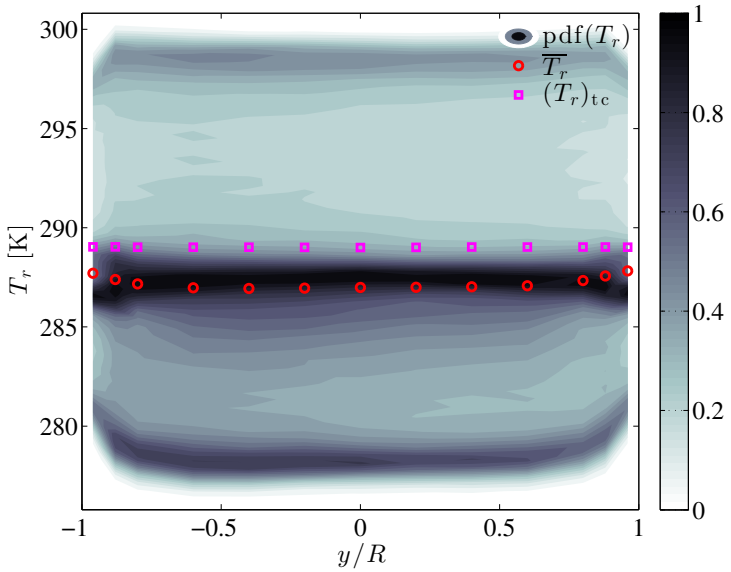

FIGURE 11. Temperature at $\dot{m}$ = 80 g/s and f_p = 60Hz.

4.2. *Distribution across the pipe section*

The traversing through the cross section was made at 7 radial points and in 12 azimuthal directions, separated by 30°. The number of traversing points were deemed to be reasonable due to the top hat character (i.e. the flow profile is relatively flat) of the mass flux and temperature profiles as will be shown later. In Fig. 12 the time averaged mass flux and temperature for the pulsating flow over the cross section are shown. In the mean ρu decreases and T increases, going from the centerline to the wall as was also seen in Fig. 9 and Fig. 11, respectively. The temperature variation is however very small and is an effect of heat transfer from the pipe wall[1] to the gas.

The phase average in the cross section is plotted for three phase instants in Fig. 13, together with the phase averaged data on the centerline for the purpose of orientation. During the deceleration phase the shape of the profiles resembles those of the mean profiles, while during the acceleration phase the temperature has the mean profile shape, but the mass flux has its largest mass flux closer to the wall. At the point of maximum flow rate the mass flux has the mean character, whereas the temperature has its highest temperature at the centerline. Furthermore, since the flow is pulsating and is open to the atmosphere downstream of the measurement module, pressure waves will reflect at the outlet boundary and interact with incident waves. Hence the shape of the pulses will be a function of flow speed and pulsation frequency. The dip in the pulse peak for the mass flux in Fig. 13, is therefore probably due to a superposition of an incident and reflected wave. It is interesting to see that despite the fact that the rotating valve set-up is far from being axisymmetric, the flow profile is still close to being axisymmetric at the measurement section 11 D downstream of the valve. It is also noteworthy that the integrated flow rate deviated from the reference ABB meter, for all flow cases with less than 4%.

[1]In this case the ambient laboratory temperature is about 5 degrees higher than the air entering the flow rig.

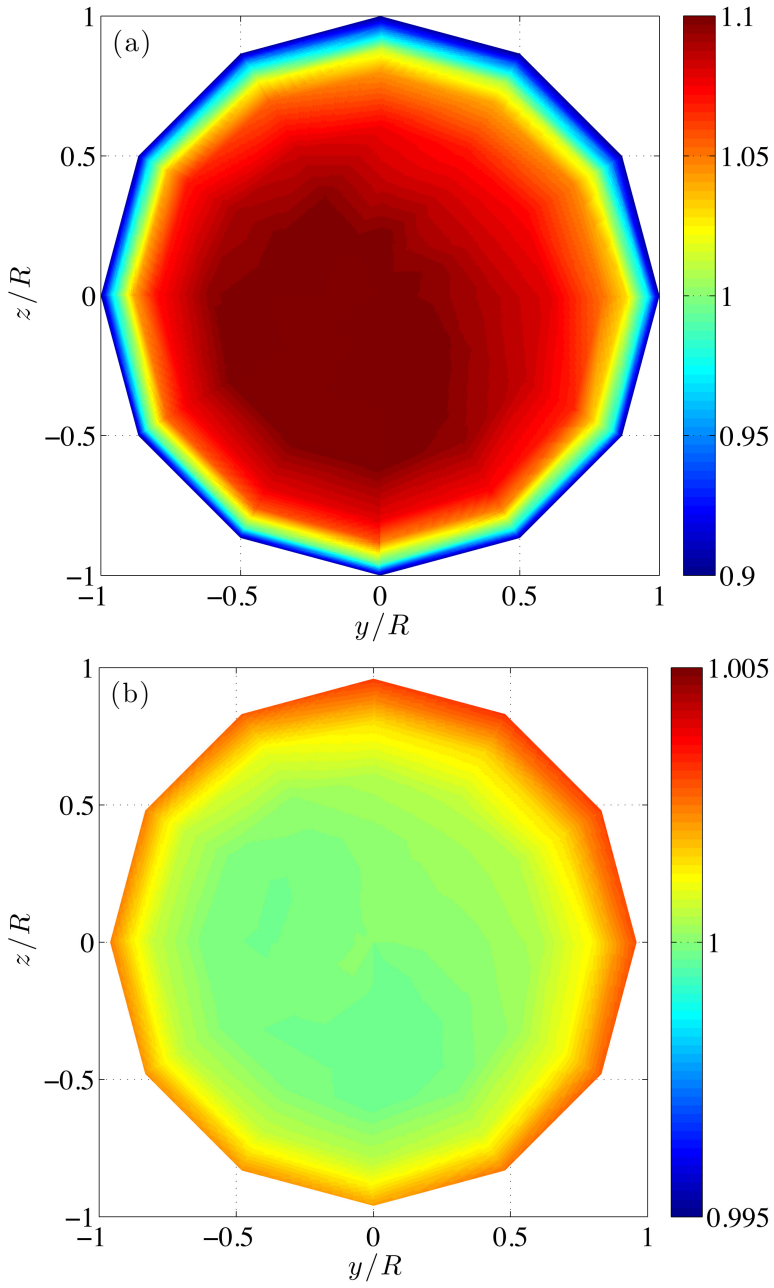

FIGURE 12. Time averaged profiles. (a) Mass flux normalized with the bulk mass flux, (b) temperature normalized with the centerline temperature.

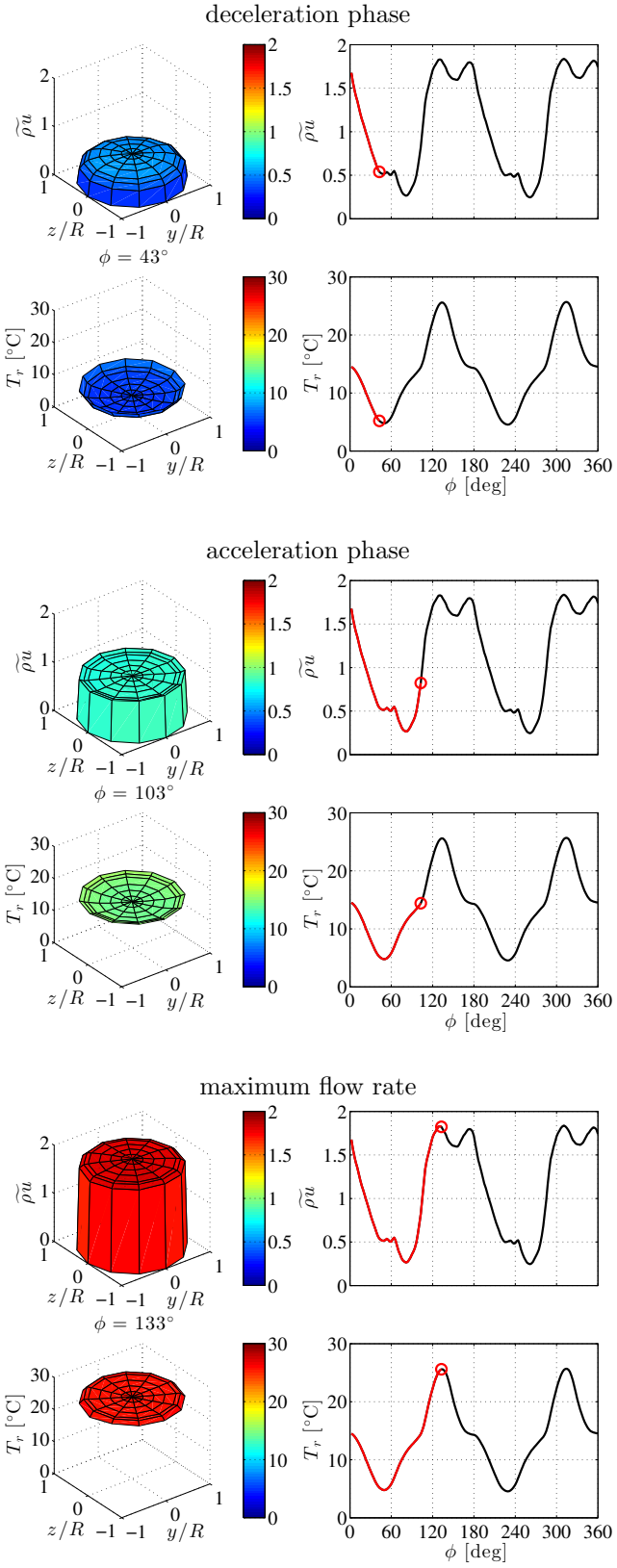

FIGURE 13. Phase averaged mass flux and temperature profiles.

5. Conclusions and ending remarks

A versatile flow rig has been developed that can be used to study pulsatile flow for internal combustion engine gas management applications. A mass flow measurement module has been developed that is able to accurately perform time resolved measurements of the mass flow distribution and temperature in both steady and pulsating flow. With this module, the flow rig can be used to experimentally study effects of pulsations and also provide accurate inflow boundary conditions for numerical simulations. The flow rig can furthermore be used to study the inflow to e.g. a turbine as well as to quantify the flow conditions downstream of a manifold, or downstream of a complicated pipe bend system.

Acknowledgements

This research was done within KTH CCGEx, a centre supported by the Swedish Energy Agency (STEM), Swedish Vehicle Industry and KTH.

References

Abdel-Rahman, A., Tropea, C., Slawson, P. & Strong, A. 1987 On temperature compensation in hot-wire anemometry. *J. Phys. E. Sci. Instrum.* **20**, 315.

Bendat, J. S. & Piersol, A. G. 1986 Random Data: Analysis and Measurement Procedures. *John Wiley & Sons*, New York, USA.

Benjamin, S. & Roberts, C. 2002 Measuring flow velocity at elevated temperature with a hot wire anemometer calibrated in cold flow. *Int. J. Heat Mass Tran.* **45**, 703–706.

Berson, A., Blanc-Benon, P. & Comte-Bellot, G. 2010 On the use of hot-wire anemometry in pulsating flows. A comment on 'A critical review on advanced velocity measurement techniques in pulsating flows'. *Meas. Sci. Technol.* **21**, 128001.

Bruun, H. H. 1995 Hot-wire anemometry: principles and signal analysis. *Oxford University Press Inc.*, Oxford, UK.

Capobianco, M., Gambarotta, A. & Cipolla, G. 1989 *Influence of the pulsating flow operation on the turbine characteristics of a small internal combustion engine turbocharger*. IMechE Conference.

Carpinlioglu, M. O. & Gundogdu, M. Y. 2001*a* A critical review on pulsatile pipe flow studies directing towards future research topics. *Flow. Meas. Instrum.* **12**, 163–174.

Carpinlioglu, M. O. & Gundogdu, M. Y. 2001*b* Presentation of a test system in terms of generated pulsatile flow characteristics. *Flow. Meas. Instrum.* **12**, 181–190.

Dijk, A. & Nieuwstadt, F. 2004 The calibration of (multi-) hot-wire probes. 1. Temperature calibration. *Exp. Fluids* **36**, 540–549.

Doblhoff-Dier, K., Kudlaty, K. & Wiesinger, M. 2010 Time resolved measurement of pulsating flow using orifices. *Flow. Meas. Instrum.* **22**, 97–103.

Durst, F., Haddad, K., Al-Salaymeh, A., Eid, S. & Ünsal, B. 2008 Mass flow-rate control unit to calibrate hot-wire sensors. *Exp. Fluids* **44**, 189–197.

Fingerson, L. & Freymuth, P. 1983 Thermal anemometers. *Fluid mechanics measurements* pp. 100–123.

Grenier, P. 1991 Effects of unsteady phenomena on flow metering. *Flow. Meas. Instrum.* **2**, 74–80.

Håkansson, E. & Delsing, J. 1994 Effects of Pulsating Flow on an Ultrasonic Gas Flowmeter. *Flow. Meas. Instrum.* **5**, 93–101.

Hebrard, P., Malard, L. & Strzelecki, A. 1992 Experimental study of a vortex flowmeter in pulsatile flow conditions. *Flow. Meas. Instrum.* **3**, 173–185.

Hultmark, M. & Smits, A. 2010 Temperature corrections for constant temperature and constant current hot-wire anemometers. *Meas. Sci. Technol.* **21**, 105404.

Kanevce, G. & Oka, S. 1973 Correcting hot-wire readings for influence of fluid temperature variations. *DISA Information* pp. 21–24.

King, L. V. 1914 On the convection of heat from small cylinders in a stream of fluid: Determination of the convection constants of small platinum wires with applications to hot-wire anemometry. *Philos. T. Roy. Soc. A.* **214**, 373–432.

Landahl, M. & Mollo-Christensen, E. 1992 Turbulence and random processes in fluid mechanics. *Cambridge University Press*, Cambridge, UK.

Laurantzon, F., Kalpakli, A., Örlü, R. & Alfredsson, P. H. 2010*a* Review on the sensed temperature in cold-wire and hot-wire anemometry. *Tech. Rep. KTH Mechanics*.

Laurantzon, F., Örlü, R., Segalini, A. & Alfredsson, P. H. 2010*b* Time-resolved measurements with a vortex flowmeter in a pulsating turbulent flow using wavelet analysis. *Meas. Sci. Technol.* **21**, 123001.

Marelli, S. & Capobianco, M. 2011 Steady and pulsating flow efficiency of a waste-gated turbocharger radial flow turbine for automotive application. *Energy* **36**, 459–465.

Mottram, R. C. 1992 Introduction: An overview of pulsating flow measurement. *Flow. Meas. Instrum.* **3**, 114–117.

Nabavi, M. & Siddiqui, K. 2010 A critical review on advanced velocity measurement techniques in pulsating flows. *Meas. Sci. Technol.* **21**, 042002.

Olczyk, A. 2008 Problems of unsteady temperature measurements in a pulsating flow of gas. *Meas. Sci. Technol.* **19**, 055402.

Paul, M., Mamun Molla, M. & Roditi, G. 2009 Large-Eddy simulation of pulsatile blood flow. *Med. Eng. Phys.* **31**, 153–159.

Perry, A. E. 1982 Hot-wire anemometry. *Clarendon Press*.

Sonnenberger, R., Graichen, K. & Erk, P. 2000 Fourier averaging: a phase-averaging method for periodic flow. *Exp. Fluids* **28**, 217–224.

Szymko, S. & Martinez-Botas, R. F. 2005 Experimental evaluation of turbocharger turbine performance under pulsating flow conditions. *ASME Turbo Expo* **6**, 1447–1457.

Vetter, G. & Notzon, S. 1994 Effect of Pulsating Flow on Coriolis Mass Flowmeters. *Flow. Meas. Instrum.* **5**, 263–273.

2

Paper 2

Time-resolved measurements with a vortex flowmeter in a pulsating turbulent flow using wavelet analysis

By F. Laurantzon[1], R. Örlü[1,2], A. Segalini[2], and P. H. Alfredsson[1,2]

[1] CICERO, KTH Mechanics, Royal Institute of Technology, SE-100 44 Stockholm, Sweden

[2] Linné Flow Centre, KTH Mechanics, Royal Institute of Technology, SE-100 44 Stockholm, Sweden

Published in *Meas. Sci. Technol.*

Vortex flowmeters are commonly employed in technical applications and are obtainable in a variety of commercially available types. However their robustness and accuracy can easily be impaired by environmental conditions, such as inflow disturbances and/or pulsating conditions. Various post-processing techniques of the vortex signal have been used but all of these methods are so far targeted on obtaining an improved estimate of the time-averaged bulk velocity. Here, on the other hand, we propose, based on wavelet analysis, a straightforward way to utilize the signal from a vortex shedder to extract the time-resolved and thereby the phase-averaged velocity under pulsatile flow conditions. The method was verified with hot-wire and LDV measurements.

1. Background

von Kármán vortex-shedding flowmeters, commonly known as vortex flowmeters, are widely used in pipe lines, automotive and industrial applications for velocity and mass flow measurements of gases, steams and liquids Baker (2005). Since the discovery by Strouhal (1878) that the frequency of the sound emitted by a wire exposed to a wind is linearly proportional to the wind speed itself, and the proposal by Roshko (1954) to expose this feature to measure the flow velocity, the vortex flowmeter has been around for more than half a century Pankanin (2005).

Such devices are nowadays commercially available in a variety of types and are preferred due to their cost-effectiveness and wide range of applicability, like e.g. in wet, contaminated or corrosive flows, and stand out due to their reliability, robustness and flexibility Reik *et al.* (2010). Although vortex flowmeters are widely used in unsteady and turbulent flow situations, as they usually prevail

in technical applications, their performance is principally designed or at least calibrated for steady flow situations. Process conditions Amadi-Echendu *et al.* (1993), environmental vibrations of the system in which the measurements are being performed Miau *et al.* (2000), upstream disturbances Venugopal *et al.* (2010) as well as pulsatile flows Grenier (1991); Al-Asmi & Castro (1992); Hebrard *et al.* (1992), e.g. caused by compressors, pumps or valves, are known to effect the accuracy of these devices Merzkirch (2005).

An example of the problem that arise in pulsating flows is demonstrated in figure 1. In figure 1a) the vortex shedding frequency behind a cylinder in a steady turbulent flow is seen and in figure 1c) the corresponding (premultiplied) spectrum. The clear peak in the spectrum makes the frequency determination unambiguous. However when the flow is pulsating such as in figure 1b) the pulsating frequency shows up strongly in the spectrum, whereas the vortex shedding frequency becomes spread out and does not even overlap with the mean flow frequency (see figure 1d). Despite the fact that the vortex signal is of the same amplitude as the pulsations the amplitude in the spectrum is much smaller.

Nonetheless, the effect of these problems can be reduced or even circumvented by special design Blodgett (1992); Zhang & Huang (2006) and post-processing techniques, in order to generate a sufficiently high and consistent signal-to-noise ratio and an output that is essentially linear over a wide flow rate. Denoising techniques for the signal from the vortex shedder based on wavelet analysis Zhang *et al.* (2004), empirical mode decomposition Sun & Zhang (2009) or Hilbert transformation Hu *et al.* (2002) have been introduced recently, but also neural networks for flow pattern prediction Sun & Zhang (2008) or data-driven filtering routines Rossberg *et al.* (2004*a*,*b*) are proposed as well. Despite these advances in the signal analysis from vortex flowmeters, the general rule of thumb regarding the effect of pulsations on flowmeters, and in particular the vortex flowmeter, has been "if you can't measure it, damp it" Mottram (1992), since pulsations are found to give rise to large deviations in the determined vortex shedding frequency Merzkirch (2005).

2. Motivation and proposed method

The fact that flow pulsations limit and complicate the application of not only vortex flowmeters has lead the community mainly towards problem solutions, that a) either eliminate sources or attenuate the amplitude of pulsation Mottram (1992) or b) apply the aforementioned post-processing techniques to denoise or decompose the signal in order to obtain an unambiguous vortex shedding frequency, f_s, and thereby mean velocity, U. Both of these routes recognize the pulsatile character of the flow as a problem and aim in avoiding or coping with it. An alternative route, which seems—to the authors knowledge—not been taken so far, is to accept the pulsatile character of the flow as the natural state, particularly in internal flows downstream valves, compressors or

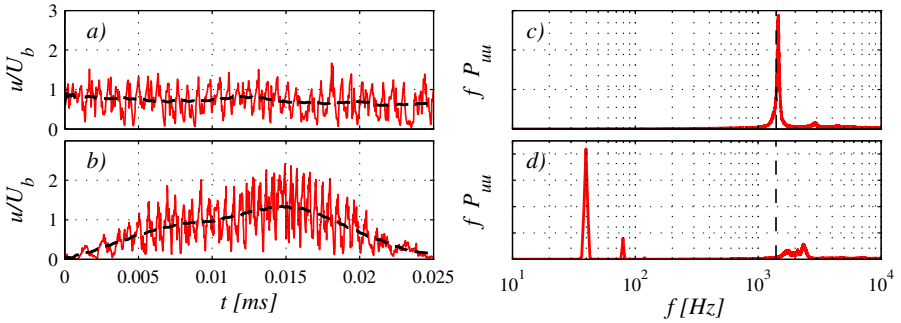

FIGURE 1. Time-series (——) signal and its moving average (- - -) from a hot-wire placed in the wake of a circular cylinder under a) steady and b) pulsatile (f_p = 40 Hz) flow conditions with a flow rate of 25 g/s. Note that the hot-wire placed in the wake measures the local minus the wake deficit velocity, which explains why the moving average is below the bulk velocity, U_b. Corresponding pre-multiplied power-spectral density (——) for the c) steady and d) pulsatile flow with the vortex shedding frequency associated with U_b (- - -). The pre-multiplied form of the power spectrum has been reported, since the vortex shedding frequency under pulsatile conditions would not show up in the usual power spectral density plot.

pumps, and exploit the features of vortex shedding to extract more than just an estimate of the mean velocity.

A phenomenon associated with vortex shedding under forcing or pulsatile flow conditions is vortex-shedding resonance, the so called lock-on phenomenon Detemple-Laake & Eckelmann (1989); Griffin & Hall (1991); Segalini *et al.* (2010). In this lock-on range, the vortex shedding frequency becomes dominated and even controlled by the pulsation frequency, f_p, (or its harmonics), and does not relate to the velocity it is exposed to Grenier (1991); Al-Asmi & Castro (1992); Miau *et al.* (2000), but rather follows f_p. Particularly, vortex shedding can be divided into three regimes Hu *et al.* (2002): 1) quasi-steady, 2) hysteresis and 3) non-interactive vortex shedding, whereas the latter regime comprises the aforementioned lock-on region, the second describes the region in which f_s exhibits a hysteresis with a lower value for f_s under acceleration and a higher frequency under deceleration. The quasi-steady regime, on the other hand, is characterized by the finding that f_s follows the periodically varying flow without phase lag. Based on this finding, the post-processed signal from vortex flowmeters should give correct estimates of U also for pulsatile flows in the quasi-steady regime Mottram & Robati (1986); Peters *et al.* (1998), which

as a role of thumb implies that $f_s/f_p > 4.4$, and still give reasonable results for the hysteresis regime, i.e. $f_s/f_p = 1.6 - 4.4$ Hu *et al.* (2002).

All of the aforementined references, suggest methods to reduce the effect of pulsations or provide advanced signal analysis tools to extract a correct U. Based on the fact that f_s follows the periodically varying flow in the quasi-steady regime without phase lag, the following idea arose: If f_s follows the instantaneous velocity, $u(t)$, without phase lag, then the instantaneous value of f_s is directly related to $u(t)$.

Following the proposed idea, the signal from a vortex flowmeter should carry not only information about U, but also $u(t)$, and could therefore be utilized to compute the phase-averaged velocity $u(\phi)$ or any other single-point statistical quantity. The instantaneous value $f_s(t)$ can be obtained through time-frequency analysis, e.g. via the short-time Fourier-transform (STFT) or wavelet based methods Hlawatsch (2008)for a recent treatment of the topic see e.g.. Through the relation proposed by Strouhal (1878) $f_s(t)$ can directly be converted to $u(t)$, from which $u(\phi)$ can be obtained through phase-averaging. Despite the triviality of the proposed method, it has—to the authors knowledge—not been reported or validated before. The aim of the present paper is therefore to introduce the described method and validate it against other experimental techniques.

3. Experimental facility and measurement techniques

To validate the proposed idea, measurements were conducted in the Laboratory of KTH CICERO (*Centre for Internal Combustion Engine Research Opus*) in a newly developed flow rig that can be used both under steady and pulsatile conditions. For the present study a straight pipe section with a diameter, D, of 38.5 mm and length of 13 D was connected to a rotating valve, as schematically illustrated in figure 2. At the downstream end of the pipe a circular cylinder with a diameter, d, of 2.99 mm, was mounted at the downstream end of the pipe. The cylinder served as the vortex shedder and it spanned the entire cross-section. Experiments were made at two flow rates of 12.5 and 25 g/s and the pulsation frequency was chosen as $f_p = 0$, 20, 40 and 60 Hz. This corresponds to a Reynolds number range of $Re_d \approx 600$ to 12000, which is within the turbulent wake region, in which the Reynolds number dependency of the Strouhal number has become negligible. For details of the CICERO flow rig as well as the pipe set-up the reader is referred to Laurantzon *et al.* (2010) and Kalpakli *et al.* (2010), respectively.

The shedding frequency was measured utilizing a hot-wire probe with a welded 5 micron tungsten wire of 1 mm length, that was operated by means of a *DISA 55M01* main frame with a *55M10* standard CTA channel, and positioned 1 d downstream of the cylinder at the centreline of the pipe. Although the flow under pulsating conditions is non-isothermal, the hot-wire

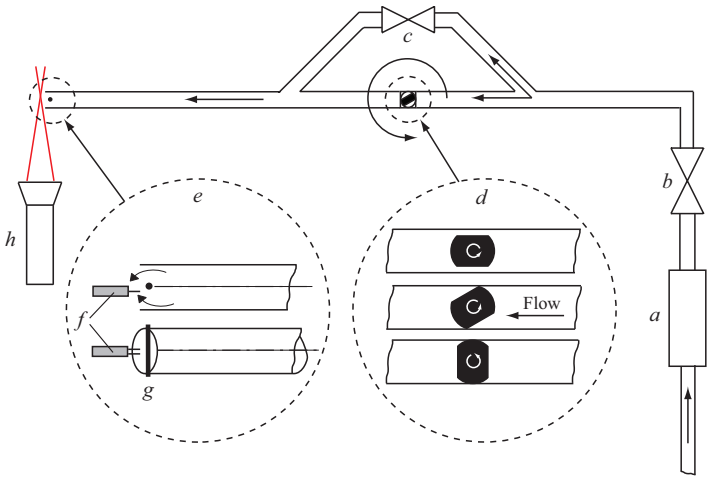

FIGURE 2. Schematic of the pipe section connected to the CICERO flow rig: *a)* Hot-film type ABB mass flow meter, *b)* main valve, *c)* bypass valve, *d)* close-up of the rotating valve, *e)* close-up of the pipe exit region, *f)* hot-wire probe, *g)* circular cylinder serving as vortex shedder, and *h)* LDV head.

readings used to verify the results from the vortex flowmeter were not corrected for pulsatile temperature variations. Previous results Laurantzon *et al.* (2010); Kalpakli *et al.* (2010), however, showed, that these effects were small for the present set-up under the selected operational conditions. To ensure a quantitative reliable validation, also supplementary laser Doppler velocimetry (LDV) measurements have been performed. The LDV system is a single component *DANTEC FlowLite* system comprising a backscatter fibre optics probe, a 400 mm lens and a BSA F/P 60 processor. The source is a He-Ne laser of 10 mW emitting light with a wave length of 632.8 nm. The seeding particles were atomized oil (*Shell Ondina 27*) that was injected at the junction between the rotating valve and the pipe section. The overall mass flow rate was furthermore monitored by a hot-film type ABB mass flowmeter, which is placed 15 m upstream the rotating valve in order to be uninfluenced by the disturbances from the rotating valve. This was done to ensure a correct bulk mean mass flow rate for the comparison of the different runs as well as for the scaling of the presented results by means of the bulk velocity, U_b.

4. Discussion of validation study

The signals from the hot-wire placed within the wake of the cylinder under steady and pulsatile conditions have already been depicted in figure 1 together with their spectral components. While a predominant peak, related to f_s is

clearly discernible in the case of steady flow, the strength of the vortex shedding almost diminishes in the presence of the energy in the pulsatile motion. Only in the pre-multiplied spectrum, which amplifies the high-frequency side, f_s is still apparent. Due to the pulsatile motion, however, which carries the vortex shedding, the determination of f_s and thereby U becomes cumbersome. This becomes particularly apparent from the deviation of the frequency related to the bulk velocity, U_b, obtained from the reference mass flowmeter to the spectral peaks related to the vortex shedding frequency. This problem is treated in many of the cited references in the beginning of this paper, where either the amplitude of f_p is damped, or the pulsatile motion is decomposed from the vortex shedding signal.

Considering now the spectrogram in figure 3(a), computed through a Morlet wavelet, the instantaneous variation of f_s can clearly be observed. Note, that in order to detect the fundamental frequency of the vortex shedding unambiguously, the wavelet transform was applied to $5 \times f_p \leq f \leq 5000$ Hz, i.e. where the lower limit has been indicated through the dashed lines. Thereby the hysteresis and non-interactive vortex shedding regimes have been excluded in the Morlet spectrogram. From figure 3(a) $f_s(t)$ can readily be obtained, which directly relates to $u(t)$, as demonstrated in figure 3(b). Performance of ten phase averages gives already a representative picture of $f(\phi)$ and thereby $u(\phi)$.

To validate the extracted phase-averaged velocity it was compared with results from hot-wire and LDV measurements. The hot-wire probe and LDV

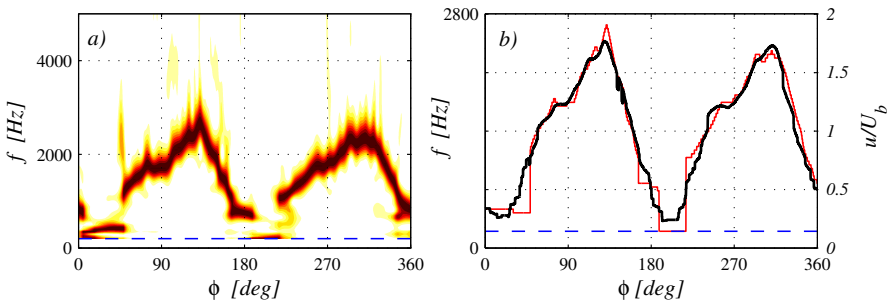

FIGURE 3. a) Morlet spectrogram of the signal shown in Fig 1b). b) Extracted instantaneous vortex shedding frequency (——) and its phase-average (——), together with its directly related velocity. A low frequency and hence low velocity limit (- - -) is set in order to avoid signal ambiguity in conjunction with the harmonics of the pulsation frequency . Note that ϕ is directly related to the time, t, in case of the instantaneous signal.

measurement volume were positioned at the same downstream position as the cylinder, but outside the cylinder wake in between the pipe wall and the cylinder. Previous results Laurantzon *et al.* (2010); Kalpakli *et al.* (2010) in the same pipe set-up have shown, that the pulsatile turbulent pipe flow exhibits a top-hat profile not only in the long-time average, but even throughout the pulsations, which justifies the displacement from the pipe centreline. The results of these three independent measurement techniques are compared in figure 4. The agreement between all three techniques is remarkable and thereby validates the proposed idea to utilize the signal from a vortex flowmeter to resolve the time-varying velocity. Note, that the number of phases used to compute the phase average for the LDV measurement was around 1000, due to the low data rate of tracer particles under pulsatile conditions. For the hot-wire measurements, around 100 averages were performed in order to smooth out the temporally fine resolved hot-wire signal. On the other hand, only 10 averages were performed for the signal from the vortex flowmeter. The number of employed averages does not effect the remarkable agreement observed here, since previous studies in pulsating pipe flows have shown, that phase-averages rather quickly convergence above 10 averages Chandran *et al.* (1979); Kalpakli *et al.* (2010).

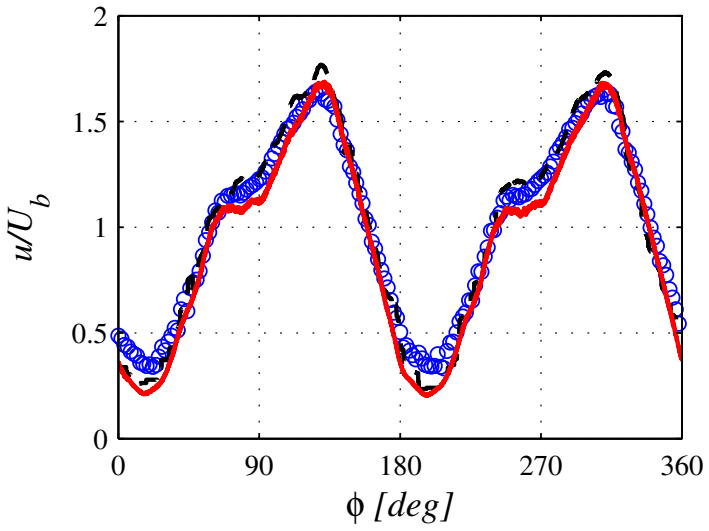

FIGURE 4. Comparison of the phased-averaged signal from the wavelet analysis of the hot-wire vortex flowmeter (- - -) given in figure 3b) with hot-wire (——) and LDV (∘) measurements performed at the same downstream location a quarter pipe diameter radially outwards from the cylinder.

Here we have only shown results for 25 g/s and 0 and 40 Hz, but the agreement between the three measurement techniques for the other performed measurements is similar and we therefore abstain from showing them here. Furthermore, various wavelets as well as STFT methods have been tested, all with quantitative similar results. It was, however, found that the Morlet wavelet gave the best signal-to-noise ratio and thereby reduced demands on the resolution for the wavelet analysis as well as phase averaging operation.

The vortex flowmeter is limited at low velocities, where f_s becomes of the same order as f_p, due to the mentioned lock-in phenomenon, but also through the Reynolds number dependence of the Strouhal number which becomes important below a Reynolds number of the cylinder of around 300 Roshko (1954); Pankanin (2005). This region has been excluded in this study, as illustrated through the dashed lines in figure 3.

5. Conclusions

Vortex flowmeters are employed in a variety of technical applications, and despite the fact that they are designed and calibrated for the operation under steady conditions, they are often exposed to pulsatile flows. The pulsatile character of the flow is known to complicate the computation of the vortex shedding frequency. Therefore a large body of literature has been devoted to suggest practical solution to reduce or avoid the pulsations prior to passing through the vortex flowmeter as well as to the development of advanced signal analysis tools, which enhance the signal-to-noise (whereas noise is here synonymous with pulsation) ratio and separates the vortex shedding phenomenon from the pulsatile motion. All of these techniques aim to provide a more accurate estimate of the mean velocity. Here, on the other hand, we propose a trivial and simple, albeit very useful, method which is based on time-frequency analysis of the raw signal. Hereby, the full information in the signal from the vortex flowmeter is exploited, in order to yield the instantaneous velocity of the pulsatile flow. The method has been tested with experimental data and compared to hot-wire and LDV measurements in a turbulent pulsatile pipe flow. The remarkable agreement between the two reference measurement techniques and the extracted velocity from the time-frequency analysis validates the proposed method.

LDV measurements can not always be performed in industrial applications, due to the need to have optical access to the internal flow and seeding particles, and hot-wires are sensitive to physical properties, e.g. temperature and humidity, which limits their application in compressible turbulent pulsating flows. Therefore, the proposed method to utilize the wavelet analysis to extract the time-resolved velocity from a vortex flowmeter, appears very promising.

Acknowledgements

This research was done within KTH CICERO, a centre supported by the Swedish Energy Agency (STEM), Swedish Vehicle Industry and KTH.

References

Al-Asmi, K. & Castro, I. 1992 Vortex shedding in oscillatory flow: geometrical effects. *Flow. Meas. Instrum.* **3**, 187–202.

Amadi-Echendu, J., Zhu, H. & Higham, E. 1993 Analysis of signals from vortex flowmeters. *Flow. Meas. Instrum.* **4**, 225–231.

Baker, R. 2005 Flow measurement handbook: industrial designs, operating principles, performance, and applications. *Cambridge University Press*, Cambridge, UK.

Blodgett, L. 1992 Theoretical and practical design of pulsation damping systems. *Flow. Meas. Instrum.* **3**, 203–208.

Chandran, K. B., Yearwood, T. L. & Wieting, D. W. 1979 An experimental study of pulsatile flow in a curved tube. *J. Biomech.* **12**, 793–805.

Detemple-Laake, E. & Eckelmann, H. 1989 Phenomenology of Kármán vortex streets in oscillatory flow. *Exp. Fluids* **7**, 217–227.

Grenier, P. 1991 Effects of unsteady phenomena on flow metering. *Flow. Meas. Instrum.* **2**, 74–80.

Griffin, O. M. & Hall, M. S. 1991 Review : vortex shedding lock-on and flow control in bluff body wakes. *J. Fluid Eng.* **113**, 526–537.

Hebrard, P., Malard, L. & Strzelecki, A. 1992 Experimental study of a vortex flowmeter in pulsatile flow conditions. *Flow. Meas. Instrum.* **3**, 173–186.

Hlawatsch, F. 2008 Time-frequency analysis: concepts and methods. *John Wiley & Sons, Inc.*, New Jersey, USA.

Hu, C., Miau, J. & Chou, J. 2002 Instantaneous vortex-shedding behaviour in periodically varying flow. *Proc. R. Soc. Lond. A* **458**, 911–932.

Kalpakli, A., Örlü, R., Tillmark, N. & Alfredsson, P. H. 2010 Experimental investigation on the effect of pulsations on turbulen flow through a 90 degrees pipe bend. *Proc. 3rd Int. Conf. on Jets, Wakes and Separated Flows* .

Laurantzon, F., Tillmark, N. & Alfredsson, P. H. 2010 A pulsating flow rig for analyzing turbocharger performance. *9th Int. Conf. on Turbocharging and Turbochargers* pp. 363–372.

Merzkirch, W. 2005 Fluid mechanics of flow metering. *Springer-Verlag.*, Berlin, Germany.

Miau, J., Hu, C. & Chou, J. 2000 Response of a vortex flowmeter to impulsive vibrations. *Flow. Meas. Instrum.* **11**, 41–49.

Mottram, R. C. 1992 Introduction: An overview of pulsating flow measurement. *Flow. Meas. Instrum.* **3**, 114–117.

Mottram, R. C. & Robati, B. 1986 Comparison of pulsation of effects on vortex and orifice flowmeter. *Fluid Control and Measurement. Pergamon* **2**, 957963.

Pankanin, G. 2005 The vortex flowmeter: various methods of investigating phenomena. *Meas. Sci. Technol.* **16**, R1–R16.

Peters, M. C. A. M., Van Bokhorst, E. & Limpens, C. H. L. 1998 Impact of pulsations on vortex flowmeter. *Proc. 9th Int. Conf. on Flow Measurement.*, pp. 185–190.

Reik, M., Höcker, R., Bruzzese, C., Hollmach, M., Koudal, O., Schenkel, T. & Oertel, H. 2010 Flow rate measurement in a pipe flow by vortex shedding. *Forsch. Ingenieurwes.* **74**, 77–86.

Roshko, A. 1954 On the development of turbulent wakes from vortex streets. *NACA Tech. Note 2913* .

Rossberg, A., Bartholomé, K. & Timmer, J. 2004*a* Data-driven optimal filtering for phase and frequency of noisy oscillations: Application to vortex flow metering. *Phys. Rev. E* **69**, 16216.

Rossberg, A., Riegler, P., Buhl, F., Herwig, J. & Timmer, J. 2004*b* Detection of improper installation from the sensor signal of vortex flowmeters. *Flow. Meas. Instrum.* **15**, 29–35.

Segalini, A., Örlü, R., Alfredsson, P. H. & Talamelli, A. 2010 Experimental study on the use of the wake instability as a passive control in coaxial jet flows. *Seventh IUTAM Symposium on Laminar-Turbulent Transition* pp. 361–366.

Strouhal, V. 1878 Über eine besondere Art der Tonerregung. *Ann. Phys.* **241**, 216–251.

Sun, Z. & Zhang, H. 2008 Neural networks approach for prediction of gas–liquid two-phase flow pattern based on frequency domain analysis of vortex flowmeter signals. *Meas. Sci. Technol.* **19**, 015401.

Sun, Z. & Zhang, H. 2009 Application of empirical mode decomposition based energy ratio to vortex flowmeter state diagnosis. *J. Cent. South Univ. Technol.* **16**, 154–159.

Venugopal, A., Agrawal, A. & Prabhu, S. 2010 Influence of blockage and upstream disturbances on the performance of a vortex flowmeter with a trapezoidal bluff body. *MEASUREMENT* **43**, 603–616.

Zhang, H. & Huang, Y. 2006 A study of mass flow rate measurement based on the vortex shedding principle. *Flow. Meas. Instrum.* **17**, 29–38.

Zhang, T., Sun, H. & Wu, P. 2004 Wavelet denoising applied to vortex flowmeters. *Flow. Meas. Instrum.* **15**, 325–329.

3

Paper 3

Experimental analysis of turbocharger interaction with a pulsatile flow through time-resolved flow measurements upstream and downstream the turbine

By Fredrik Laurantzon, Ramis Örlü, Antonio Segalini, Nils Tillmark & P. Henrik Alfredsson

KTH Mechanics, SE-100 44 Stockholm, Sweden

IMECHE CONF TRANS (In Print) 2012

The inflow to and outflow from turbochargers are highly complex and, in particular, pulsating. Nevertheless, most studies of turbocharger performance are conducted under steady conditions. Hence, there is a great interest in determining and under-standing turbocharger performance maps under pulsatile conditions. The highly complex flow field constitutes a challenge for time-resolved flow measurements by means of conventional measurement techniques. In a recent paper by Laurantzon et al [Meas. Sci. Technol. **20** 123001 (2010)], time-resolved bulk flow measure-ments under pulsatile conditions have been obtained via wavelet analysis of the signal from a vortex flow meter. Here, this method has been used in order to obtain time-resolved performance maps based on the mass flow both upstream and down-stream of the turbine. The results show that the turbine has a large damping effect on the mass flow pulsations, but that the pulse shape is to a high degree preserved while passing through the turbine, and that the time-dependent filling and emptying of the turbine case make the quasi-steady assumption invalid, if the whole turbine stage is considered.

1. Introduction

At KTH CCGEx, Competence Centre for Gas Exchange, KTH works together with vehicle industry in Sweden within the area of gas management of internal combus-tion engines, where turbo charging is a focal point. Essential in this respect are turbocharger performance maps, which in most cases are obtained under steady conditions. The inflow to and outflow from turbochargers, on the other hand, are highly complex and, in particular, pulsating, see e.g. Capobianco *et al.* (1989); Baines (2010). Hence, there is a great interest to understand how turbocharger performance maps behave under pulsatile conditions. The highly complex flow field, including high speeds, back flow, strong

secondary flows, non-isothermal conditions, strong and rapid pulsations etc. constitutes a challenge for time-resolved flow measurements.

While commonly employed measurement techniques such as thermocouples and Pitot-tubes do not even guarantee a correct time-averaged reading under pulsating conditions, hot-wires provide time-resolved mass-flux readings (see review in Laurantzon (2010)). Thermal anemometry techniques also need time-resolved temperature measurements, due to the necessity of temperature compensation. Time-resolved temperature measurements in the context of typical engine pulsating frequencies are not possible with standard thermocouples, but cold-wire anemometry may give the frequency response needed. However, cold-wires are impractical due to their fragility, see e.g. Capobianco (2006). The highly inhomogeneous flow field also necessitates several measurement points across the flow in order to obtain a good estimate of the averaged mass flow rate. In a recent paper by Laurantzon *et al.* (2010*a*), time-resolved bulk flow measurements under pulsatile conditions were obtained via time-frequency analysis using wavelet analysis of the signal from a vortex flow meter. The advantage of this method is that neither velocity calibration, nor temperature compensation are needed, thereby constituting an optimal technique for the purpose of the present work. Furthermore, as shown in Laurantzon *et al.* (2010*a*) the utilization of this technique directly provides an estimate of the time-resolved bulk velocity from a single point measurement, thereby qualifying the technique in particular for the inhomogeneous and non-isothermal flow upstream and downstream of a turbine.

For a long time many authors have debated the use of steady state turbocharger maps, i.e. maps obtained without inflow pulsations, since this would imply that the flow through the turbine is quasi-steady. However, the unsteady flow through the turbine due to pulsations is close to quasi-steady for low pulse frequencies, e.g. Costall *et al.* (2005), and the rotation rate of the impeller of the turbine is fairly constant during the pulsating cycle due to high angular momentum of the turbine-compressor combination. However the filling and emptying of the volute is highly unsteady giving rise to a failure of the quasi-steady model, see for instance Aymanns *et al.* (2012). Hence, the turbine overall characteristics will be dominated by the transient behavior of the gas in the volute. This complex problem remains a challenge, especially for engine simulations, but also for turbine design.

Within the CICERO laboratory at KTH CCGEx, a pulsatile flow rig has been developed and has recently been used to investigate the effect of pulsations on the flow field upstream and downstream a turbine and thereby assess the turbine performance under pulsatile conditions, Laurantzon *et al.* (2010*b*). In the present paper, the vortex flow meter has been utilized in order to obtain turbocharger performance maps under pulsatile conditions. In particular the effects of mass flow rate and pulsation frequency have been investigated. Results indicate that the pulse shape of the mass flow rate signal to a high degree

is preserved, albeit damped, while passing through the turbine. Furthermore, the expected time-dependent mass storage in the turbine housing is confirmed and analyzed.

The paper is organized as follows. In Section 2 a description of the flow rig design including the utilized instrumentation is given, while Section 3 outlines the employed time-resolved mass flow rate measurement technique by means of wavelet analysis. Section 4, presents the results in terms of pulsation frequency and flow rate, whereas conclusions and plans for future work are given in Section 5.

2. Experimental set-up

The flow rig is supplied with dried compressed air through a pipe system from compressors and tanks stored away from the laboratory. The mass flow rate is accurately measured by a hot film flow meter connected to the laboratory inlet line. In the laboratory, upstream the flow rig, the air passes an electric heater (2 in Fig. 1) increasing the gas temperature to avoid it from dropping below the dew point downstream the turbine (5 in Fig. 1). To obtain pulsating flow a valve that can be rotated to give a time varying open area (3 in Fig. 1) is connected to the line downstream the heater. The valve consists of a ball, planed on two opposite sides along the axis of rotation, and tightly fitted into a circular pipe. A frequency controlled AC motor rotates the ball causing the valve to open twice per revolution (see detail in Fig. 1). To be able to vary the pulse modulation degree of the turbine inlet flow, the ball valve is connected in parallel with a single pipe with a control valve (4 in Fig. 1). The turbine is connected through a 1 m long straight pipe to the pulse generator.

To resolve the large temporal flow variations the sensors mounted upstream and downstream of the turbine have a high frequency response, a feature not necessary in the compressor line where the flow is almost steady. The pressures in the turbine line were measured with piezo-resistive pressure transducers, whereas the pressure transducers in the compressor line were of differential membrane type.

The time varying recovery temperatures were measured with cold-wires (made of tungsten with a diameter of 5 micron) connected to a Dantec Streamline anemometer. For the flow speeds used here the recovery temperature is close to the stag-nation temperature. Two sensors were used, one positioned upstream and one downstream the turbine. The calibration of the cold-wires was done in-situ at low speed by means of thermocouples. On the compressor side thermocouples were used to measure the temperature.

The unsteady inlet and outlet turbine flow velocities were obtained by vortex shedding flow meters, which will be described in some detail in Section 3. The flow up-stream of the turbine is fairly uniform and without swirl,

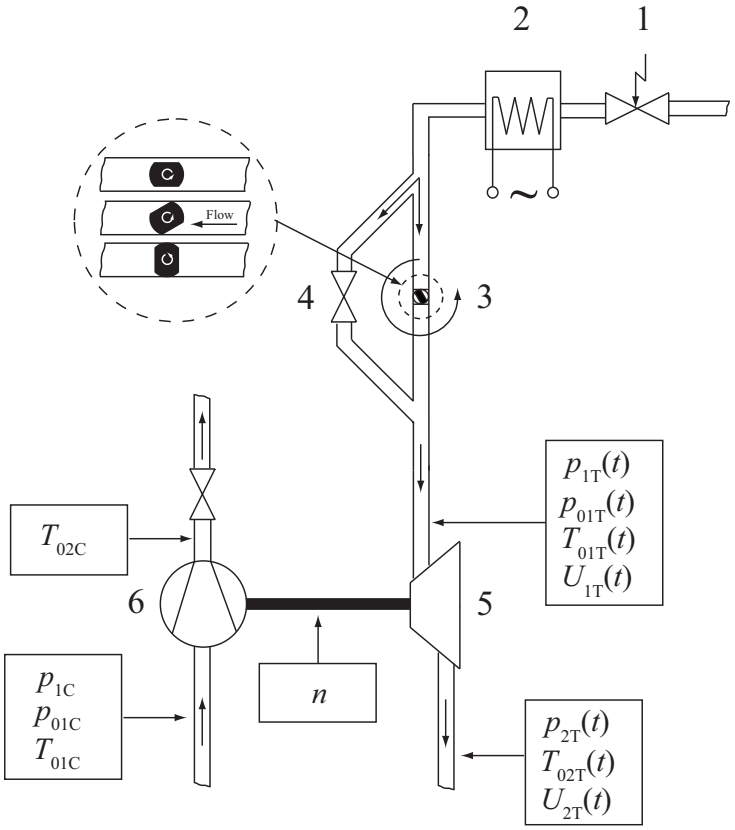

FIGURE 1. Schematic representation of the CICERO flow rig system and its instrumentation. 1. Inlet regulator valve, 2. Electric heater, 3. Pulse generator, 4. By-pass line, 5. Turbine, 6. Compressor.

whereas the swirl on the downstream side is substantial and has to be suppressed through a honeycomb section, in order to obtain a reliable output from the vortex meter.

The sampling of the various transducer signals was done phase-locked with respect to the angular position of the ball valve. Typical sampling time was 20 seconds for all measured quantities with a sampling frequency of 15.6 kHz.

3. Time resolved measurements with a vortex shedder flow meter

Vortex shedding flow meters are based on the detection of vortices shed periodically from a body. Here a circular cylinder located along a diameter of the pipe was used as the shedding element. The circular cylinder generates a flow pattern known as the von Karman vortex street and experimental evidences Norberg (1994); Fey *et al.* (1998) show that the shedding frequency scales with the flow velocity and the cylinder diameter. The non-dimensional frequency $St = fd/U$ (also called Strouhal number) is approximately constant (≈ 0.20), although there is a small Reynolds number dependence. The shedding frequency f has been shown to be proportional to a velocity close to the bulk velocity U, for a given cylinder with diameter d, see Laurantzon *et al.* (2010*a*). This measurement technique has been developed in our laboratory in order to obtain time re-solved flow measurements in pulsating flows. One condition that has to be fulfilled is that the pulsating frequency f_p is sufficiently low relative to the vortex shedding frequency f, so that there is a clear distinction between them. A general rule of thumb to avoid signal ambiguity is to let $f/f_p > 4.4$ Mottram & Robati (1986); Peters *et al.* (1998), see also the discussion in Laurantzon *et al.* (2010*a*). By choosing a suitable diameter of the cylinder it is usually possible to obtain such a scale separation. The vortex shedding frequency is detected by means of hot-wire anemometry and wavelet analysis described below is used to obtain the instantaneous frequency.

There are two major advantages with this technique as compared to direct measurement of velocity with hot-wire anemometry; namely that here the hot-wire does not need to be calibrated since the hot-wire is only used to detect the shedding frequency. Moreover, the measured quantity has been found to be close to the bulk velocity see Laurantzon *et al.* (2010*a*). In order to get the instantaneous mass flux also the density needs to be determined, which is obtained by using the gas law with the measured time resolved pressure and temperature. A schematic design of the meter is depicted in Figure 2. For unidirectional flow the shedding occurs downstream the cylinder and only hot-wire 2 is used. However, if reversed flow occurs, the upstream hot-wire will detect the flow velocity variation during the flow reversal. This design is thus suitable for pulsating flow, where quite large back flow rates may occur.

If the bulk velocity $U(t)$, is time dependent, the vortex shedding frequency is frequency modulated by the variation in flow rate. The instantaneous frequency can-not be obtained with classical Fourier analysis and instead the wavelet technique has been used as a straightforward way to find the time varying frequency. A continuous wavelet transform of a function $u(t)$ is defined through a convolution with a wavelet function $\psi(t)$

$$\tilde{u}(\tau, a) = \int_{-\infty}^{\infty} \left[u(t) \frac{1}{\sqrt{a}} \psi^*\left(\frac{t-\tau}{a}\right) \right] dt \tag{1}$$

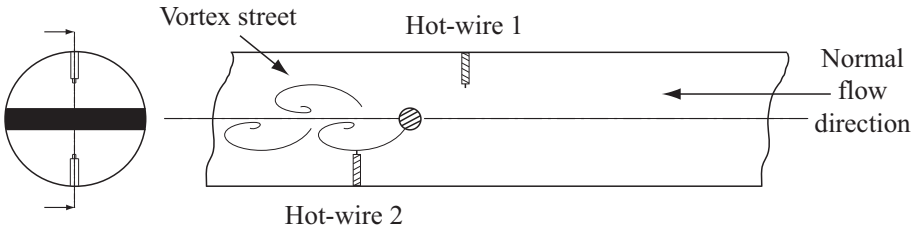

FIGURE 2. Schematic of a pipe section with the vortex shedding flow meter.

The schematic design of the meter is depicted in Fig. 2. For uni-directional flow the shedding will occur downstream the cylinder and only hot-wire 2 is used. However, if reversed flow occurs, the upstream hot-wire will detect the flow velocity variation during the flow reversal. This design is thus suitable for pulsating flow, where quite large back flow rates may occur.

In a sense, the wavelet transform can be viewed as the correlation of the function $u(t)$ with the complex conjugate of the wavelet function $\psi(t)$ shifted and dilated in time through the parameters a and τ. Thus, the stronger the resemblance of the function $u(t)$ with $\psi[(t-\tau)/a]$, the larger the magnitude of the wavelet coefficient. The time shift τ defines the window middle-point, while the scale a defines the width of the observed signal and is related to the instantaneous frequency $f(t)$ through the relationship $f(t)a = K$ where K is a proportionality constant which depends on the chosen wavelet. More details about the wavelet transform properties can be found in specialized textbooks such as Hlawatsch (2008).

The analysis can be summarized by means of Fig. 3, see also Laurantzon *et al.* (2010*a*). This case shows pulsating flow at a pulse frequency of $f_p = 80$ Hz. In Fig. 3(a) the time signal for the anemometer output voltage for two periods is shown. The pre-multiplied power spectral density (PSD) can be seen in Fig. 3(b); showing the large energy content at the pulse frequency f_p, and some at its harmonics. Another aggregation of energy starts at about $50f_p$, which is related to the vortex shedding of the cylinder. Since the PSD does not give more information than just the frequency range where most of the energy is concentrated, other evaluation methods have to be employed. In Fig. 3(c) the so-called wavelet spectrogram for the signal is illustrated. From this the time varying frequency of the vortex shedding can be extracted to give $f(t)$ and hence $U(t)$ as shown in Fig. 3(d). The example shown below is just for two periods, but if the entire time series is considered, a phase average can be obtained from the individual periods, as in Fig. 3(d). Noteworthy is that for this test case there was no backflow and the lowest velocity corresponded

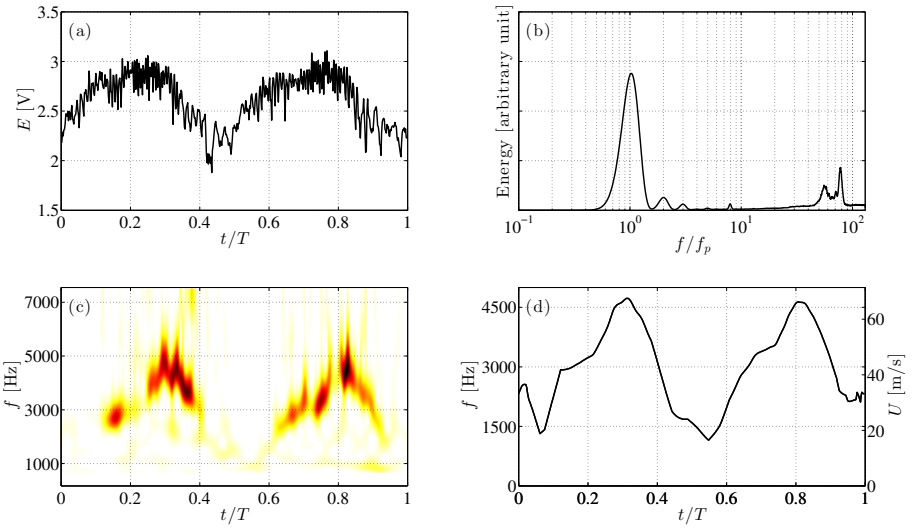

FIGURE 3. The evaluation of the signal from the vortex shedding flow meter. (a) Time signal. (b) PSD of the time signal. (c) Wavelet spectrogram. (d) The extracted time resolved frequency.

to a shedding frequency at approximately $25f_p$, hence there was no ambiguity between the pulse and shedding frequencies.

4. Results

In this section, results from both steady and pulsating turbine measurements will be demonstrated. Specifically the effect of phase shifting the signals will be shown. Typically the data is phase averaged for 400 pulse cycles. Furthermore, all phase averaged data will be presented with two pulses i.e. corresponding to a full revolution of the pulse generator.

There is a certain distance between the locations of the upstream and downstream sensors, and this gives rise to a time lag between the phases for the respective quantities under pulsating flow. This time lag should equal the time it takes for the disturbance pulse to travel between the two stations i.e.

$$\tau_0 = \frac{\Delta x}{a + u} \tag{2}$$

where Δx is the path length between the stations, u is the average velocity along the path and a the speed of sound which has been estimated as $a \approx 20T^{1/2}$ (where T is the mean temperature in Kelvin). However, there exist several problems involved in this method to find the time lag τ_0. Firstly, the distance

Δx cannot be unequivocally defined through the turbine without more detailed measurements of the path lines in the space between the two sensors, secondly both u and a will vary in both space and time. Hence, instead we determined τ_0 from the peak in the cross correlation between the same quantities, e.g. between the static pressure upstream and downstream the turbine

$$\phi(\tau) = \lim_{T\to\infty} \frac{1}{T} \int_{-T/2}^{T/2} p_1(t)p_2(\tau + t)dt \tag{3}$$

It should however be emphasized that it is important to do the correlation between the same quantities, since for instance velocity and pressure in one point in a flow field are in general out of phase in unsteady flow.

Despite the uncertainty related to employing Eq. (2), it can be used as a check for the order of magnitude of the cross correlation. For the tested flow cases, the local velocity was small compared to the speed of sound (roughly $0.15a$ at most for this study), moreover the path travelled in the turbine was a small fraction compared to the rest of the piping system, between the sensors. An approximate delay can be obtained by using the time average of u and a, and by approximating the axial distance travelled through the turbine with some characteristic length scale of the turbine e.g. the distance from the inlet to the outlet. The time lag obtained from the cross correlation, Eq. (3) is approximately 4.5 ms for all cases reported, which corresponds fairly well to the time lag estimated with Eq. (2). Note that this time lag will vary depending on the flow case, i.e. the pulsating frequency and the mean flow rate, and is to a high degree governed by the speed of sound a. But since the temperature variations were moderate, the time lag did not change considerably from case to case. In addition to this phase shift an adjustment for the different sensor locations upstream the turbine was done. The time lag between two instruments located downstream the turbine was negligible and all the upstream measured quantities were related to the same reference plane, namely the location for the upstream stagnation pressure sensor.

4.1. *Effects of pulsation frequency*

In Fig. 4, the mass flow downstream the turbine $\dot{m}_2$, is shown vs. the mass flow upstream $\dot{m}_1$. Both the time dependent variation during the pulse cycle, which shows a closed loop, and the mean values (shown as a filled circle in Fig. 4) are shown. In Fig. 4(a), the directly measured values are shown, i.e. without any phase shifting. The values of the mean mass flow rates at the upstream and down-stream sides are similar and also close to the value of the system mass flow meter (105 g/s) which gives confidence in the flow measuring technique. One can also observe that the pulsation amplitude is heavily damped downstream the turbine. The phase shifted flow rates are plotted in Fig. 4(b); and for this case the relation between the flow rates is close to a straight line. To further estimate the similarity between any two upstream and downstream quantities,

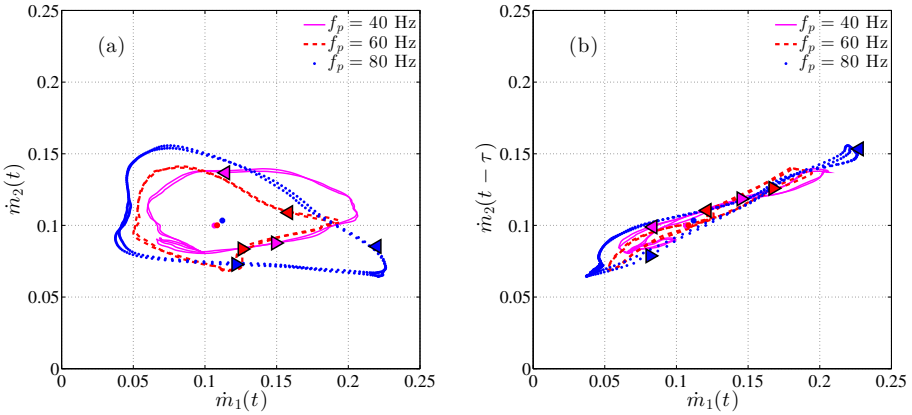

FIGURE 4. Outlet mass flow as function of inlet mass flow. (a) Directly measured values. (b) Outlet mass flow phase shifted to correlate with inlet mass flow. Mean mass flow rate 105 g/s, at f_p 40 Hz (solid), 60 Hz (dashed) and 80 Hz (dotted) pulse frequency. The circles show mean values and arrows indicate loop path.

the correlation coefficient can be used. The correlation coefficient between two fluctuating signals u_1 and u_2, is defined as

$$r_{u_1 u_2} = \frac{\Sigma u_{1i}^{'} u_{2i}^{'}}{\sqrt{\Sigma (u_{1i}^{'})^2 \Sigma (u_{2i}^{'})^2}} \tag{4}$$

where prime denotes the fluctuating part of the signal. The coefficient for $\dot{m}_1$ and $\dot{m}_2$, was for all cases greater than 0.95, where a coefficient of 1 in Fig. 4 means perfect correlation. Hence, although damped with more than a factor of two, the pulse shape was to a large degree preserved.

Fig. 5 shows the turbine map for the three different pulse frequencies, where the upper row is the unaltered values and the lower row shows the phase shifted ones. As a comparison four points from steady flow measurements are plotted together and a polynomial of second degree is applied for visual aid. Here we see that the steady points are close to the mean as obtained from the pulsating flow case for all frequencies. As pointed out in Baines (2010), the quasi-steady assumption is usually made in the zero and simple one-dimensional models. However as shown in Fig. 5, the area spanned during the pulse cycle, sometimes called the hysteresis area, is just slightly decreased when phase shifting is applied, which indicates that the quasi-steady assumption is invalid for the flow through the turbine. Further, as can be seen in Fig. 5, the loop path upstream the turbine is clockwise, whereas it is counter clockwise

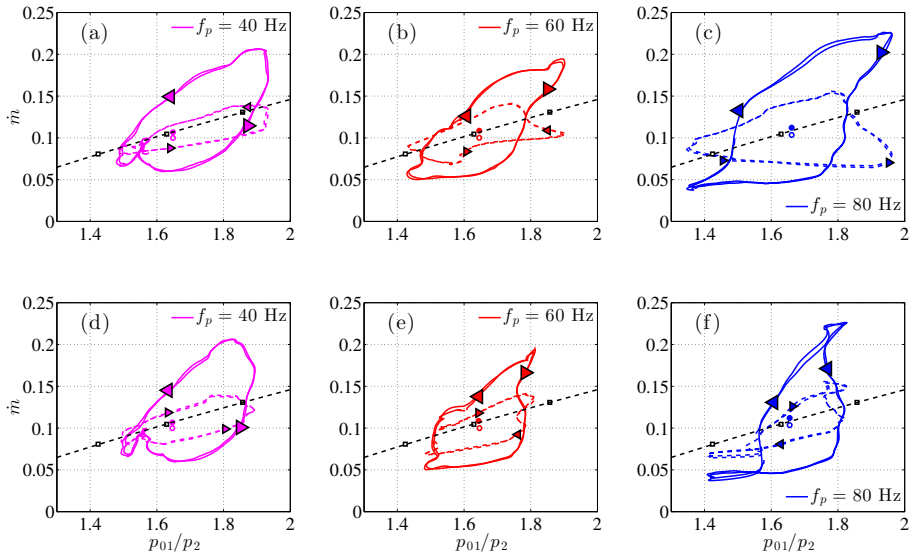

FIGURE 5. Turbine map at a mean mass flow rate 105 g/s, at different pulse frequencies. The upper row plots are instantaneous, the lower row plots are phase shifted. Upstream flow (solid line) and downstream flow (dashed line). Black dashed line is obtained from steady flow measurements. Full and open circles show mean value for upstream and downstream flow respectively. Arrows indicate loop path.

downstream the turbine. The reason for this is illustrated by means of Fig. 6, which shows the flow case in Fig. 5(a). Here, the acceleration and retardation phases are marked for a given expansion ratio. If one considers the upstream flow rate, it is clear that it is higher at the acceleration phase as com-pared to the retardation phase. Thus, the hysteresis path must be clockwise for the upstream mass flow and vice versa applies for the downstream mass flow.

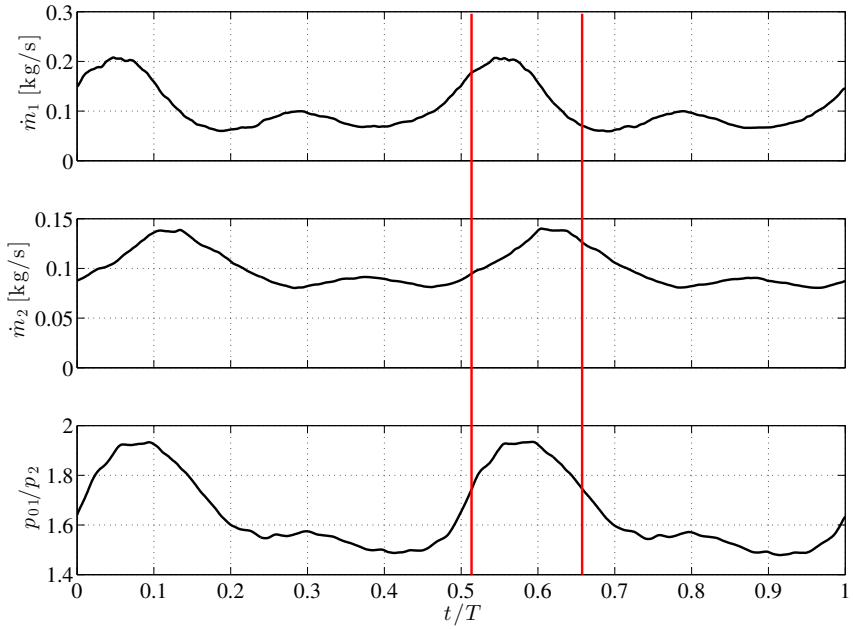

FIGURE 6. Phase averaged data for one period (flow case from Fig. 5(a)). Mass flow rate upstream turbine (upper), mass flow rate downstream turbine (middle) and expansion ratio (lower). The two vertical lines are for visual aid and shows acceleration and retardation phase respectively at the same expansion ratio.

4.2. *Effects of flow rate*

Figs. 7 and 8 shows the same quantities as in Figs. 4 and 5 respectively, although here the pulse frequency is instead held constant whereas four different flow rates are shown. In Fig. 7(a), the relation between the measured mass flow rates upstream and downstream the turbine are shown and as expected the mass flow variation during the pulse cycle increases for increasing flow rate. In Fig. 7(b) phase shifting is applied for maximum correlation between the upstream and down-stream side and now it is clear that the in and out flow follow each other, although the outflow amplitude is damped with about a factor of two. In Figs. 7(c) and 7(d) the flow rates are normalized with the average flow rate and it is clearly seen that in this format the curves more or less overlap, hence the behaviour is independent of the flow rate in this flow range. Finally, in Fig. 8, the turbo map for these different flow rates are plotted

together. In Fig. 8(a) the maps are plotted without any time shift whereas in Fig. 8(b) all data are shifted to correlate with p_{01}. There is no large difference between the maps on the upstream side between Fig. 8(a) and (b), since the upstream mass flow rate and p_{01} are measured almost at the same position, whereas the map using the downstream mass flow changes significantly. The steady response is plotted as the dotted line and can be compared with the mean values obtained from the pulsating flow given as symbols. As can be seen the steady points agree well with the mean of the pulsating flow. In Figs 8 (c) and (d) the same data are plotted but normalized with the mean pressure ratios and mass flow rates, respectively, showing that the path followed in the turbine map is fairly independent of the flow rate.

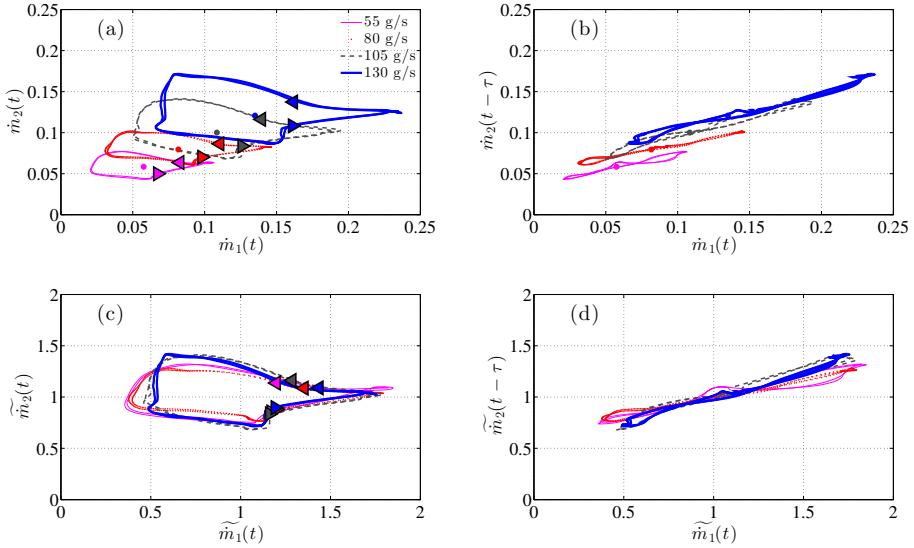

FIGURE 7. Different flow rates at 60 Hz pulse frequency. The average flow rates are 55 g/s (solid thin), 80 g/s (dotted), 105 g/s (dashed) and 130 g/s (solid thick). (a) Instantaneous. (b) Shifted. (c) Instantaneous normalized with time average. (d) Shifted normalized with time average.

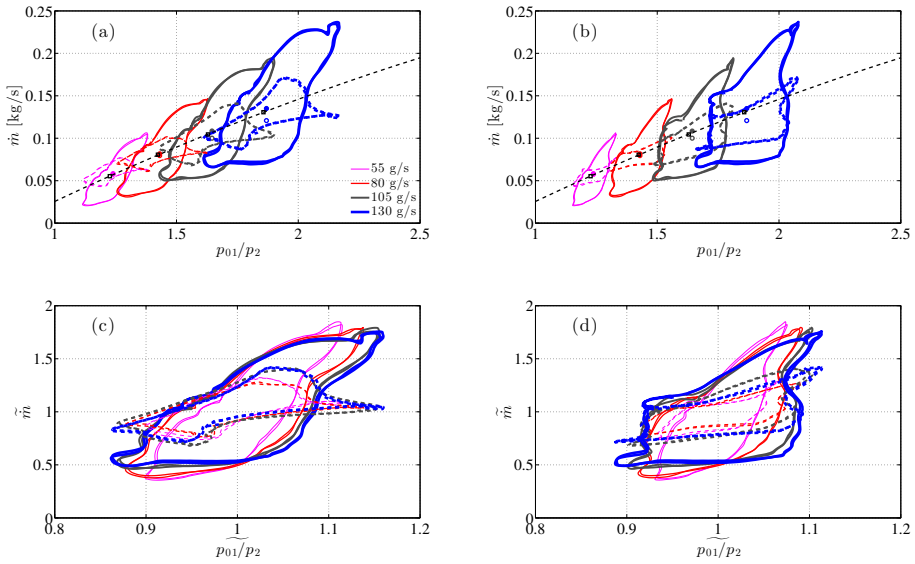

FIGURE 8. Turbine map at mean mass flow rate 55 g/s, 80 g/s, 105 g/s and 130 g/s (increasing line thickness), at 60 Hz pulse frequency. Solid line is upstream flow, dashed line is downstream flow. Black dashed line is turbine map from steady measurements. (a) Instantaneous. (b) Phase shifted, (c) and (d) same as (a) and (b) but normalized with mean values.

5. Conclusions and future work

In the present work, time resolved measurements of pressure, temperature and velocity were obtained both upstream and downstream a turbine of a turbocharger. A newly developed mass flow meter based on wavelet analysis of the vortex shedding behind a cylinder is shown to be able to accurately describe the pulsating mass flow rate.

In this work it is demonstrated that the pulse shape to a high degree is preserved after passing the turbine. Although the characteristic looping curves dominate in the pulsating flow case, the time averaged value agrees fairly well with the corresponding steady flow points.

The mass flow rate and expansion ratio were phase shifted in order to test the quasi-steadiness of the flow through the turbine, however even for the shifted values the hysteresis plots in the turbine map is not a single valued function, as would be expected if the flow is quasi-steady. Thus, the study

confirms that the time dependent mass storage in the turbine case makes the quasi-steady assumption invalid, at least for the turbine as a whole.

The present data form a unique experimental database of the flow through a turbine that can be used for checking present and future turbine models.

Acknowledgements

This work has been carried out within KTH CCGEx. Kim Karlström and Göran Rådberg are acknowledged for their skillful work in setting up the flow rig.

References

Aymanns, R., Scharf, J., Uhlmann, T. & Lückmann, D. 2012 A Revision of Quasi Steady Modelling of Turbocharger Turbines in the Simulation of Pulse Charged Engines *16th Supercharging Conf., Dresden*.

Baines, N. 2010 Turbocharger turbine pulse flow performance and modelling – 25 years on. *9th Int. Conf. on Turbochargers and Turbocharging, London, ImechE* pp. 347–362.

Marelli, S. & Capobianco, M. 2006 Turbocharger turbine performance under steady and unsteady flow: test bed analysis and correlation criteria *8th Int. Conf. on Turbochargers and Turbocharging, London, IMechE*, pp. 373-385.

Capobianco, M., Gambarotta, A. & Cipolla, G. 1989 Influence of the pulsating flow operation on the turbine characteristics of a small internal combustion engine turbocharger. *Proc. 2nd Int. Conf. on Turbochargers and Turbocharging, London, IMechE*, pp. 63-70.

Costall, A., Szymko, S., Martinez-Botas, R. F., Filsinger, D. & Ninkovic, D. 2005 Assessment of Unsteady Behaviour in Turbocharger Turbines. *ASME Turbo Expo 2006* **6**, 1023–1038.

Fey, U., Konig, M. & Eckelmann, H. 1998 A new Strouhal-Reynolds-number relationship for the circular cylinder in the range $47 < \mathrm{Re} < 2 \times 10^5$. *Phys. Fluids* **10**, 1547–1549.

Hlawatsch, F. 2008 Time-frequency analysis: concepts and methods. *John Wiley & Sons, Inc.*, New Jersey, USA.

Laurantzon, F. 2010 Flow Measuring Techniques in Steady and Pulsating Compressible Flows. *Licentiate thesis, KTH Mechanics, TRITA-MEK 2010:09, ISBN 978-91-7415-824-3*.

Laurantzon, F., Örlü, R., Segalini, A. & Alfredsson, P. H. 2010*a* Time-resolved measurements with a vortex flowmeter in a pulsating turbulent flow using wavelet analysis. *Meas. Sci. Technol.* **21**, 123001.

Laurantzon, F., Tillmark, N. & Alfredsson, P. H. 2010*b* A pulsating flow rig for analyzing turbocharger performance. *9th Int. Conf. on Turbochargers and Turbocharging, London, IMechE* pp. 363–372.

Mottram, R. C. & Robati, B. 1986 *Comparison of pulsation of effects on vortex and orifice flowmeter*. Fluid Control and Measurement.

Norberg, C. 1994 An Experimental Investigation of the Flow Around a Circular-Cylinder - Influence of Aspect Ratio. *J. Fluid Mech* **258**, 287–316.

Peters, M. C. A. M., Van Bokhorst, E. & Limpens, C. H. L. 1998 Impact of pulsations on vortex flowmeter. *Proc. 9th Int. Conf. on Flow Measurement.*

Paper 4

4

Vortex shedding flow meters: accuracy assessment and extension towards industrial configurations

By
F. Laurantzon[1], A. Segalini[2], S. Reifarth[3], R. Örlü[1,2] and P. H. Alfredsson[1,2]

[1] CCGEx, KTH Mechanics, Royal Institute of Technology,
[2] Linné Flow Centre, KTH Mechanics, Royal Institute of Technology
[3] CCGEx, KTH Machine Design, Royal Institute of Technology,
SE-100 44 Stockholm, Sweden

Submitted

Experiments under different inflow conditions in pipes have been performed in order to assess the potential of a new generation of cylindrical vortex flow meters able to characterize the instantaneous bulk velocity in highly turbulent environments. The shedding frequency is sensed by a hot-wire downstream of the cylinder and is evaluated by using wavelets in case of pulsating flows as recently proposed by Laurantzon et al [Meas Sci Technol (2010), **21**:123001]. The optimal sensor position downstream the cylinder and along its axis has been investigated with fully developed inflow conditions and practical indications on the positioning are provided. The accuracy of the velocity estimation is around ±5% for a generic inflow but it can be improved significantly by focussing on a specific configuration. The use of a microphone as an alternative to a hot-wire to sense the shedding frequency has also been attempted with success under steady and pulsating conditions, to extend the usefulness of the technique to more harsh industrial applications.

---

1. Introduction

When a two-dimensional bluff body is immersed in a flow, vortices of opposite circulation will form in the wake behind the body. For steady flow these vortices are shed with an alternate pattern at a regular frequency. The intimate relationship between the shedding frequency, f_{VS}, and the upstream velocity, U, was deduced by Strouhal (1878) and can be expressed by means of the dimensionless frequency (the so called Strouhal number)

$$\mathrm{St} = f_{VS} d/U, \tag{1}$$

where d is usually taken as the cross section length scale. By looking at the functional dependence of the shedding frequency it can be demonstrated that the Strouhal number is primarily a function of Reynolds number, Re, and of the characteristic shape of the vortex shedder. However, when the flow is confined by solid walls the vortex shedding phenomenon is altered and new geometrical parameters will enter the analysis, such as the blockage ratio d/D, where D is the hydraulic diameter of the confining wall.

An attractive feature of vortex shedding flow meters is that the Strouhal number usually is expected to be fairly constant for a large range of Reynolds numbers. As an example, for a circular cylinder St ≈ 0.21 in the turbulent wake Re regime, namely within $200 < \mathrm{Re}_d < 1 \times 10^5$, (see reference Reik *et al.* (2010)). The constant St (or its weak Re dependence) property has important practical implications, first of all that the shedding frequency is approximately proportional to the oncoming velocity. Assuming that confinements have no effects on the Reynolds number dependence of the vortex shedding frequency, it is natural to use this property to measure indirectly the magnitude of the flow velocity. This is also possible under extreme conditions where other anemometric systems are not suitable or reliable (e.g. under back-flow conditions or fast changing unsteady inflows as well as under highly non-isothermal conditions) or will need a continuous maintenance (or calibration).

According to Igarashi (1999) three properties are essential for a high performance vortex flow meter, namely low pressure loss, strong and stable shedding and a stable detection of the vortex shedding frequency. While the first two are related to flow properties, the third one is associated to the measurement device and its working principle. The best route to generate some vortices shed at an approximately constant frequency is by means of bluff bodies with a sharp edge at the point of flow separation, so that the wake width becomes approximately constant as well as the shedding frequency. As concluded by Venugopal & Agrawal (2011), the commercial vortex flowmeters are usually based on simple shapes like trapezoid and triangular, due to its ease in manufacturing and patent issues. Hence there is no need to explore new vortex shapes for steady flow conditions. However this is not true for highly turbulent flows where the incoming flow direction is continuously changing and the wake width with fixed separation points could exhibit inflow direction dependence, with consequent erroneous estimation of the velocity. This issue (usually neglected since the instantaneous transverse velocity component is small compared to the bulk velocity in pipes) becomes more severe for complex turbulent flows under pulsating conditions, where a cylindrical geometry should be preferred, since the shedding would be independent of the flow direction[1].

[1]Eventual adjustment times of the wake structure after a sudden change in flow directions are expected to be small or with a time scale smaller than the one of the shedding.

For vortex flow meters used in industrial pipe flows, the flow is usually turbulent and confined by the tube walls and indeed the vortex device will experience fully three dimensional flow Reik *et al.* (2010). Another important issue is the optimal blockage ratio of the vortex flow meter; a high blockage ratio is preferred, since it accelerates the flow and gives a stronger signal, and less scatter in the St-relation, but on the other hand it will become intrusive and give a higher pressure loss, and its presence will affect the measured velocity. A blockage ratio of $d/D \approx 0.3$ was shown to be optimal by Venugopal *et al.* (2010). For a recent review on vortex flow meters the reader is referred to Pankanin (2005).

In this study a circular cylinder is used as the vortex shedder and the shedding frequency is obtained from the signal processing of hot-wire and microphone time series. As previously mentioned, from the point of view of steady laminar (or low turbulence level) flow measurement, a circular cylinder flow meter presents many disadvantages since the separation point will vary with Reynolds number for a cylinder Achenbach & Heinecke (1981). However, the purpose with the present study is by no means to find the best geometrical design for the vortex shedder, but here the aim is rather to find a robust technique that is able to measure the instantaneous bulk velocity in strongly unsteady gas flows as e.g. encountered in the in- and outflow to internal combustion engines.

The remainder of the paper is organized as follows. The next section provides a description of the facilities used in the present experiments. The analysis is then introduced in fully developed pipe inflow conditions in section 3 and then extended to industrial configurations in section 4. As an alternative to the use of hot-wire anemometers to detect the shedding frequency, a flush mounted microphone configuration is tested and the preliminary results under steady and pulsating inflow conditions are discussed in section 5 after which section 6 concludes the paper by summarizing the main results.

2. Experimental setup

The experiments were conducted at two separate pipe flow facilities. The first is a straight pipe flow facility intended for basic turbulence research and has an upper Reynolds number limit at $\mathrm{Re}_D = U_b D/\nu \approx 34000$ (where U_b, D and ν are the bulk velocity, the pipe diameter and the kinematic viscosity, respectively), whereas the latter is intended for combustion engine related flow research and can provide Reynolds numbers up to about 5×10^5. These facilities and their instrumentation will be described individually in the two subsequent sections.

2.1. *Fully developed turbulent pipe flow experiment*

The pipe flow experiments were performed in the *Fluid Physics Laboratory* of *KTH Mechanics* in a pipe with inner diameter $D = 60$ mm and length $100D$ as

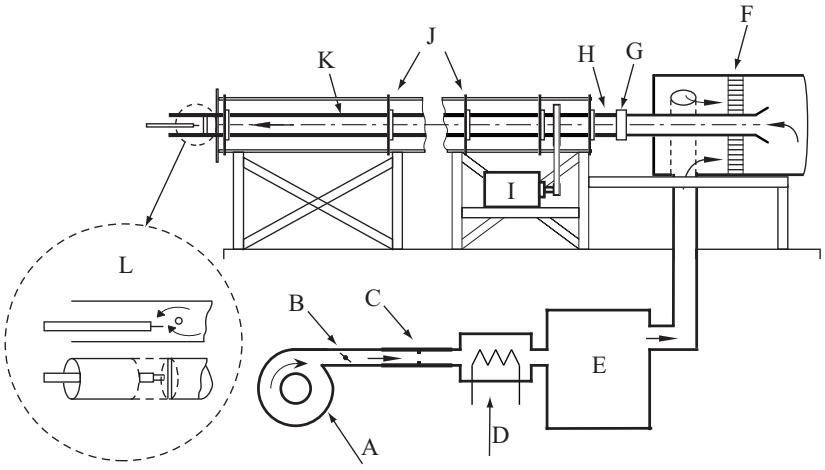

FIGURE 1. Schematic description of the experimental setup. (**A**) Centrifugal fan, (**B**) Valve, (**C**) Flow meter (orifice plate), (**D**) Electrical heater, (**E**) Distribution chamber, (**F**) Stagnation chamber, (**G**) Coupling between stationary and rotating pipe, (**H**) Honeycomb, (**I**) DC motor, (**J**) Ball bearings, (**K**) Rotating pipe, (**L**) Vortex shedding measurement location.

schematically shown in figure 1. A detailed description of the facility can be found in Örlü (2006).

The air is provided by a centrifugal fan (**A**) with a butterfly valve (**B**) for flow rate adjustment, downstream of which a flow meter (**C**) monitors the flow rate. The flow meter output is directly related to the Reynolds number Re_D and the calibration relation has been obtained by a number of velocity profile measurements. Downstream the flow meter a flow distribution chamber (**E**) splits the flow into three different pipes, that are symmetrically connected to the stagnation chamber (**F**) in order to ensure a symmetric flow with no swirl in the settling chamber. A bell mouth shaped entrance first feeds the flow into a one meter long stationary section, which is connected to the rotating pipe (**K**) through a rotating coupling (**G**). In the first part of the pipe a honeycomb (**H**) is mounted, which straightens up the flow. Thereafter the flow develops along the pipe. Roughly $1D$ upstream the pipe outlet, a circular cylinder is mounted, spanning the entire pipe diameter, to serve as a vortex shedder. The cylinder is interchangeable and three different cylinder diameters, d, were used, namely 1.7, 3 and 5 mm, i.e. d/D varies from 0.028 to 0.083.

The pipe outlet is far enough from the surrounding walls and the floor, ensuring that the experiments reported here are unaffected by physical boundaries. The pipe is made of seamless steel and has a honed inner surface. The

outer pipe surface is insulated, such that $T \approx$ const over the whole pipe length. The temperature was measured at the pipe outlet by means of a thermocouple of K type. The maximum temperature variation in the flow during the measurements is about 0.3 K. Furthermore, the flow temperature is typically 1 K above the ambient due to the turbulent frictional heating.

Experiments were carried out at Re_D ranging from 7800 to 34000, hence corresponding to $\mathrm{Re}_d = U_b d/\nu \geq 220$ for the smallest cylinder used, which is within the turbulent wake region.

The shedding frequency at the vortex shedder (**L**) was measured utilizing a hot-wire probe with a welded 5 μm tungsten wire of 1 mm length, that was operated by means of a *Dantec StreamLine* main frame with a *90C10* standard CTA module. Calibration of the hot-wire was performed in a nozzle calibration facility at the same temperature as during the measurements. The hot-wire was held by means of support arms connected to a stepper motor, that enabled automatic positioning of the hot-wire probe. With this 2D traverse, the hot-wire can be traversed in both the downstream and the radial direction. Data acquisition and control of the stepper motor was managed by a PC with a *NI-6250* acquisition board. Typically for each data point 30 seconds of data were acquired at a sampling frequency of 20 kHz.

2.2. *Pulsating pipe flow experiment*

In order to broaden the Reynolds number range and to obtain flow conditions similar to those in the gas exchange system, complimentary measurements were performed at the *CICERO Laboratory* of *KTH CCGEx*. A schematic description of the apparatus is depicted in figure 2 whereas a detailed description of the facility can be found in Laurantzon *et al.* (2010a).

In short the facility has a compressor system that can deliver 0.5 kg/s of dry air. In the flow loop a high quality ABB thermal mass flow meter ((**a**) in Fig. 2) gives the flow rate, before the air passes a 18 kW regulated heater (**c**) to a pulse generator (**e**) that is placed upstream the flow meter (**f**) under investigation. The frequency of the pulsations is controlled by an AC-motor, which can create pulsating frequencies up to 100 Hz. The pulsation amplitude is directly controlled by the flow rate and the amount of flow through a bypass (**d**) of the pulse generator. An orifice plate flow meter (**b**) is used to check the system flow meter calibration. Two pipes were investigated with 40 mm and 56 mm inner diameter, respectively. For both pipe diameters, an upstream straight pipe section of about $30D$ was used in order to reduce the effect of upstream obstacles on the shedder readings. Five different cylinders with diameters 1, 2, 3, 3.2 and 4 mm, were employed as vortex shedders. Three experiments were carried out with different upstream conditions. One with the 40 mm diameter pipe connected downstream the pulse generator, while the two other experiments were for the 40 and 56 mm diameter pipes, where the pipes

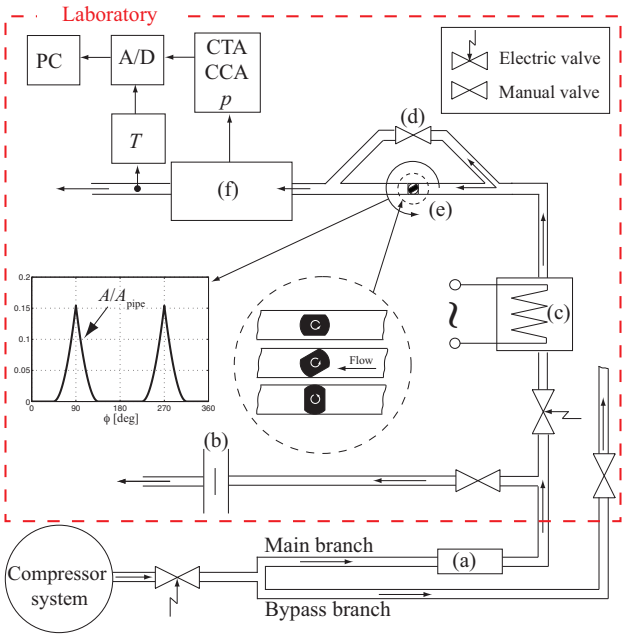

FIGURE 2. A schematic description of the flow rig. (**a**) Thermal mass flow meter (ABB), (**b**) orifice plate, (**c**) electric heater, (**d**) by-pass branch, (**e**) pulse generator, (**f**) hot-wire/cold-wire unit.

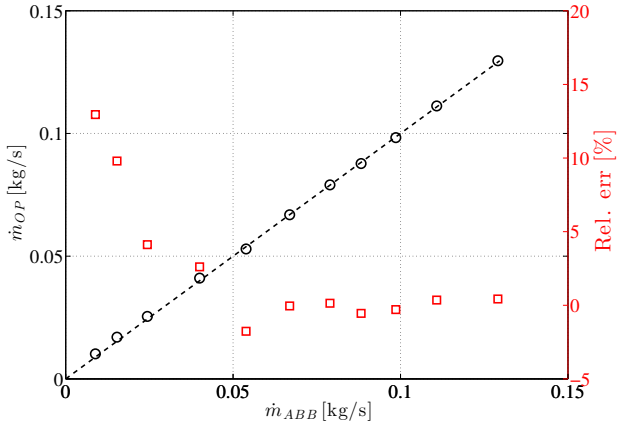

FIGURE 3. (*Left axis*) Mass flow rate estimation. Orifice plate vs. hot-film flow meter (ABB). (*Right axis*) Relative error of the ABB sensor with respect to the orifice plate.

were connected downstream the orifice plate (**b**). This was done in order to assert an accurate flow rate estimation, since the system reference flow meter becomes inaccurate for a mass flow $\dot{m} < 40$ g/s, as can be seen in figure 3, where the flow rate obtained with orifice plate is plotted against the flow rate measured by means of the hot-film flow meter (ABB).

Two techniques were employed to detect the shedding frequency. A hot-wire was used with instrumentation similar to that of the facility described in section 2.1. However here the hot-wire was fixed behind the cylinder perpendicular to the flow without the possibility to traverse the probe. Therefore a Pitot tube was employed instead to obtain the velocity profiles with the same traversing equipment as described in the previous section.

Time resolved measurements in pulsating flow with a hot-wire have been performed previously, see Laurantzon *et al.* (2010b). The benefits with the hot-wire used as a detector of the shedding in pulsating flow is the high signal-to-noise ratio (SNR) and its high frequency response. On the other hand, the wire is fragile and is easily destroyed by particles in the flow or strong vibrations of the pipes. Because of this, a new measurement approach was developed that is both more robust and that can be used in harsh environments such as those encountered in internal combustion engines, where the flow is pulsating, gases often contain particles and the whole engine is vibrating. This measurement device measures the pressure fluctuations due to the vortex shedding directly on the cylinder body. It consists of a hollow circular cylinder with a small hole at its half length. A microphone is flush mounted at one end of the cylinder as schematically shown in figure 4. In this way, the microphone is protected from the actual gas flow and any particles in the gas. The microphone is from *Brüel and Kjær Type 4941*, has a sensitivity of 0.09 mV/Pa and can manage frequencies up to 20 kHz.

There are a couple of phenomena that have to be considered when designing this microphone-based vortex flow meter. Frequencies that are not related to the shedding (such as standing waves, Massey (1998)) can appear, increasing the noise content of the signal. Another frequency that can appear in cavities with a thin neck leading to the cavity is the Helmholtz resonance frequency, see e.g. Sieverding *et al.* (2000), given by the relation

$$f_H = \frac{a}{2\pi}\sqrt{\frac{A_n}{V_c L_n}} \tag{2}$$

where a is the speed of sound, V_c is the volume of the cavity, A_n and L_n are the area and length of the neck, respectively. Apparently, f_H can be partially controlled by the geometric design of the shedder. However the geometric shape must at the same time be optimized to achieve fast frequency response of the system. In order to achieve a high frequency response for a tube-pressure

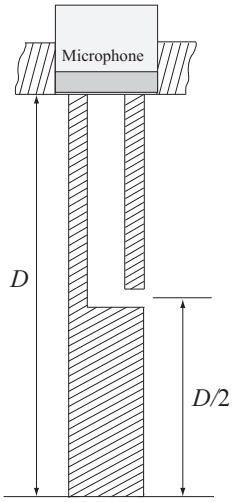

FIGURE 4. Schematic representation of the cylinder with the microphone. The hole to the cylinder cavity is located in the middle of the pipe cross section and it is possible to turn the hole in arbitrary orientation relative the flow normal direction.

transducer system, short tubes with large diameters are preferable (Tijdeman (1965)).

3. Results in fully developed pipe conditions

3.1. *Analysis of the shedding frequency*

As discussed in the introduction, the vortex flow meter is based on the vortex shedding phenomenon observable in the wake behind a cylinder (see e.g. Kundu (2012)). The presence of the incoming turbulent pipe flow velocity is not expected to affect the dynamics significantly, since the approaching mean velocity profile will nearly be flat with a variation of the order of $0.1U_b$ for $r < D/4$. The presence of intense velocity fluctuations is not expected to modify the shedding process due to the absolutely unstable nature of the vortex shedding phenomenon behind bluff bodies, see for instance Schmid (2001). The confinement due to the pipe wall, on the other hand, is potentially able to affect the vortex dynamics because complex three-dimensional interactions between vortices shed by the cylinder and characteristic wall turbulence eddies will occur close to the wall. By assuming the probe to be located at a fixed position downstream the cylinder with a statistically steady inflow, the vortex shedding frequency, f_{VS}, is related to the operating parameters by the functional dependence

$$f_{VS} = F\left(U_b, D, d, \rho, \mu\right) , \tag{3}$$

where ρ and μ are the fluid density and dynamic viscosity, respectively. By means of the Buckingham theorem, it is possible to simplify equation (3) to

$$\mathrm{St}_d = \frac{f_{VS} d}{U_b} = G\left(\mathrm{Re}_d, \frac{d}{D}\right), \tag{4}$$

where the Strouhal number, St_d, the cylinder Reynolds number, $\mathrm{Re}_d = \frac{\rho U_b d}{\mu}$, and the blockage ratio, d/D, are recognized. In the case of the infinitely long cylinder, this latter parameter is not able to affect the dynamics (being zero) and the Strouhal number becomes a function only of the Reynolds number Re_d. However, when $d/D > 0$ the functional relationship (4) shows that a dependence of the Strouhal number on both Reynolds number and blockage ratio is theoretically possible. Figure 5(a) and (b) shows the Strouhal number *versus* cylinder Reynolds number, Re_d, and pipe Reynolds number, Re_D, respectively, for three different blockage ratios obtained in the fully developed pipe facility described in section 2.1. It is evident that the blockage ratio is able to affect the Strouhal number significantly beyond the measurement uncertainty. Furthermore, the increase of the dimensionless frequency is consistent with the decrease of blockage ratio.

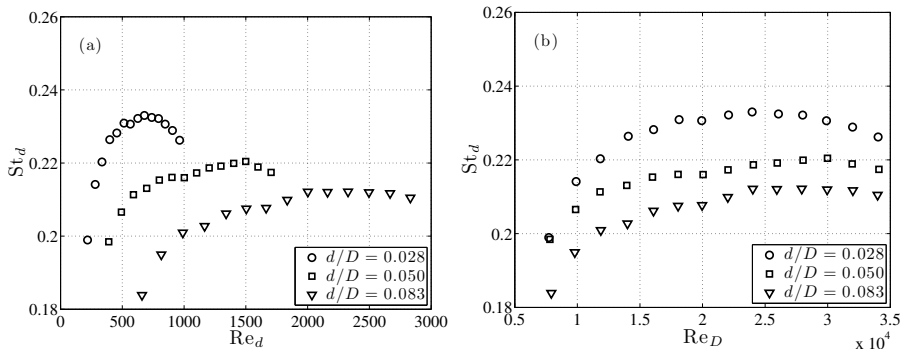

FIGURE 5. Strouhal number St_d as function of the Reynolds number for different values of the blockage ratio d/D. (a) Re_d. (b) Re_D. Measurements were performed at the pipe centerline.

3.2. *Space robustness*

A practical issue investigated in the present work is the optimal probe position in terms of both shedding frequency determination and accuracy. In order to determine this region the probe was traversed in the pipe middle plane normal to the cylinder axis spanning the streamwise, x, and radial, r, pipe directions. $x = 0$ and $r = 0$ identify the cylinder axis which is the origin of the local reference

frame used in this section. From the analysis of the various time series, it is possible to evince that inside a region defined by $2 \leq x/d \leq 20$ and $1 \leq r/d \leq 3$, the flow dynamics are dominated by a constant shedding frequency despite the turbulent inflow. Outside this region the shedding signal is not unambiguous anymore.

The optimal position can now be defined as the position where the measured spectral peak frequency f_{VS} is "dominant" compared to the rest of the spectrum. This evaluation can be accomplished by introducing the operator E_u that is the energy content between $a < f < b$, namely

$$E_u(a,b) = \int_a^b P_{uu}(f)\,df\,. \tag{5}$$

A new index, Ψ, can then be introduced as

$$\Psi = \frac{E_u(f_{VS}-B, f_{VS}+B)}{E_u(0, f_{VS}-B) + E_u(f_{VS}+B, +\infty)}\,. \tag{6}$$

This Ψ parameter is the ratio between the energy of the shedding phenomenon and the energy of the remaining part of the spectra and can heuristically be thought as a signal-to-noise ratio (SNR), if one consider the remaining part of the spectra just due to turbulent noise uncorrelated to the shedding frequency. Figure 6 shows a contour plot for two different Reynolds numbers of the Ψ parameter with half-band $B = 0.2 f_{VS}$. Both experiments clearly show a maximum of Ψ in the neighborhood of $x/d = 5$ and $r/d = 1.5$, where the shedding energy is more than 80% of the remaining spectral energy.

3.3. *The vortex shedding along the cylinder*

Given the optimal position of the sensing hot-wire as determined in the previous section, the hot-wire was placed in this position to be traversed from one pipe wall to the other parallel to the cylinder. This was done to appreciate the signal behavior close to the wall and to establish a suitable area for the estimation of the bulk velocity along the cylinder. As a reference for the subsequent section, the mean velocity profile of the pipe flow obtained with a calibrated hot-wire, albeit without cylinder, can be seen in figure $7(a)$.

The Ψ parameter (defined in equation 6) is plotted in figure $7(b)$ against the radial position in the pipe. Here Ψ is notable higher for the smallest cylinder, this is mainly because the shedding frequency is higher in this case and so the remaining turbulence level is lower. Moreover, the frequency band is bigger, being proportional to the shedding frequency, f_{VS}. The two other cylinders have however about the same level, which is somewhat counterintuitive as we would expect that Ψ should decrease with increasing cylinder diameter.

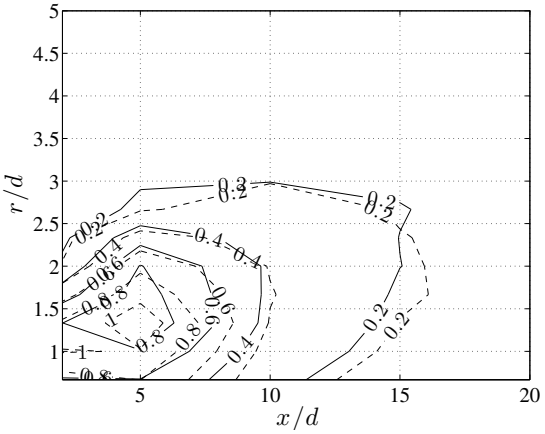

FIGURE 6. Contour plot of the Ψ parameter for half-band $B = 0.2f_{VS}$ in different spatial positions at $\mathrm{Re}_D = 24000$ (*solid lines*) and $\mathrm{Re}_D = 34000$ (*dashed lines*) for $d/D = 12$.

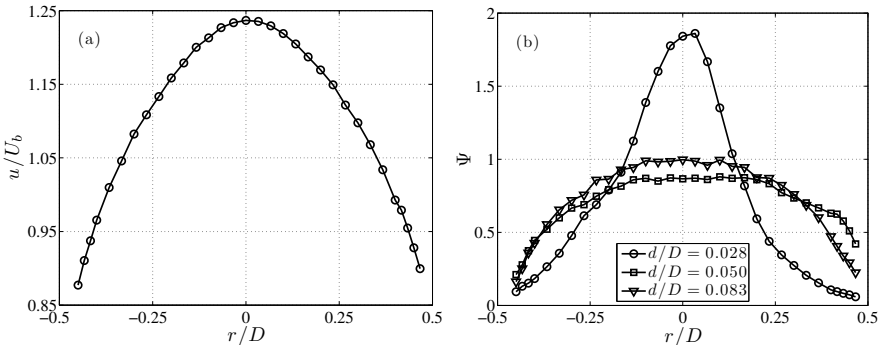

FIGURE 7. (*a*) The velocity profile from hot-wire measurement without cylinder. (*b*) The signal-to-noise ratio estimation along the cylinder. For $\mathrm{Re}_D = 24000$

The corresponding dimensionless frequency can be seen in figure 8, where it can be observed that the Strouhal number decreases with increasing cylinder diameter and it extends for a significant part of the flow near the pipe centerline. It can also be noted that the largest cylinder diameter shows a more uniform frequency distribution along the pipe diameter.

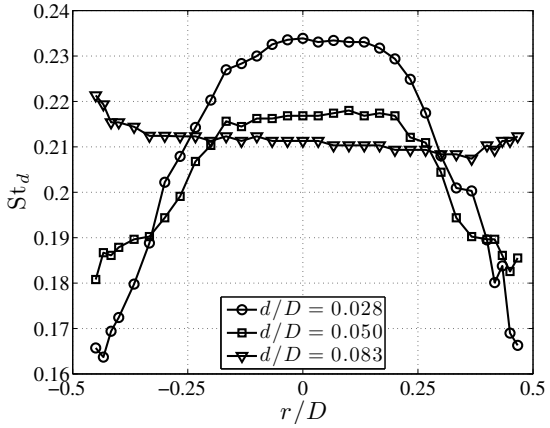

FIGURE 8. The Strouhal number St_d based on the bulk velocity, U_b, for the three different cylinder diameters.

4. Vortex shedder in industrial configurations

With the results discussed under fully developed conditions in the previous section, we subsequently investigated the robustness of the shedding phenomenon under different pipe configurations with different upstream conditions. Different pipe configurations (discussed in section 2.2) were therefore tested with the same nominal vortex shedder in order to assess practical measurements uncertainties in real operating conditions, where the incoming flow can differ significantly from fully developed pipe flow conditions. In order to distinguish between the different industrial pipe realizations, table 1 provides a list of symbols used for each experiment, that will be employed throughout this section. In figure 9 the comparison between the fully developed pipe velocity profile against two measurements sets from the industrial pipe configuration is reported. As evident from the figure, the structure of the velocity profile is completely affected, with a particular flat resulting profile with the pipe $D40^a$ with the pulse generator mounted upstream.

The comparison of the measured Strouhal number as function of the cylinder Reynolds number, Re_d, and pipe Reynolds number, Re_D, is reported in figure 10 for all the experiments available (including the fully developed conditions). A moving average is provided together with an error band of amplitude ±5% of the local average value. The large measurement scatter is mostly due to strong alterations of the inflow rather than measurement uncertainties (which are of the order of 1% due to the uncertainties in the bulk velocity measurements from the ABB hot-film flowmeter). Therefore both plots underline the importance of upstream conditions on the bulk velocity determination with the

Experiment	$D40^a$	$D40^b$	$D40^c$	$D56^d$	$D56^e$	$D60^f$
Symbol	○	•	•	□	∗	▽

TABLE 1. (a) The vortex shedder is placed downstream the pulse generator. (b) The pulse generator is omitted. (c) Repetition of (b), to check repeatability. (d) The pulse generator omitted. (e) Measurement with microphone downstream pulse generator. (f) Reference measurements in the turbulence pipe flow facility.

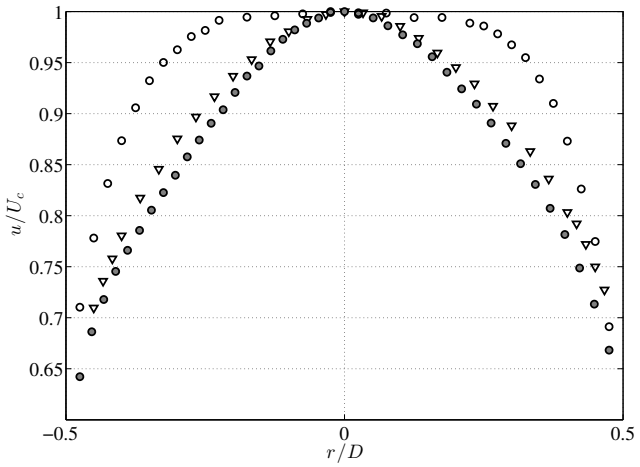

FIGURE 9. Velocity profile scaled with centreline velocity, along the pipe outlet. ▽:Re = 24000, •:Re = 99000, ○: Re = 135000.

vortex shedder approach and it can clearly be stated that, even for developing flows, the accuracy of the estimation is of the order of ±5% of the real value.

According to the local average distribution, the Strouhal number increases for $\mathrm{Re}_D < 1 \times 10^5$ while it starts to decrease mildly above, albeit this latter statement is not strongly supported by the experimental results due to the large scatter. However, it should be pointed out that this Reynolds number transition has already been observed in wind tunnel experiments (Norberg (1994)).

It is worth noting that while the Reynolds number based on the cylinder diameter, Re_d, affects the shedding process directly, the pipe Reynolds number, Re_D, shows a more compact scatter distribution, despite the change of the blockage ratio of a factor 4. This fact underlines that confinement effects and

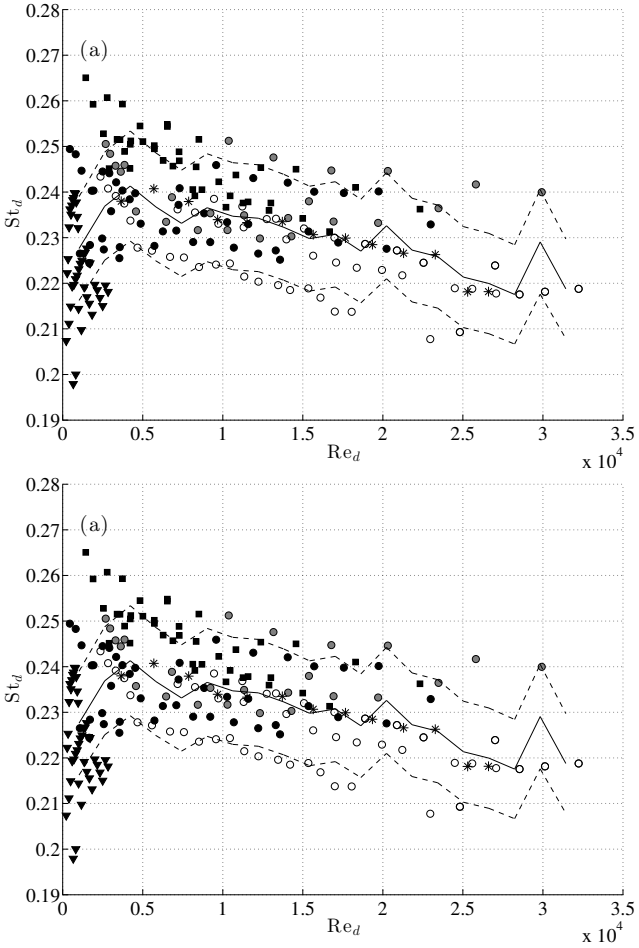

FIGURE 10. Strouhal number as function of Reynolds number. (a) Cylinder Reynolds number Re_d. (b) Pipe Reynolds number Re_D. The symbols are defined in table 1.

profile non-homogeneities (related to Re_D) are strongly affecting the shedding process.

Figure 11 shows the scatter plot between Strouhal number and blockage ratio, d/D. While under fully developed conditions there was a clear decreasing trend with the increase of the blockage ratio (c.f. figure 5), the inclusion in the analysis of the industrial data suggests a similar trend, despite the scatter. However the effect of the blockage ratio cannot generally be evaluated, but it must still be assessed for a specific inflow condition. For the sake of simplicity

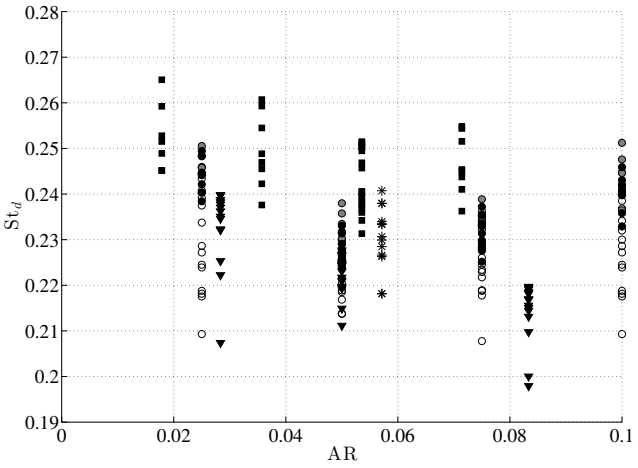

FIGURE 11. Strouhal number as function of blockage ratio, i.e. aspect ratio (AR).

it will here be assumed that the blockage ratio has only a weaker effect than the Reynolds number on the Strouhal number. However it must be said that the pipe Reynolds number includes the blockage ratio in its definition, since $\mathrm{Re}_D = \mathrm{Re}_d D/d$.

A possible way to quantify the shape of the incoming velocity profile is the ratio between the maximum velocity and the bulk velocity $\gamma = U_\mathrm{c}/U_\mathrm{b}$. In the limit $\gamma \to 1$ the velocity profile becomes a top-hat profile while for fully developed conditions $\gamma \approx 1.25$ with a weak logarithmic dependence with the Reynolds number, Re_D, (see e.g. Schlichting (2006)). As a rule of thumb, it can be stated that if γ is away from the fully developed state, then strong modifications to the fully developed velocity profile took place. Figure 12 reports a subset of the available data where a characterization of the incoming velocity profile was also performed. For the fully developed conditions, the increase of γ is associated with a decrease in Reynolds number and to a consequent decrease of the Strouhal number. However, this is not the case for the other experiments that show a completely opposite trend. Again, no firm conclusion can be stated from the analysis of figure 12 but it can be said that the γ parameter should enter the analysis performed in section 3.1, if a generalization of equation (4) is pursued.

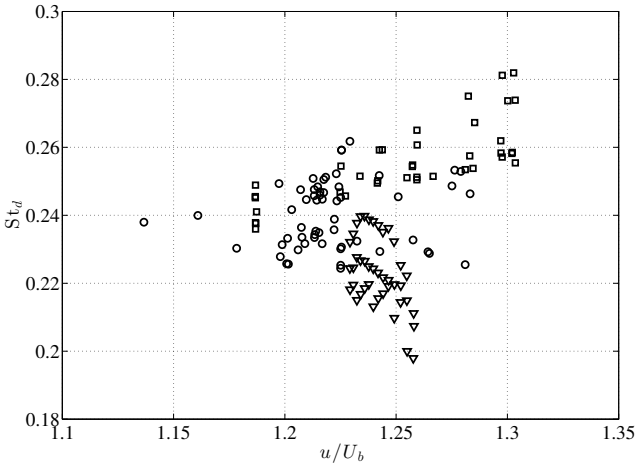

FIGURE 12. Strouhal number as function of γ ratio, i.e. u/U_b.

5. Bulk velocity estimation by means of microphone measurements

In the previous section it was demonstrated that a hot-wire located in the wake of a circular cylinder is able to determine with reasonable accuracy the instantaneous bulk velocity. However in real applications the use of hot-wires will necessitate continuous maintenance due to the fragility of the sensor. A possible alternative to the local velocity measurement is the use of a pressure sensor since the two quantities are associated through a Poisson equation (Mathieu (2000)). This practically means that the pressure is non-locally affected by events that will happen in the neighborhood with an intensity that decays as the inverse of the distance squared.

A test series was performed to determine the performance of a microphone measurement device under different operating conditions. It was found that the orientation of the shedder showing the highest SNR was at 90 degrees relative the normal flow direction, i.e. perpendicular to the flow direction, where the minimum of the local static pressure is expected[2]. This means that the flow in both directions can be detected with the same signal quality without discerning the flow direction.

5.1. *Steady conditions*

Under steady state conditions, the microphone setup was tested in a mass flow range from 25 to 350 g/s. Fig. 13 shows the power spectral density (PSD) for

[2]Cf. potential flow past a circular cylinder, where the pressure coefficient $C_p = 1 - 4\sin^2\theta$, has a minimum value for $\theta = 90°$.

hot-wire measurements in comparison to microphone measurements. Whereas the hot-wire spectra shows clear peaks at the shedding frequency, the spectra for the microphone, shows a scattered frequency content at lower Re, but clearer peaks at higher flow rates. Such disturbances can lead to problems in the measurements of pulsating flows, since part of the pulse might lie in a region with high noise content in the signal. They are believed to be the result of a Helmholtz resonance and/or standing waves in the cylinder cavity. An estimation of the Helmholtz frequency with equation (15), gives $f_H \approx 1500$ Hz, which may explain the noise at the lowest frequencies in the Fig. 13. A geometric optimization aimed at the reduction of this noise or at moving this resonant frequency away from the region spanned by the shedding peak has not been attempted in the present work.

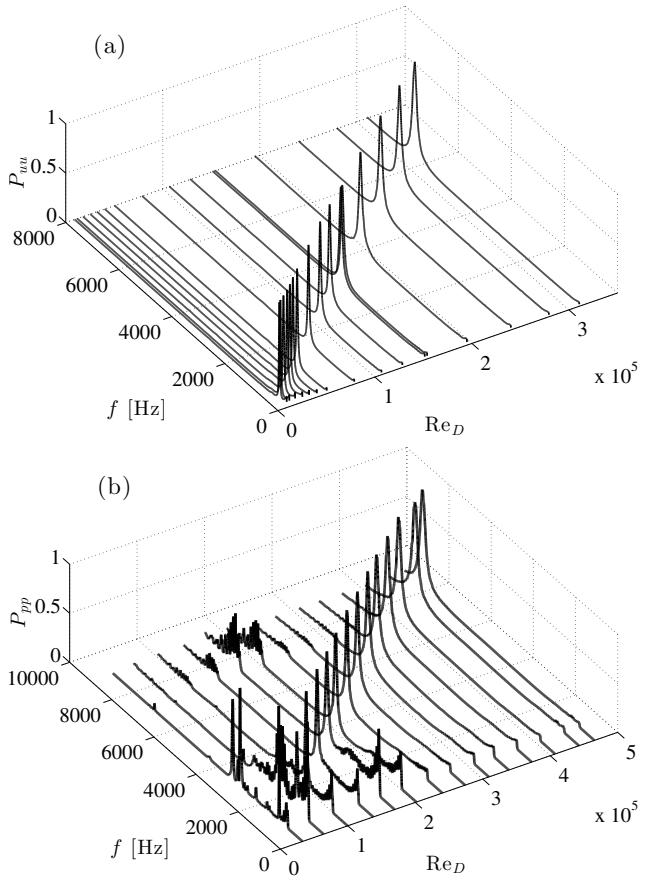

FIGURE 13. Power spectral density (PSD). Obtained with (a) Hot-wire. (b) Microphone.

5.2. *Pulsating conditions*

The microphone as a vortex shedding detector was employed for the pulsating flow study. Two different mean flow rates were studied, namely 80 g/s and 150 g/s for pulse frequencies f_p ranging from 10 Hz to 100 Hz, with steps of 10 Hz.

As discussed in the previous section, the spectra of the microphone signal has a frequency ambiguity problem at low mass flow rates where it becomes difficult to distinguish between the shedding peak and the peak of the Helmholtz resonance. This was confirmed for the 80 g/s case, were a significant noise content was found in the wavelet map. Therefore, in order to validate the technique, only results from the 150 g/s case will be shown. Two examples are shown in figure 14 and 15, at pulsating frequencies 30 and 60 Hz, respectively. In part (a) of the figures, the spectrogram of the wavelet transform is

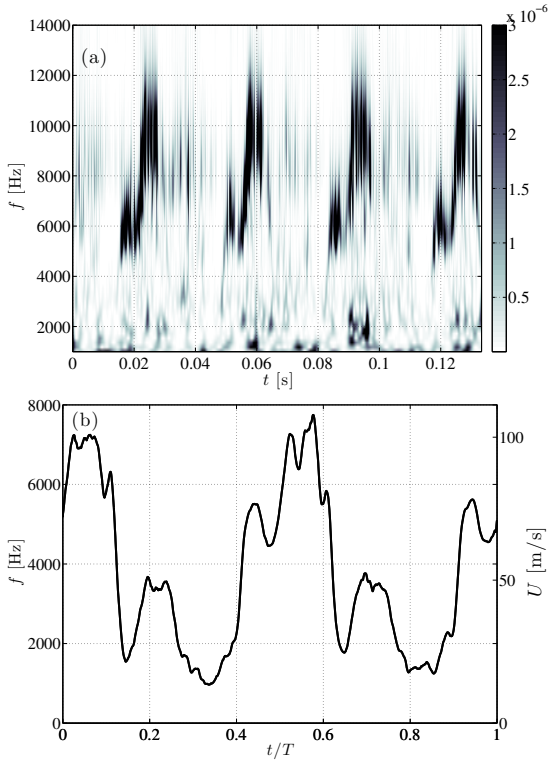

FIGURE 14. Pulsating flow at f_p = 30 Hz (T=0.033 sec) and mean mass flow rate 150 g/s. (a) Spectrogram. (b) The extracted frequency (left vertical axis) and velocity (right vertical axis).

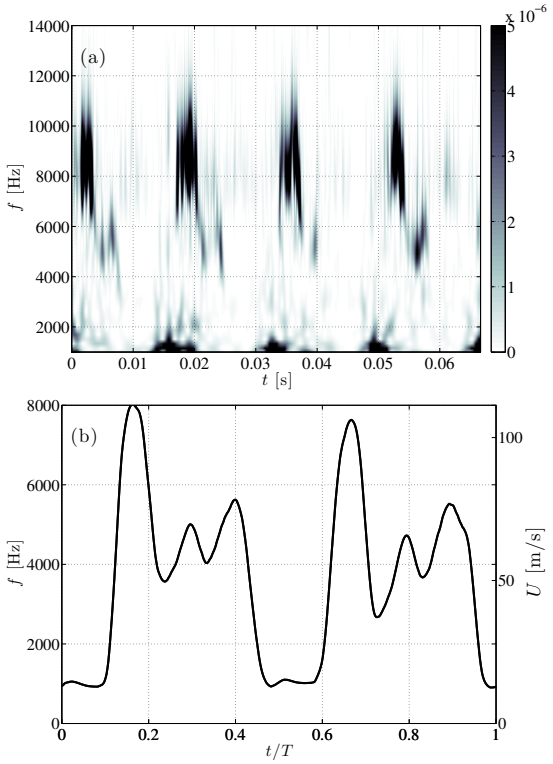

FIGURE 15. Pulsating flow at f_p = 60 Hz (T=0.017 sec) and mean mass flow rate 150 g/s. (a) Spectrogram. (b) The extracted frequency (left vertical axis) and velocity (right vertical axis).

shown for four pulses while part (b) shows the extracted frequency and velocity determined with the assumption of a constant Strouhal number. The data shown here are phase averaged (for about 300 cycles) over a complete rotor revolution of the pulse generator, i.e. for two pulses, which explains the small differences of the pulse shape. The Reynolds number for 150 g/s is around $\mathrm{Re}_D \approx 2 \times 10^5$, which in steady flow corresponds St $\approx$ 0.235, as obtained by means of figure 10. The accuracy of the velocity estimation can of course be increased if the variation in Reynolds number during the pulse is taken under consideration. However, the mean of the flow rate obtained with a constant St number, gave a deviation from the mean reference flow rate with less than 5% for all pulse frequencies, which can be viewed as acceptable, in light of the error band width in the Strouhal number determination discussed in section 4. Above all it should be kept in mind that the novelty in the method is that the

instantaneous bulk speed can be measured sufficiently well even under harsh conditions as they are encountered in industrial flows.

6. Conclusions

Experiments were carried out in order to find a relevant correlation between St and Re for vortex shedding behind a circular cylinder in a pipe. Three cylinders were used with blockage ratio d/D of 0.028, 0.050 and 0.083 respectively. For the purpose of obtaining a reasonable estimate of the Strouhal number, the blockage factor d/D as well as the Reynolds number based on the pipe diameter, Re_D, must be taken into account. For this choice of the scaled Strouhal number St'_d, the estimated bulk velocity U_b, deviates less than 3% of the measured bulk velocity, as opposed to the often used relationship $\mathrm{St} = f(\mathrm{Re}_d)$ or St= 0.21, where the deviation is about 12% and 13% respectively.

A simple but effective way to determine the optimal sensor location to detect the vortex shedding frequency with high signal-to-noise ratio has been proposed.

The first test series with a microphone to sense the vortex shedding frequency shows potential for that method. As the whole setup is more robust than a hot-wire setup, it can be used in internal combustion engine related flows. Furthermore, the choice of a circular cylinder as a shedder offers an isotropic shedding even if the inflow deviates slightly from the streamwise direction, furthermore because the hole to the microphone is oriented perpendicular to the normal flow direction, similar signal quality will be obtained if flow reversal occurs, which is an attractive feature of the technique. Although some further development is needed to reduce signal ambiguity at low flow rates, the technique seems suitable for time resolved measurement under harsh conditions where alternative techniques are not available.

Acknowledgement

This work was carried out with CCGEx, a competence centre sponsored by the Swedish Energy Agency, Swedish vehicle industry and KTH.

References

Achenbach, E. & Heinecke, E. 1981 On vortex shedding from smooth and rough cylinders in the range of Reynolds numbers 6×10^3 to 5×10^6. *J Fluid Mech* **109**, 239–251.

Bergh, H. Tijdeman, H. 1965 Theoretical and experimental results for the dynamic response of pressure measuring systems. National Lucht- en Ruimtevaartlaboratorium.

Igarashi, T. 1999 Flow resistance and Strouhal number of a vortex shedder in a circular pipe. *JSME Int J B-Fluid T* **42**, 586–595.

Kundu, P.K, Cohen, I.M. 2004 Fluid Mechanics. Elsevier.

Laurantzon, F., Tillmark, N. & Alfredsson, P.H. 2010 A pulsating flow rig for analyzing turbocharger performance. *9th International Conference on Turbochargers and Turbocharging*, 19-20 May 2010 pp. 363–372.

Laurantzon, F., Örlü, R., Segalini, A. & Alfredsson, P. 2010 Time-resolved measurements with a vortex flowmeter in a pulsating turbulent flow using wavelet analysis. *Meas. Sci. Technol.* **21**, 123001.

Massey, B., Ward-Smith, J. 1998 Mechanics of fluids. Taylor Francis Ltd.

Mathieu, J. 2000 An introduction to turbulent flow. Cambridge University Press

Norberg, C. 1994 An Experimental Investigation of the Flow Around a Circular-Cylinder - Influence of Aspect Ratio. *J Fluid Mech* **258**, 287–316.

Örlü, R. 2006 Experimental study of passive scalar mixing in swirling jet flows. Licentiate thesis, KTH.

Pankanin, G. 2005 The vortex flowmeter: various methods of investigating phenomena. *Meas. Sci. Technol.*, 16:R1-R16, 2005.

Reik, M., Höcker, R., Bruzzese, C., Hollmach, M., Koudal, O., Schenkel, T. & Oertel, H. 2010 Flow rate measurement in a pipe flow by vortex shedding. *Forsch. Ingenieurwes.* **74**, 77–86.

Schlichting, H. 2006 Boundary layer theory. McGraw-Hill.

Schmid, P., Henningson, D.S. 2001 Stability and Transition in Shear Flows. Springer.

Sieverding, C., Arts, T., Denos, R. & Brouckaert, J. 2000 Measurement techniques for unsteady flows in turbomachines. *Exp Fluids* **28**, 285–321.

Strouhal, V. 1878 Über eine besondere Art der Tonerregung. *Ann Phys* **241**, 216–251.

Venugopal, A. & Agrawal, A. 2011 Review on Vortex Flowmeter-Designer Perspective. *Sensor Actuat A-Phys* **70**, 8–23.

Venugopal, A., Agrawal, A. & Prabhu, S. 2010 Influence of blockage and upstream disturbances on the performance of a vortex flowmeter with a trapezoidal bluff body. *Measurement* **43**, 603–616.

Paper 5

5

Response of common flowmeters to unsteady flow

By Fredrik Laurantzon, Ramis Örlü, Nils Tillmark and P. Henrik Alfredsson

CCGEx, KTH Mechanics, SE-100 44 Stockholm, Sweden

Technical Report

This report gives information on the response of several different types of flow meters to pulsating flows. The flow meters tested are based on pressure difference measurements (the venturi flow meter and Pitot tube), hot-film meter, as well as turbine and vortex flow meters. All flow meters were investigated using both steady and different pulsating frequencies and amplitudes. The problems associated with reverse flow during pulsations are also highlighted in the study.

---

1. Introduction

Flow meters in technical applications often measure under non-ideal circumstances, i.e. the flow is disturbed in some sense. Flow disturbances can basically be of two types, namely a non-ideal flow distribution across the flow cross section or the flow is unsteady, i.e. the flow rate is pulsating (Grenier 1991). An example of the former is an asymmetric velocity distribution at the outlet of a pipe bend located close to the flow meter, while pulsations related to internal combustion engine flows are an example of unsteady flows. Non-ideal flow distributions and unsteadiness can also appear simultaneously, see e.g. Timité *et al.* (2010). While the impact of steady flow disturbances on flow meters is well documented, and empirical compensation/correction schemes can be applied, unsteady flow disturbances still constitute a challenge for accurate flow measurements of even the mean flow rate. One of the complications related to unsteady flows is flow reversal, that can occur for instance in separated, highly swirling and periodic flows, as e.g. encountered in intake and exhaust pipings in reciprocating machineries (Persoons *et al.* 2004). Most measurement techniques have in common that they are only suited for uni-directional flow, hence large errors can be expected if flow reversals occur, since the signal may be rectified.

Common approaches to deal with flow disturbances is to try to attenuate the disturbance, e.g. by means of flow conditioners or by damping the pulsations (Mottram 1992; Blodgett 1992), or through the use of sophisticated post

processing techniques (Atkinson 1992; Rossberg *et al.* 2004). Another route is to try to resolve the time dependent fluctuations in the flow (Doblhoff-Dier *et al.* 2010; Laurantzon *et al.* 2010), and determine the mean flow directly from the time-resolved signal. The last approach demands that the technique has an inherent high frequency response.

1.1. *Some common flow meters for industrial processes*

In most industrial processes one is interested to obtain the mean flow rate of a gas or a liquid. Such flow meters can be based on many different principles, such as differential pressure flow meters (orifice plate, venturi, Pitot tube etc.), vortex flow meters, turbine flow meters and hot-film flow meters. These are all standard techniques for measurements in steady flows, but are usually unsuited for pulsating flow.

The use of differential pressure flow meters in unsteady flows is usually not recommended in the literature (Doblhoff-Dier *et al.* 2010). Although efforts have been made to study the influence of pulsating flows on orifice plates (Gajan *et al.* 1992), time resolved measurements with orifice plates (Doblhoff-Dier *et al.* 2010) and pulsating flows with a Pitot tube (Nakamura *et al.* 2005). General and common conclusions from these studies are, that fast pressure transducers are necessary to obtain accurate results, and moreover to be aware of that the time average of the pressure does not necessary correspond to the time average of the flow rate (due to the so called square root problem).

Extensive studies regarding the effects of pulsations on vortex flow meters have been performed and can be found in e.g. Grenier (1991) and Hebrard *et al.* (1992), where it is concluded that large metering errors occur for vortex flow meters in pulsating flows, see also the discussion in Laurantzon *et al.* (2010).

The responsiveness of the turbine flow meter is proportional to the density of the fluid and are mainly used for liquid flows. Turbine flow meters are also known to overestimate the mean flow rate in pulsating flows. This is due to the fact that the flow meter responds more rapidly to an increase in the flow rate than to a decrease (Atkinson 1992). The magnitude of this error depends upon the physical design of the turbine meter (rotor inertia, diameter, blade angle, etc.) and the flow condition present (flow rate, fluid density, pulsation frequency, amplitude and modal structure or wave shape), see e.g. McKee (1992).

The perhaps most utilized technique in pulsating flows is thermal anemometry (either hot-wire anemometry (HWA) or hot-film anemometry (HFA)), due to its high frequency response. This technique is also popular to use in combustion engine related flows (Persoons *et al.* 2004) and turbo machinery flows (Sieverding *et al.* 2000). However, thermal anemometry techniques sense the magnitude of the mass flow rate but can not discriminate the direction of the flow. Although, different techniques have been proposed to obtain both the

direction and the magnitude of the flow, see for instance Sokolov & Ginat (1992), Persoons *et al.* (2006) and Li & Naguib (2003), it has been questioned whether the technique is suitable when flow reversal occurs, since the heat transfer is not well defined when the velocity passes through zero and changes direction (Berson *et al.* 2010). Moreover, a non-isothermal flow field complicates the measurements for techniques that are based on heat-transfer, since the anemometer output is also related to the ambient, i.e. fluid, temperature (Ardekani & Farhani 2009). In order to obtain accurate results also the temperature needs to be measured time-resolved (or at least pulse-resolved) and simultaneously to enable a temperature compensation of the flow meter readings.

1.2. *The aim and layout of this paper*

The aim with the present study is to assess the effects of pulsations on some different flow meters, and to obtain time resolved measurements in order to obtain an accurate estimation of the real flow rate. The emphasis in this study will be on flow meters suitable for flows in inlet and exhaust systems of reciprocating internal combustion engines, as well as their feasibility to obtain time resolved data. A thorough analysis will be given for these flow meters, which in this study are: the venturi flow meter, the hot-film flow meter and the Pitot tube. The available literature for the behavior of these meters in pulsating flows is quite limited. Additionally one commercially available vortex flow meter and one turbine flow meter are included in the study. They have built-in processing with digital filters with response times of the order of 0.1s, implying that a steady output signal is obtained even under pulsating conditions and they are not suitable to give time resolved measurements under pulsating flow conditions. However they are included here in order to assess whether they have a potential to be used to measure the mean mass flow rate under such conditions.

The outline of the remainder of the report is as follows: section 2 presents and describes the experimental set-up and instrumentation. The main results are presented and discussed in section 3, whereas section 4, summarizes and concludes the present work. Three appendices are also included dealing with some specific issues of the study.

2. Experimental set-up

Experiments were carried out in the KTH-Cicero laboratory, that since 2011 is part of CCGEx, a centre for research related to gas exchange in internal combustion engines. The flow rig and experimental set-up is schematically depicted in Fig. 1 and a detailed description of the facility can be found in Laurantzon (2009). The facility has a compressor system that can deliver 0.5 kg/s of dry air. In the flow loop a high quality ABB thermal mass flow meter (Fig. 1(a)) gives the flow rate, before the air passes a 18 kW regulated

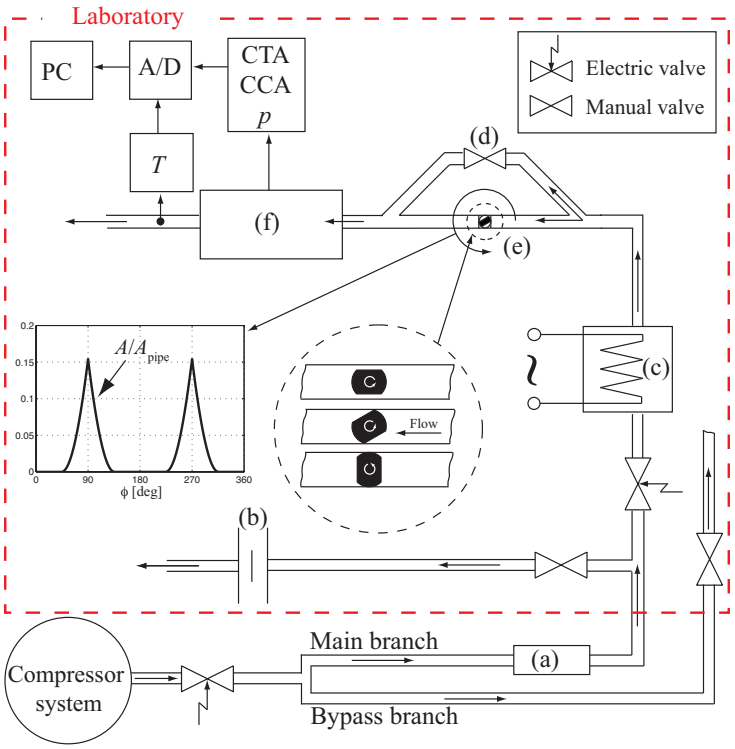

FIGURE 1. A schematic of the flow rig. (a) Thermal mass flow meter (ABB), (b) orifice plate, (c) electric heater, (d) by-pass branch, (e) pulse generator, (f) hot-wire/cold-wire unit.

heater (c) to a pulse generator (e) that is placed upstream the flow meter (f) under investigation. The frequency of the pulsations is controlled by an AC-motor, which can create pulsating frequencies up to 100 Hz. The pulsation amplitude is directly controlled by the flow rate and the amount of flow through a by-pass (d) of the pulse generator. An orifice plate flow meter (b) is used to check the system flow meter calibration.

In the present study a number of different flow meters have been tested under stationary and pulsating flow conditions. Since the flow meters have different geometrical shapes, it was necessary to utilize slightly different pipe connections. For all flow meter installations the piping was at least 10 D upstream and 5 D downstream from the flow meter position respectively, in order to assure well controlled flow conditions at steady flow. The downstream pipe was open to the atmosphere without any constriction.

It should also be noted that, although factory calibrations exist, some of the flow meters have been calibrated in-house prior to use. This is the case

for the hot-film flow meter, the vortex flow meter and the turbine meter, in order to ensure that all measurement techniques are calibrated against the same reference mass flow reading. The calibration was done against the mass flow rate measured by the system reference, which is located sufficiently far upstream the pulse generator that it is virtually unaffected by the pulsations. The output of the hot film flow meter is directly related to ρu, i.e. the mass flux. The vortex flow meter and the turbine meter are, however, responding to the volume flow. In these two latter cases the density of the gas at the meter position had to be estimated. An estimate is obtained by measuring the instantaneous pressure upstream and downstream the meter as well as the stagnation pressure and temperature. Although the flow through the flow meters is not isentropic, it is, however, a reasonable approximation which is used in order to estimate the average density.

The hot-film flow meter has a frequency response that limits its ability to make time resolved measurements at high pulsating frequencies. The venturi flow meter and the Pitot tube are usually not meant for use in pulsating flows, however by using flush mounted pressure transducers with short response times and cold-wires to capture the stagnation temperature fluctuations, they can be used as well to determine the instantaneous mass flow rate under pulsating conditions.

In the following each flow meter and its instrumentation are described in more detail.

2.1. *Venturi flow meter*

The venturi flow meter used in this study is a venturi meter used in Volvo heavy duty trucks to measure the EGR flow rate (see Fig. 2). In the present tests it was located approximately 1000 mm downstream the pulse valve. The flow meter was connected to the pulse valve section by a straight pipe (L = 750 mm), with an inner diameter of 55 mm. The meter outlet was connected to a temperature measurement section and a 400 mm long pipe, leading to the ambient air. The device has moreover two static pressure taps, where the first tap is located at the upstream end of the meter and the second tap is located at the throat. The cross section areas at pressure tap positions are A_1=2083 mm^2 and A_2=568 mm^2, respectively. For the stationary measurements a differential pressure transducer was used, which was connected by plastic tubes to the two pressure taps. An absolute pressure transducer was also connected to the upstream pressure tap. This arrangement gives good accuracy also at low flow speeds, where the pressure difference is small. This arrangement was, however, not suitable for the pulsating flow measurements, since the tubing-pressure transducer system had a too slow response to enable accurate measurements of the pressure difference. Instead, two fast response, absolute pressure transducers (*Kulite WCT-312M-25A*), were flush mounted at each pressure tap, in order to record the instantaneous variations in the pressure.

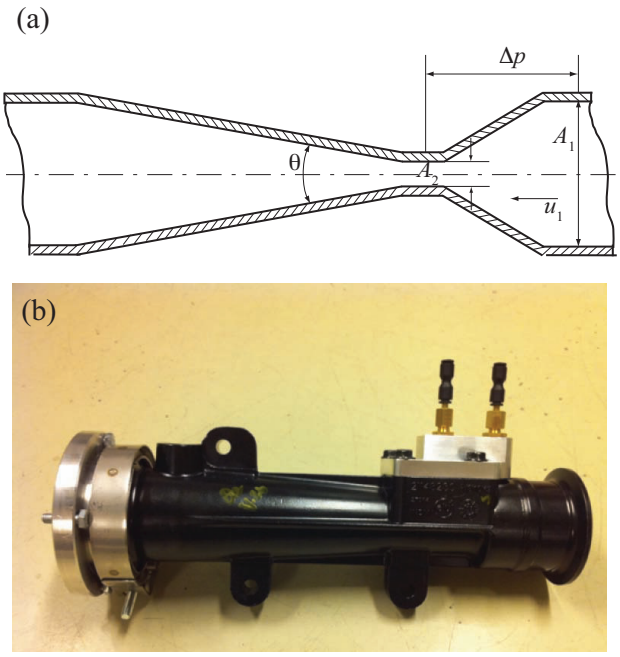

FIGURE 2. Venturi flow meter, (a) principal design, (b) photo. The flow direction is from right to left.

Directly downstream the venturi flow meter, a temperature measurement module with a Pt100 sensor and a cold-wire were mounted. The Pt100 sensor was used during steady flow measurements, but also served as a calibration reference for the cold-wire temperature sensor used for pulsating flow. Under steady conditions the gas stagnation temperature T_0, was assumed to be constant both in time and along the venturi meter. However during pulsating flow the stagnation temperature will vary. The cold wire measures the recovery temperature T_r, which for the Mach number range considered here can be assumed to be close to the stagnation temperature T_0. If the pulsating flow can be viewed as quasi-steady we can assume that the stagnation temperature is constant along the venturi at each instant of time. For the quasi-steady approach to be used, it is necessary that the distance between the sensors Δx is small compared to the wavelength of the pressure wave λ, i.e. $\Delta x << \lambda$.

2.2. *Pitot tube*

The Pitot tube was mounted in a short pipe module with inner diameter D=40 mm, situated approximately 1.5 m downstream the pulse valve. The Pitot tube with an outer diameter of 5 mm and an inner diameter of 2.5 mm

was mounted through a hole in the pipe wall. At the pipe wall/Pitot tube interface, a fast response pressure transducer (*Kistler 4045A5*), was flush mounted, but with a small volume in between. A short distance upstream (approximately 43 mm) at the tip of the Pitot tube, a fast pressure transducer (*Kulite WCT-312M-25A*), flush mounted at the pipe wall, measured the static pressure.

The same temperature measurement module used with the venturi meter set-up, was used also in this set-up. The temperature module was mounted about 3 pipe diameters downstream the Pitot tube.

2.3. *Hot-film flow meter*

The hot-film flow module tested, was provided by Scania, and is in their application used to measure the amount of intake air to the engine. It was studied in a set-up with a circular PVC pipe connected to the pulse generator. The PVC pipe has a diameter D=69 mm, and length L=1765 mm, with the outlet open to the laboratory. The actual hot-film module was located about 19 D downstream the pulse generator, and the distance between the hot-film and the outlet was 6 D, while the hot film meter was mounted inside the PVC pipe.

The module contains a hot-film for registration of the mass flux ρu and a thermistor for temperature measurements that are used for compensation of variations in temperature. The hot-film device was taken from a commercial flow meter with a given calibration chart. However for this specific installation, it was re-calibrated in order to comply with the present geometry.

Since back flow can occur in strongly pulsatile flows, laser Doppler velocimetry (LDV) measurements was performed in order to qualitatively as well as quantitatively assess the presence of back flow. This was conducted under the same flow conditions but without the hot film present. To enable LDV measurements, the PVC pipe was replaced with a Plexiglas pipe, and a glass section with a length of 200 mm was placed at the location of the hot-film meter. The length of the combined sections was the same as the PVC pipe with the hot-film mounted. This was both to get an idea about the amplitude of the velocity fluctuations, but also to identify the location of back flow. The effect of back flow will be further discussed in Appendix C.

2.4. *Vortex flow meter*

The vortex flow meter used in this study is a commercial *Yokogawa DY050* vortex flow meter, where the measurement section has a diameter of 50 mm and a length of 200 mm and is equipped with flanges at both ends. Furthermore, upstream the vortex flow meter a 15 D long pipe was connected to the pulse valve module. Since the meter measures the volume flow rate, the density had to be estimated in order to compare it with the reference ABB flow meter. For this purpose, a fast response pressure transducer (*Kulite B57*) was flush mounted just upstream the vortex flow meter module, whereas the same pipe

module used for the Pitot tube measurement, was located just downstream the meter. Finally a temperature module was placed downstream the Pitot tube pipe module. From these measurements of the pressure upstream and downstream the device as well as the stagnation pressure and temperature, an "average" fluid density at the location of the vortex meter was estimated.

To exemplify the worst case scenario for the density determination we considered the highest flow rate which was 215 g/s. In this case the pressure drop was about 12 kPa between the two pressure taps, with an upstream pressure of 160 kPa. Assuming isentropic conditions in the flow between the pressure transducers would give a density difference of about 6% between the two pressure tap locations. To obtain the mass flow rate, the average pressure and the stagnation pressure measured by the Pitot tube were used to determine the local Mach number. The temperature was then determined from the energy equation by knowing the Mach number and the stagnation temperature. The density was thereafter obtained using the perfect gas law.

2.5. *Turbine flow meter*

The turbine flow meter used in the experiment is of type *GL-FL3* from *GL Flow*, which is a commercial volume flow meter used e.g. to measure the flow of natural gas. The set-up for this meter was similar to that of the vortex flow meter. However, the diameter of the measurement section of the turbine flow meter is 40 mm. The difference in diameter between the upstream piping and the turbine flow meter was adjusted with a short smooth convergent pipe section. To estimate the mass flow rate an average density of the gas was estimated in a similar way as for the vortex flow meter, described in section 2.4. However in this case the pressure difference across the meter is much larger, at 215 g/s the pressure upstream the meter was 191 kPa and the pressure drop 41 kPa. Of course, this increases the uncertainty in the determination of the density to be used when calculating the mass flow rate.

During pulsating conditions the output from the turbine flow meter was constant, and the variable mass flow rate under pulsating conditions was determined from the density variations obtained from the pressure and temperature measurements.

3. Results

In this section we describe the measurements carried out with the different flow meters, both under steady and pulsating flow. Some of the flow meters were calibrated in-house before their use. This is done under well known steady conditions with the use of the ABB reference flow meter, thereby establishing a relation between the flow meter output and the real flow rate. This relation is then assumed to be valid and is employed under pulsating flow conditions.

3.1. *Venturi flow meter*

Here, we present steady and pulsating measurements with the venturi flow meter obtained from Volvo as described in Sec. 2.1. The steady flow measurements were made using a differential pressure transducer between the pressure tap at the upstream wide section and the section having the smallest cross section area. For the pulsating flow two absolute pressure transducers were used to measure the upstream and downstream pressures.

3.1a. *Stationary flow.* For stationary flow through constriction flow meters, such as the venturi flow meter, the estimation of the mass flow rate can be done in several ways. One way is to assume incompressible and isentropic flow and to apply corrections for the compressibility as described in the ISO standard ISO-5167 (2003).

However in many applications this will not give reliable results and here we will analyze the flow meter using the compressible flow equations described in the following.

It shall also be mentioned that the venturi flow meter can be run in two different regimes, i.e. non-choked and choked conditions, respectively. Under choked conditions the Mach number reaches unity at some position along the venturi (at the smallest section from a gas dynamic point of view). The behaviour in the two regimes are quite different as will be shown below. For the venturi the outlet in the present set-up is connected directly to the atmosphere. This makes the outlet pressure equal to the atmospheric one, whereas the flow rate is changed by changing the inlet pressure.

From the measured data it is possible to calculate the mass flow rate through the venturi from the isentropic relations. The mass flow rate is given by the conservation of mass

$$\dot{m} = \rho A u \,. \tag{1}$$

It can be rewritten in terms of pressure, Mach number and total temperature to yield

$$\dot{m} = \frac{p_1 A_1 M_1}{\sqrt{RT_0}} \sqrt{\gamma \left(1 + \frac{\gamma - 1}{2} M_1^2\right)}. \tag{2}$$

The Mach number at the upstream cross section M_1 can be obtained from

$$M_1^2 = \frac{2}{\gamma - 1} \left[1 - \left(\frac{p_2}{p_1}\right)^{(\gamma-1)/\gamma}\right] \left[\left(\frac{A_1}{A_2}\right)^2 \left(\frac{p_2}{p_1}\right)^{-2/\gamma} - 1\right]^{-1} \tag{3}$$

since the pressures p_1 and p_2 are measured and the area ratio A_1/A_2 is known. For more details regarding the derivation of these equations, see Laurantzon (2010).

In order to illustrate the behavior of the venturi meter 10 different mass flow rates ranging from 0 g/s to slightly above 200 g/s were used for the stationary measurement. This flow range includes both non-choked (7 measured points including zero flow rate) and choked conditions (3 measured points).

The measured mass flow rate is plotted as function of the pressure difference $\Delta p = p_1 - p_2$ in Fig. 3(a), where p_1 is measured upstream the venturi contraction and p_2 is measured in the middle of the (geometrically) smallest section. Together with the measured data the calculated mass flow rates from Eq. (2) are also plotted in the figure. As can be seen there exist two different regimes, one up to a pressure difference of about 40 kPa and another above that value. In the first regime the mass flow rate increases almost parabolically with the pressure difference, which is what is expected for incompressible flow. In the upper regime there is a linear trend with increasing pressure. For choked flow we would expect the flow rate to increase linearly with the stagnation pressure which is reflected as the linear trend in the Fig. 3(a).

The agreement between the calculated values and the measured mass flow rates are overall good, however at small pressure differences there are some discrepancies which probably are related to increased uncertainties at low pressure differences. At high pressure ratios (in the choked regime) the calculated values are higher than the measured by 1.2 to 1.7 %.

In Fig. 3(b) the mass flow rate is instead plotted as function of the pressure ratio p_2/p_1, together with the theoretically obtained results (based on the measured area and pressure ratios). The choked flow regime is now clearly seen around a pressure ratio of 0.62. From the isentropic relationships we know that at the critical condition[1] the pressure ratio $p^*/p_0 = 0.528$ which is smaller than the measured pressure ratio. However $p_1 \approx 0.98 p_0$ based on the inlet Mach number $M_1 = 0.15$, but does not explain the large difference. The obvious conclusion is that the measured pressure at the throat is not at the smallest, in a gas dynamic sense, section. Thus, the air at the second pressure tap is not at the critical condition, but at a Mach number less than unity, and the flow is further accelerated in the straight part of the nozzle until it reaches the critical condition.

As the upstream pressure is increased the flow rate increases, and the Mach number at the venturi throat will reach unity for a high enough difference pressure (or rather pressure ratio). The mass flow rate then becomes a linear function of the stagnation pressure. This feature is apparent for the three last points in Fig. 3(a), where the linear dependence between mass flow rate $\dot{m}$ and

[1]The critical condition is the reference state where the flow is sonic. Critical conditions will be denoted with an asterisk.

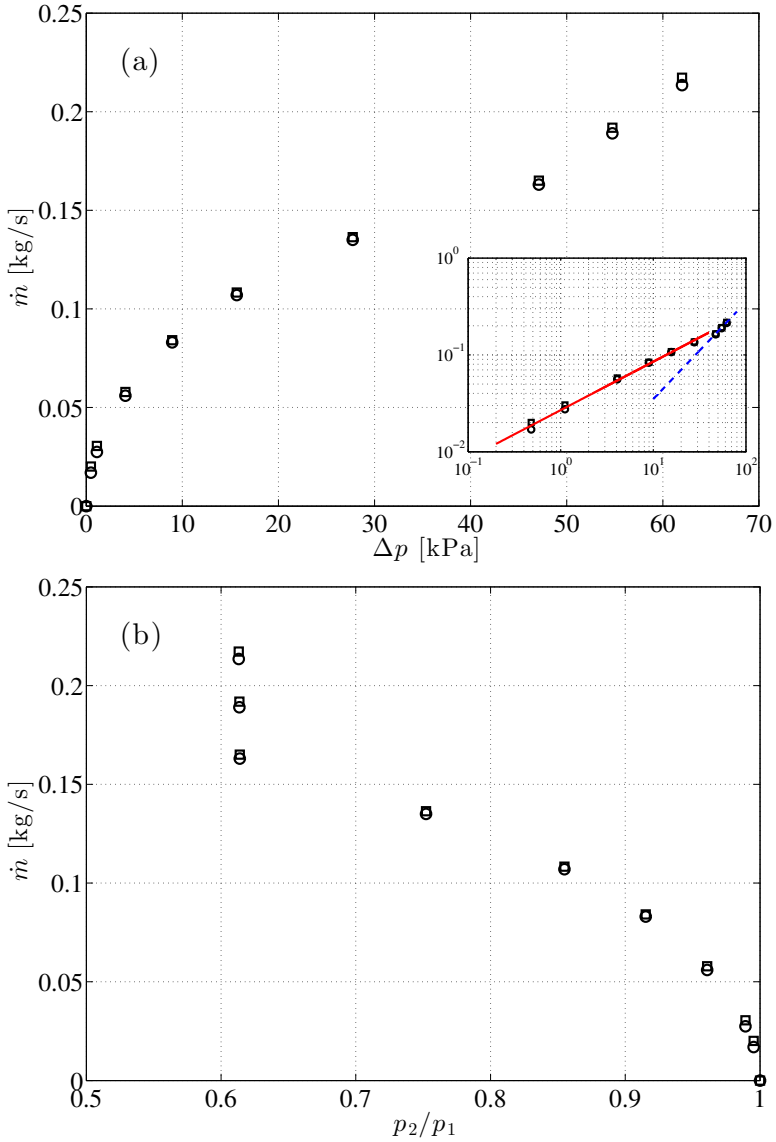

FIGURE 3. Mass flow rate for the venturi flow meter for stationary flow as function of (a) the pressure difference $\Delta p = p_2 - p_1$, (b) the pressure ratio p_2/p_1. □: Calculated flow rates from measured flow data and venturi geometric data. ○: Mass flow rate according to the ABB reference flow meter. The data from (a) is also shown in the insert as a log-log plot, where a square (solid) and linear (dashed) fit are made.

the difference pressure Δp is apparent[2]. The expression for the mass flow rate under choked nozzle flow conditions is

$$\dot{m} = \frac{p_0 A^*}{\sqrt{RT_0}} \sqrt{\gamma \left(\frac{2}{\gamma + 1} \right)^{(\gamma+1)/(\gamma-1)}}. \tag{4}$$

If we instead write it as function of p^*, the above relation can be rewritten to obtain

$$\dot{m} = \frac{p^* A^*}{\sqrt{RT_0}} \sqrt{\frac{\gamma(\gamma + 1)}{2}}. \tag{5}$$

If we again consider Fig. 3 we find that the mass flow rate obtained with the venturi deviates from the reference flow meter with a maximum of about 2%, and hence the theory gives a fairly good estimate of the flow rate. For the three largest flow rates for which the flow is choked, the Mach number M_1, based on the pressure and area ratios p_2/p_1 and A_1/A_2, respectively, is calculated to 0.156. In turn, this Mach number implies that $M_2 = 0.882$. Furthermore, the measured pressure ratio p_2/p_1 at choked flow is 0.614, whereas it becomes 0.537 if the isentropic relation

$$\frac{p_2}{p_1} = \frac{p_2/p_0}{p_1/p_0} = \left(\frac{1 + \dfrac{\gamma - 1}{2} M_1^2}{1 + \dfrac{\gamma - 1}{2} M_2^2} \right)^{\gamma/(\gamma-1)} \tag{6}$$

is employed. This result together with the fact that the pressure is measured at the middle of the throat section, suggests that the flow becomes sonic further downstream at the end of the throat section. This hypothesis is substantiated by the analysis in Appendix A.

3.1b. *Pulsating flow.* The response of the venturi flow meter to pulsating flow was investigated at two mass flow rates, i.e. 80 g/s and 130 g/s. For 80 g/s the frequency of the pulsating flow ranges from 10 up to 80 Hz in steps of 10 Hz, whereas for 130 g/s, measurements were made at pulse frequencies of 40, 60 and 80 Hz. As mentioned before, for the pulsating flow cases the pressures p_1 and p_2 were measured directly with an absolute pressure transducer mounted directly on the pressure tap.

The estimation of the mean mass flow rate under pulsating conditions can be done in two ways. One possibility is to calculate the mean pressures of

[2] Δp is in fact linearly proportional to p_0 at choked conditions.

p_1 and p_2 and thereafter determine a mean Mach number M_1 from Eq. (3). This will however in our cases, lead to drastic overestimation of the flow rate. The other possibility is to assume that the flow is quasi-steady, and to employ Eq. (3) at each time instant to calculate the instantaneous value of M_1. In this way, the time resolved mass flow rate can be obtained from Eq. (2), and the mean value of the time varying quantity can be determined. These two method are compared in Table 1.

Method	10 Hz	20 Hz	30 Hz	40 Hz	50 Hz	60 Hz	70 Hz	80 Hz
Mean (80)	1.365	1.387	1.500	1.395	1.210	1.108	1.177	1.073
Inst. (80)	1.023	1.062	1.092	1.052	1.001	1.013	1.007	1.016
Mean (130)	-	-	-	1.129	-	1.087	-	1.116
Inst. (130)	-	-	-	1.034	-	1.020	-	1.049

TABLE 1. Mass flow rate estimation (normalized with the reference mass flow rate of 80 and 130 g/s respectively) for the two methods, where "Mean" denotes the method where the flow rate is determined from the mean values of the pressures, whereas for "Inst." the time resolved mass flow rate is used to determine the mean mass flow rate.

From the results in Table 1, one can conclude that it is preferable to obtain the mean mass flow rate after the instantaneous mass flow rates are calculated. This is a consequence of the so called square root problem, easiest illustrated through the inequality

$$\frac{1}{T}\int_0^T \sqrt{\Delta p}\; dt \leq \sqrt{\frac{1}{T}\int_0^T \Delta p\; dt} \tag{7}$$

The largest deviation from the reference flow meter is about 9% if the mean value is determined as an average of the time resolved signal, whereas it deviates as much as 50% if the average of the pressure is taken and the mean value calculated from that.

To fully appreciate how the pressures p_1 and p_2, the stagnation temperature T_0, the pressure ratio p_2/p_1, mass flow rate $\dot{m}$ as well as the Mach numbers M_1 and M_2, varies under the pulsations, these quantities are shown phase-averaged in Fig. 4 for one flow case. It should be noted, that the pressures and the (stagnation) temperature are measured, whereas the mass flow rate and Mach numbers are calculated based on these measurements.

In Fig. 4 one observes that during part of the pulse cycle the pressures p_1 and p_2 are almost identical which implies that the flow rate is close to zero. One can also see that there is a plateau in the Mach numbers M_1 and M_2 that indicates that the flow is choked. According to the stationary case (cf. Fig. 3),

choking occurs approximately at a mass flow rate of $\dot{m} \approx 0.15$ kg/s which seems to be the case also here. Hence the assumption of quasi steady flow seems to be appropriate. Also for this case we observe that M_2 at choking is less than unity, again implying that critical conditions are reached further downstream. The temperature variation during the pulsation is about 13 K and the lowest temperatures are seen at low flow rates.

In Fig. 5, the rest of the flow cases are collected for all pulse frequencies at 80 g/s where Fig. 5(a) shows the phase average of the mass flow rate. Here one can see that the pulse shape is altered when the pulse frequency is increased. One also observes that the flow does not reach choking conditions. An interesting aspect is that the number of pulsations recorded in the mass flow rate is twice that of the pulse frequency, for the two highest pulse frequencies. The reason for this is not clear, but is probably due to pulse reflections in the system and needs to be investigated further. Fig. 5(b) shows the probability density function (pdf) for the mass flow rate. One can observe that the concentration of the pdf at low flow rate, for f_p at 20–50 Hz can be an indication of back flow, since also the mean mass flow rate is slightly overestimated in these cases.

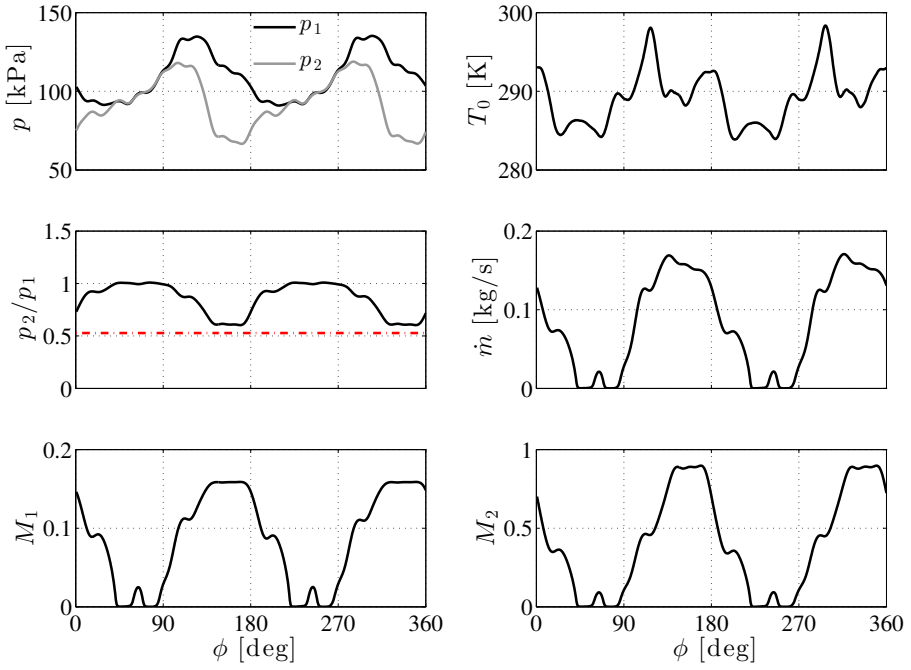

FIGURE 4. Phase averaged venturi flow meter data at 80 g/s and 40 Hz pulse frequency.

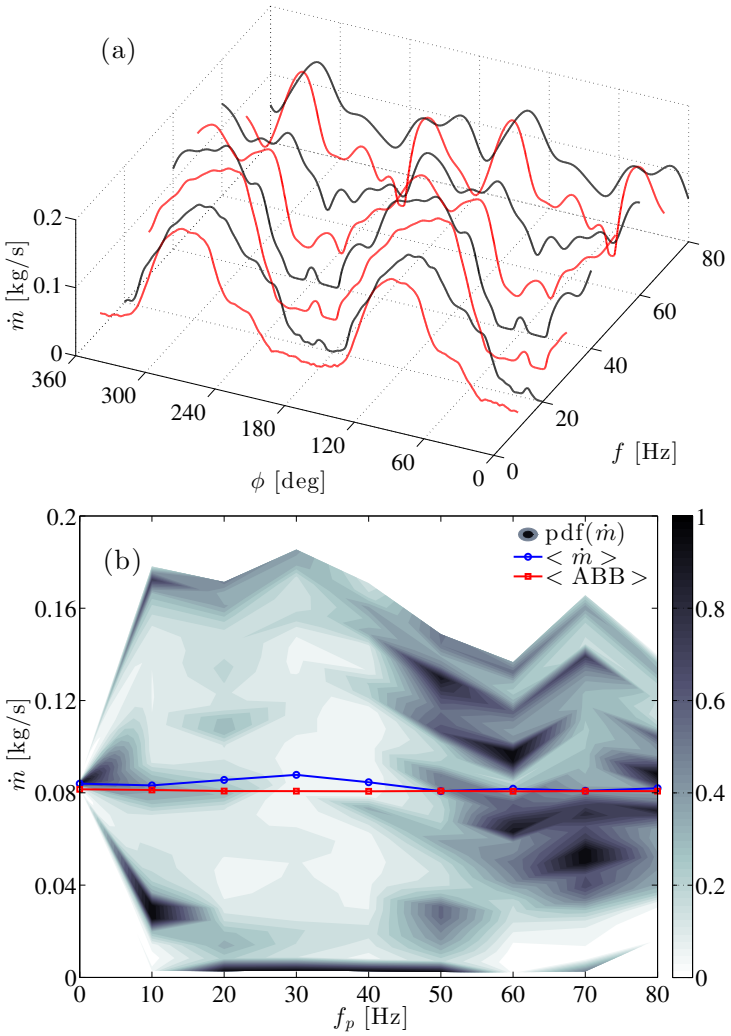

FIGURE 5. The mass flow rate for different pulse frequencies at 80 g/s mean flow rate. (a) Phase averaged flow rate (with alternating line color to enhance the visibility). (b) Probability density function, normalized with its maximum value.

Moreover, from the pdf, it is apparent that a large range of the flow rate is captured by the technique for all pulse frequencies.

3.2. *Hot-film flow meter*

3.2a. *Stationary flow.* The hot-film flow meter was first calibrated under steady flow conditions and thereafter tested under pulsating flow conditions. Typical steady flow calibrations of the hot film are shown in Fig. 6. It shows an acceptable adherence to King's law but in this case it is directly calibrated against the mass flow rate such that

$$E^2 = A + B\dot{m}^n \tag{8}$$

where A, B and n are all least square fitted to obtain the best agreement with the calibration points. For the employed meter A is very close to E_0^2, i.e. the voltage at zero mass flow rate, but the exponent n is 0.67 which is substantially higher than the original value in King's law. However one should remember that King's law is valid for an infinitely long cylinder. In the experiment the meter was oriented in both the standard flow direction and in the reverse direction, in order to determine if the signal is different under possible back flow. As can be seen in Fig. 6, the curves almost collapse, indicating that the output signal is rather independent of the flow direction.

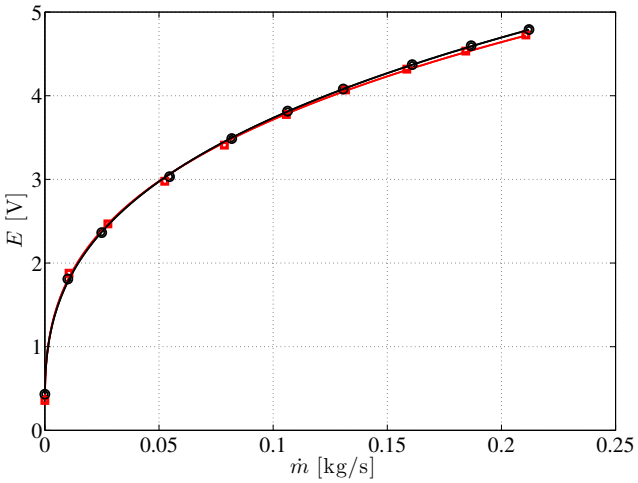

FIGURE 6. Hot film calibration curves for the Scania hot-film meter. Measured points with the meter oriented in its flow direction (circles). Measured points with the meter oriented in the reverse direction (squares). Solid lines represent Eq. (8) fitted to the data.

3.2b. *Pulsating flow.* Here results are presented for the case with a mean flow rate of 80 g/s and pulse frequencies ranging from 4 to 80 Hz. Similar results

were also obtained for 130 g/s but these are not presented here. The results for 80 g/s are shown in Fig. 7 where the mean mass flow rate as well as the fluctuations around the mean in terms of the pdf are given as function of the pulse frequency.

For low pulse frequencies a large span of values are seen in the pdf, indicating that the hot-film is fully able to resolve the pulsations in the flow. The average value is also close to that measured by the system flow meter, i.e. 80 g/s. The span of the fluctuations gradually decreases to 20 g/s even though the average value is still consistent with that of the system flow meter. However in the range of 30–50 Hz the hot-film overestimates the mean flow rate considerably, whereas at higher frequencies (≥ 60 Hz) it falls back to the actual value. Another observation is that the span of the mass flow rate fluctuations decreases as the pulse frequency increases, which may be expected since the frequency response of the hot-film system is rather limited.

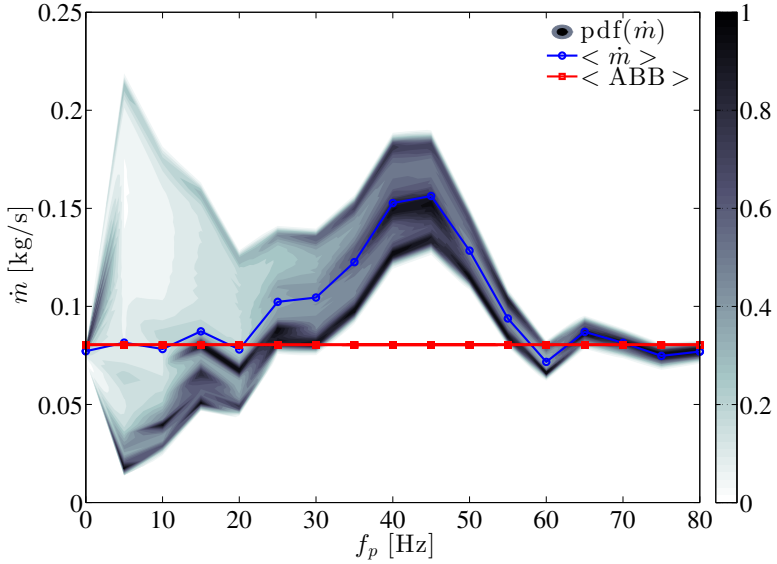

FIGURE 7. Mass flow rate measurements with the hot-film flow meter. The estimated mass flow plotted against pulse frequency together with the pdf showing the pulsation range. Mean mass flow rate obtained from the hot film (blue), reference mass flow rate (red).

3.3. *Pitot tube*

A possibility to measure the flow rate in both stationary and pulsating (under the assumption of quasi-steadiness) flow is to use a Pitot tube immersed in the

flow to determine the stagnation pressure (p_0) combined with measurement of the static pressure (p) at the wall. From these values the Mach number at the position of the probe can be determined. The mass flow rate is determined from

$$\dot{m} = C\frac{pAM}{\sqrt{RT_0}}\sqrt{\gamma\left(1+\frac{\gamma-1}{2}M^2\right)}, \tag{9}$$

where the Mach number is determined from the isentropic relation i.e.

$$\frac{p_0}{p} = \left(1+\frac{\gamma-1}{2}M^2\right)^{\gamma/(\gamma-1)}. \tag{10}$$

A is here the pipe cross section area at the position of the Pitot tube. The stagnation temperature T_0 also needs to be measured. C is a parameter that takes into account that the velocity measured by the Pitot tube is not the average velocity across the pipe section. For fully developed turbulent profiles, the ratio of average u_m to maximum (centerline) velocity u_c is given by a power law velocity distribution

$$\frac{u_m}{u_c} = \frac{2n^2}{(n+1)(2n+1)}, \tag{11}$$

where the parameter n is a function of the Reynolds number Re, see e.g. Benedict (1980). For Reynolds numbers typical of the present study $n = 7$ giving $u_m/u_c = 0.82$. The parameter C should correspond to the ratio in Eq. (11). In order to take this into account the set-up can be calibrated against the system mass-flow meter to determine C under steady conditions. However, under pulsating conditions one has to assume that the ratio between the instantaneous Mach number obtained from the Pitot tube and the cross section averaged Mach number is the same.

In order to find the mass flow rate under pulsating conditions it is necessary to make time resolved measurements of both the static pressure as well as the stagnation pressure. To do so in the present experiments the pressure transducers were mounted directly on the probe tubing for the Pitot tube and directly at the wall tap for the static pressure measurements.

3.3a. *Stationary flow.* The measurements under stationary conditions, were mainly done in order to calibrate the mass flow rate obtained from the Pitot tube against the reference mass flow meter. Since the Pitot tube measures

the total pressure at the centerline, and the *bulk velocity* is in general lower than the centerline velocity, the mass flow estimated with the Pitot tube will overestimate the flow rate. Hence, this ratio has to be determined by means of the calibration. As is shown in Fig. 8, the mass flow rate obtained from the Pitot tube measurements overestimates the actual flow rate with approximately 14%. The linear dependence between the two methods indicates that the parameter C in Eq. (9) is independent of flow rate in the stationary case. However this percentage is quite much lower than obtained from Eq. 11 and is probably due to the fact that the profile is not fully developed and is therefore more of a top-hat profile as compared to the fully developed one.

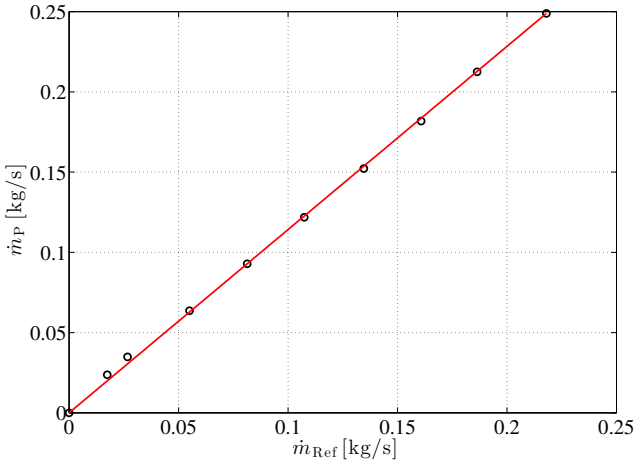

FIGURE 8. The mass flow rate obtained with the Pitot tube vs. the reference ABB flow meter. The solid line is a linear fit to the data.

3.3b. *Pulsating flow.* The pulsating flow measurements were performed at the same flow rates and pulse frequencies as for the venturi flow meter. The stagnation and static pressures p_0 and p were both sampled at 10 kHz, but had to be low-pass filtered afterwards due to the high frequency noise content in the signal due to a Helmholtz resonance (see Appendix B). To obtain the flow rate the pressure signals are first sampled and phase averaged individually and the pressure ratio p_0/p was calculated from the phase averaged signals. From the pressure ratio the Mach number is calculated and together with the static pressure and stagnation temperature the mass flow rate is calculated using Eq. (9). Here it is assumed that the ratio between the instantaneous mass flow rate and that measured by the Pitot tube i.e. parameter C is the same in the stationary and the pulsating flow. It was observed that for short periods, when the flow was rapidly accelerating, the recorded pressure ratio was less than unity, which

of course is not possible physically, but can be due to a time lag in the Pitot tube measurements. For these periods the pressure ratio was set to zero, i.e. the Mach number and thereby also the flow rate were both set to zero.

In Fig. 9, the measured quantities p_0, p as well as the pressure ratio p_0/p and the measured stagnation temperature T_0 are plotted together with the calculated M and $\dot{m}$. For the 40 Hz pulsation case one peak in pressure and mass flow can be seen for each pulse from the pulse generator. In this case one can see that the pressure ratio becomes less than one for a short period, and during that period the Mach number and mass flow are set equal to zero. By averaging the mass flow rate one obtains a flow rate which overestimates the reference value of 80 g/s by 7.7%.

The phase averaged mass flow rate for all pulse frequencies can be seen in Fig. 10(a). The tendency is that the flow situation becomes more complicated, the higher the pulse frequency. The reason for the multiple peaks in the flow rate for higher frequencies is probably due to reflections in the pipe system, however this needs to be further investigated. Considering e.g. the "worst" case at 80 Hz pulse frequency, averaging the mass flow rate here gives in contrast to the 40 Hz case, an underestimation of the flow rate by 8.3%. One can also

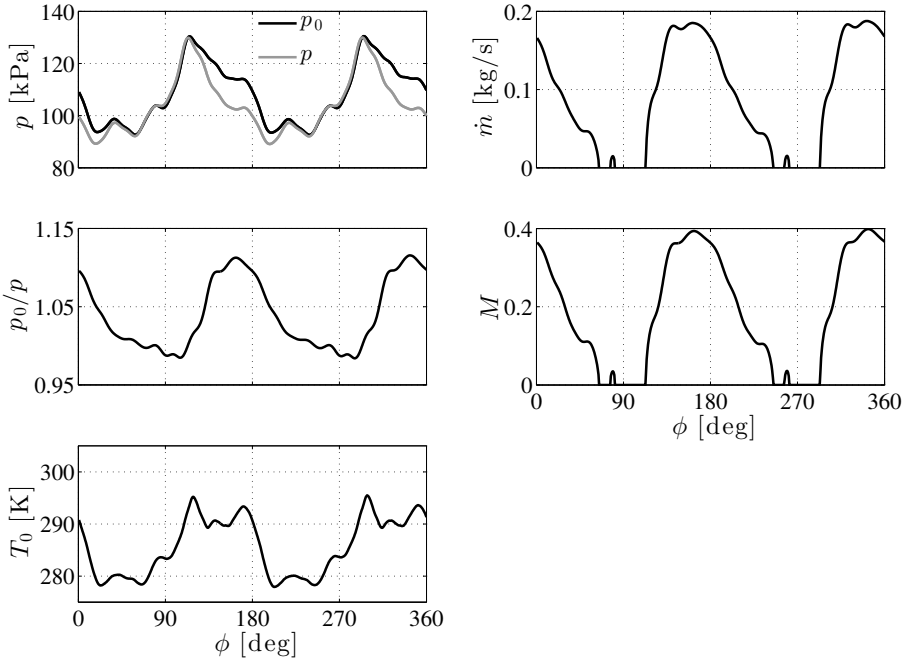

FIGURE 9. Pitot tube measured phase averaged quantities at 80 g/s flow rate and 40 Hz pulse frequency.

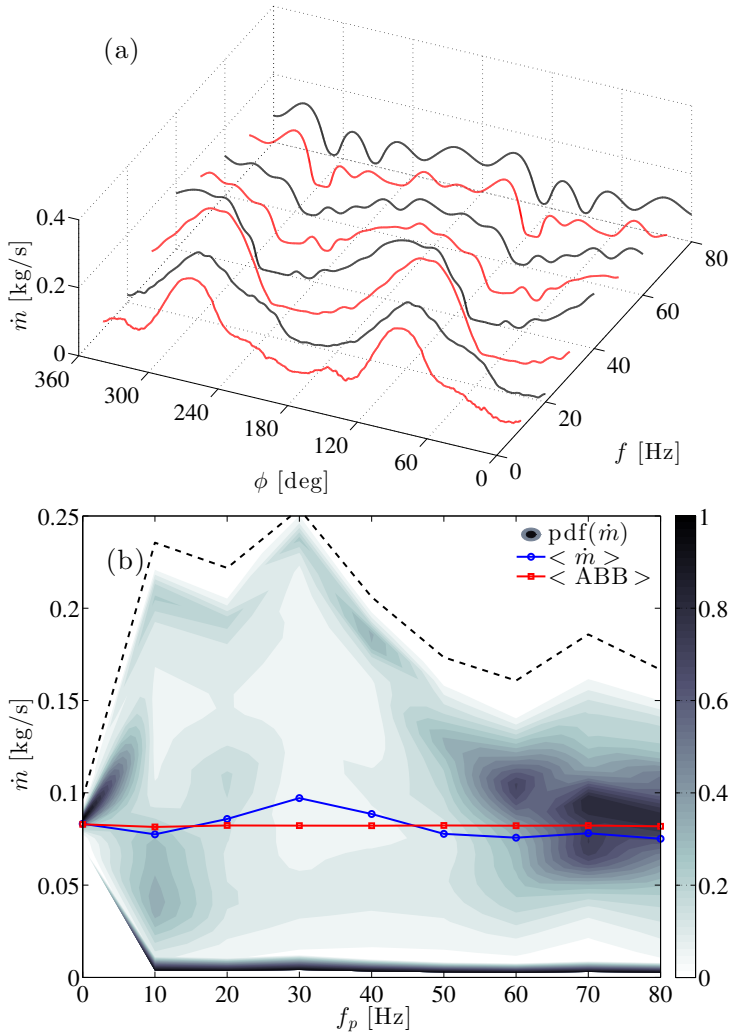

FIGURE 10. Pitot tube mass flow rate variations for different pulse frequencies. (a) Phase averaged data (with alternating line color to enhance the visibility). (b) Pdf of the time signal. The dashed line represents the upper mass flow rate limit observed for the pdf.

notice in Fig. 10(b) that the flow rate is overestimated in the cases where the pdf is accumulated towards low flow rates, thus indicating back flow. The reason for the underestimation of the flow rate for pulse frequencies above 40 Hz is

probably due to the factor C, which should be higher in pulsating flow, since the velocity profile usually is flatter in pulsating flow as compared to stationary.

3.4. *Vortex and turbine flow meters*

The measurements performed with the vortex and the turbine flow meters were done both in stationary and pulsating flow. These flow meters respond to the velocity and are therefore in principle sensitive to the volume flow. As shown below this is confirmed by the measurements, so in order to compare with the reference mass flow meter, the density of the gas at the flow meter for each flow rate needs to be determined. The output voltage signals are averaged in the microprocessor of the meters and therefore the output does not show any variations in time for the pulse frequencies used here.

3.4a. *Stationary flow.* Two similar steady tests were conducted for both the vortex and the turbine flow meter. One with the outflow direct to the laboratory and the other with a regulating valve at the outflow such that the pressure in the measuring section could be increased and thereby also the gas density. This was done in order to verify that the flow meter responds to the volume flow. 10 mass flow rates were used, starting at 0 g/s going up to about 215 g/s. However for the three lowest flow rates the vortex flow meter does not register any flow. For the non-pressurized case the pressure downstream the flow meter varies between 0 and 50 kPa above ambient, whereas for the pressurized case it is kept at 100 kPa above ambient.

The measurements for the turbine flow meter and the vortex flow meter under pressurized and non-pressurized conditions are given in Fig. 11. The output is fairly linear with the flow rate, and as can be seen the pressurized and non-pressurized measurement points seem to collapse on the same line, hence showing that the flow meters respond to the volume flow rate and that the output is independent of the density. One can notice from the plot that the squares (representing non-pressurized flow), are shifted upwards to a higher volume flow rate compared to the circles (representing pressurized flow). This is obviously due to the fact that for a given mass flow rate, the volume flow rate will increase if the density is lowered.

3.4b. *Pulsating flow.* In pulsating flow the output from both meters did not show the pulsations but was steady. The instantaneous mean density is estimated with pressure measurements upstream and downstream the devices, together with measurements of the stagnation pressure and temperature downstream the flowmeters. If one first considers the turbine, for the low frequencies the turbine flow meter shows too high values[3], but for the higher frequencies one obtains values that are within ±1% of the value obtained from the system

[3]The overregistration of flow rate for the turbine flow meter in pulsating flow is a well known problem (McKee 1992).

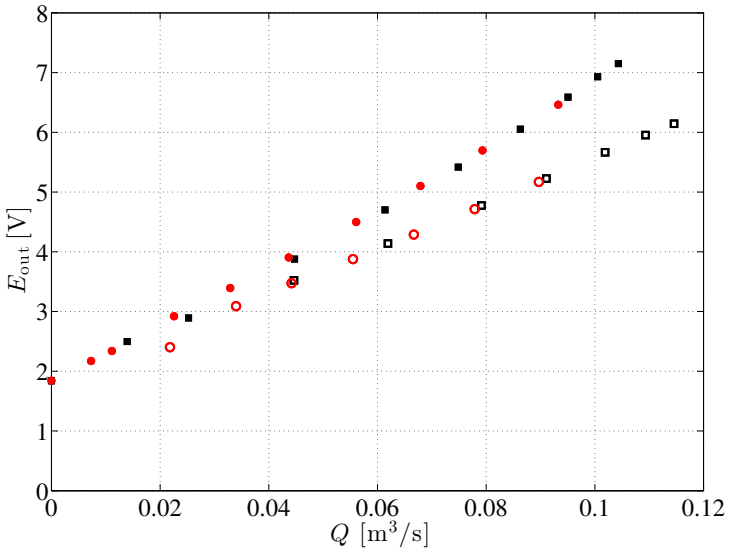

FIGURE 11. Output from the turbine flow meter (filled symbols), and the vortex flow meters (open symbols) as function of the volume flow rate. ○: Pressurized flow. □ Non-pressurized flow.

mass flow meter. The averaging process of the vortex flow meter gives fairly accurate results for all pulse frequencies as shown in Sec. 4. A summary of all pulsating flow results is given in Sec 4

4. Summary

This section summarizes the behavior of the flow meters in pulsating flow in Table 2. Furthermore, it should be emphasized that these values depend on how the averaging procedure is done. All values in the table are obtained by averaging the time resolved output from the venturi, Pitot and hot-film flow meters as well as the time resolved measurements of pressure and temperature. The latter quantities are needed in order to obtain the density of the gas at the position of the vortex and turbine flow meters.

The worst results are obtained for the hot-film flow meter in the range 30-50 Hz. As shown in Appendix C there is quite a large time period where there is reverse flow (back-flow) for this frequency range. The hot-film flow meter rectifies the signal for reverse flow which then gives an overestimate of the flow rate and therefore a substantial error.

The turbine flow meter shows a substantial overestimate of the flow rate for low frequencies. This is probably because of the well known phenomenon that the turbine meter accelerates more rapidly than it decelerates. However

at high pulsating frequencies its inertia will make it rather insensitive to the pulsations.

For high pulsation frequencies, where there is no back flow, one may in general say that all flow meters give rather good results.

TABLE 2. Mean mass flow rate for different flow meters at pulsating conditions and at the reference rate ~ 80 g/s[1]. The flow rates are normalized with the reference flow meter.

Flowmeter	10 Hz	20 Hz	30 Hz	40 Hz	50 Hz	60 Hz	70 Hz	80 Hz
Venturi	1.02	1.06	1.09	1.05	1.00	1.01	1.00	1.02
Pitot	0.95	1.04	1.18	1.07	0.95	0.92	0.95	0.92
Hot-film	0.98	0.97	1.29	1.89	1.63	0.92	1.12	1.00
Vortex	0.98	0.99	1.08	1.01	0.97	1.00	0.97	1.00
Turbine	1.24	1.21	1.18	1.07	1.03	1.00	1.01	1.00

[1] The deviation from this value is for all cases less than 3%.

Acknowledgement

This work was carried out with CCGEx, a competence centre sponsored by the Swedish Energy Agency, Swedish vehicle industry and KTH.

Appendix A - Flow rate through the venturi nozzle at choked conditions

The throat of the venturi nozzle used in this study is not distinct, but has some distance of "more or less" constant cross section area. Assume that the flow in the throat section, from the second pressure tap to the end of the throat, where we assume that the Mach number is unity (denoted as location 3), develops according to adiabatic one-dimensional flow theory with friction (so called Fanno-flow, see for instance Anderson (2002)). This distance is short and is of the order of the throat diameter. Consider the relation

$$\frac{4fL}{D} = \frac{1 - M_1^2}{\gamma M_1^2} + \frac{\gamma + 1}{2\gamma} \ln\left[\frac{(\gamma + 1)M_1^2}{2 + (\gamma - 1)M_1^2}\right]. \tag{12}$$

If $L \simeq D$ then the ratio $4fL/D$ becomes 0.02, assuming that the friction factor $f = 0.005$. This corresponds to a Mach number of about 0.88, which is close to what we estimated in section 2 from the measured pressure ratio.

Furthermore, using the Fanno flow theory, we can express the pressure ratio in terms of Mach numbers as

$$\frac{p_2}{p_1} = \frac{M_1}{M_2}\sqrt{\frac{2 + (\gamma - 1)M_1^2}{2 + (\gamma - 1)M_2^2}}. \tag{13}$$

It is possible to obtain a general expression for the pressure ratio between the pressure at Mach number M and the pressure at critical condition by substituting $M_2 = 1$ and M_1 to just an arbitrary Mach number M, with the corresponding pressures p^* and p respectively, to become

$$\frac{p}{p^*} = \frac{1}{M}\sqrt{\frac{\gamma + 1}{2 + (\gamma - 1)M^2}} \tag{14}$$

If the Mach number is 0.88 Eq. 14 shows that the pressure ratio $p/p^* = p_2/p_3$ is about 1.16. With the previous measured and estimated values we have that $p_2/p_1 = 0.614$ and $p_3/p_1 = 0.537$ and hence, $p_2/p_3 = 0.614/0.537 = 1.14$, showing a good agreement with the theoretical pressure ratio.

Appendix B - The Helmholz resonator

It was noted that the signal from the Pitot tube showed a high frequency component at a certain, more or less, fixed frequency for different flow rates and pulse frequencies. This implies that it is not coupled to the flow, but to something else. This phenomenon only occurred for the transducer connected to the Pitot tube. Thus, a hypothesis was that the Pitot tube connection between the transducer and the tube functioned as a *Helmholtz resonator*. The resonance in a pressure transmitting tube-cavity combination is a well known phenomenon (see e.g. Sieverding *et al.* 2000). The Helmholtz eigenfrequency

f_r is given by

$$f_r = \frac{a}{2\pi}\sqrt{\frac{A_t}{LV}}, \tag{15}$$

where a is the speed of sound, A_t is the throat cross section area, L is the length of the throat and V is the volume of the cavity.

In order to investigate if the Pitot tube system acts as a Helmholtz resonator, a qualitative analysis of the response from the pressure transducer was performed. For this analysis, measurements at stationary conditions were performed when the pressure transducer was screwed in the bottom of its thread. The distance between the face of the pressure transducer and the Pitot tube gives rise to a cylindrical cavity volume with an estimated height of 0.5 mm and with the diameter of the pressure transducer, which is 13 mm. Together with the length of the Pitot tube $L = 44$ mm and the cross section diameter of the Pitot tube $D_t = 1.8$ mm, the resonance frequency can be determined from Eq. (15) to about 1.6 kHz. A spectrum obtained from the time signal of the pressure transducer connected to the Pitot tube can be seen in the top plot of

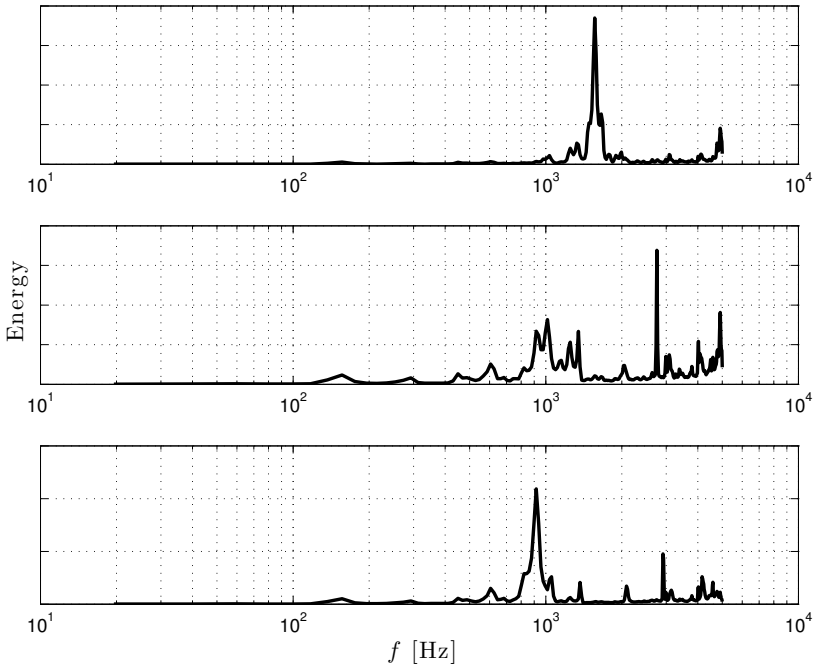

FIGURE 12. Pre-multiplied spectrum from three cases of chamber size, to test the hypothesis of a Helmholtz resonator. The chamber volume increases from the top to the bottom plot.

Fig. 12, where most of the energy is concentrated to about 1.55 kHz. The two lower plots are obtained when the pressure transducer was unscrewed in two steps, i.e. the cavity volume was increased in two steps. This would, according to Eq. (15), imply a lower resonance frequency, which also can be observed from the spectra. Hence the hypothesis that the high frequency content of the Pitot tube signal is due to a Helmholz resonance seems to be confirmed.

Appendix C - LDV measurements to assess flow reversal

Since flow reversal is a frequent phenomenon in pulsating flows and most utilized flow measurement techniques cannot determine the flow direction, laser Doppler velocimetry (LDV) was used to assess whether back flow occurs or not. In the following an analysis of the flow characteristics at the position of the hot-film flow meter will be done, in order to show why the over-prediction in flow rate for this device was prevalent only for certain pulse frequencies (cf. Sec. 3.2b).

LDV measurements were carried out at the pipe centerline both inside the pipe and at the pipe outlet. For these measurements the PVC pipe was replaced with a Plexiglas pipe with the same dimensions but without the hot-film sensor. The result from the measurements at the pipe outlet can be seen as solid lines in Fig. 13. Here a substantial amount of back flow can be observed at 40 and 50 Hz. On the other hand the velocity always seems to be positive at 10, 70 and 80 Hz pulse frequency.

Since the flow pulsations within the pipe may change with the position due to reflections at the end of the pipe, it was deemed necessary to also measure at the position of the hot-film sensor. These measurements are shown in the right column of Fig. 13, together with the measurement at the pipe outlet. It is evident that large back flow occurs for those frequencies that give rise to the largest deviation in mass flow estimation, for the hot-film measurements. At the two lowest frequencies, i.e. 20 and 40 Hz there is a strong correspondence between the measurements at the outlet and inside the pipe, whereas for the higher frequencies the signals seems to be partly out of phase.

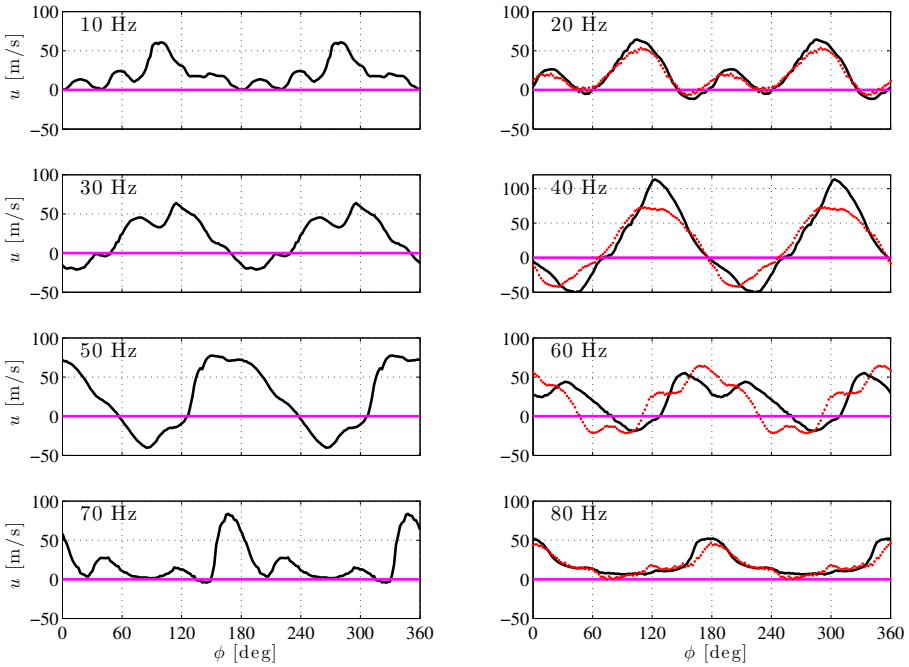

FIGURE 13. The phase averaged velocity, measured by LDV at the pipe outlet (black solid), and at the glass section (red dotted). The horizontal line is for visual aid.

Manipulation of the LDV signal

Since the utilized hot film has a certain upper frequency limit (~ 30 Hz), it will function as a low pass filter. The LDV time signal is assumed to describe the true velocity variation during the pulses. Hence it should be possible to let the LDV signal u_{LDV} be an input to a linear time invariant system and obtain the hot-film signal $\dot{m}_{HF}$ as an output. Since the LDV gives the velocity its corresponding mass flow rate will be estimated from the mass flow rate of the hot film. Due to this, the analysis will be of qualitative nature. If we assume that the hot-film responds with a system time delay τ, and that it to a first approximation can be described as a first order system, we can write

$$\dot{m}(t)_{LDV} = \dot{m}(t)_{HF} + \tau \frac{\partial[\dot{m}(t)_{HF}]}{\partial t}. \tag{16}$$

Taking the Fourier transform $\mathcal{F}$, of the above equation, we obtain the linear system

$$Y(\omega) = H(\omega)X(\omega), \tag{17}$$

where the input $X(\omega)$ is the transform of $\dot{m}_{LDV}$, the output $Y(\omega)$ simulating $\dot{m}_{HF}$ and $H(\omega) = 1/(1 + i\omega\tau)$ is the system transfer function. The simulated output is then obtained as

$$y(t) = \mathcal{F}^{-1}(Y(\omega)). \tag{18}$$

However, since the hot film senses the magnitude of the flow rate, irrespectively of the flow direction, as concluded from Fig. 6, we shall use the absolute value of $\dot{m}(t)_{LDV}$, to get $X(\omega)$. In Fig. 14, the LDV signal together with its absolute value is plotted together with the true output from the hot film and the simulated output $y(t)$, obtained from the LDV signal with the time delay τ, where τ was found to correspond well to the previously mentioned frequency response. Fig. 14(a) shows a case with negligible back flow, so we can see that the mean of the LDV signal is close to that of the hot film. In Fig. 14(b), the back flow is instead strong. In this case the mean of the simulated hot film signal is by far overestimated relative to the mean of the LDV signal, but close to the mean of the absolute value of the LDV signal. We can also conclude from both cases that the simulated signal shows fair agreement with the observed behavior of the hot film signals.

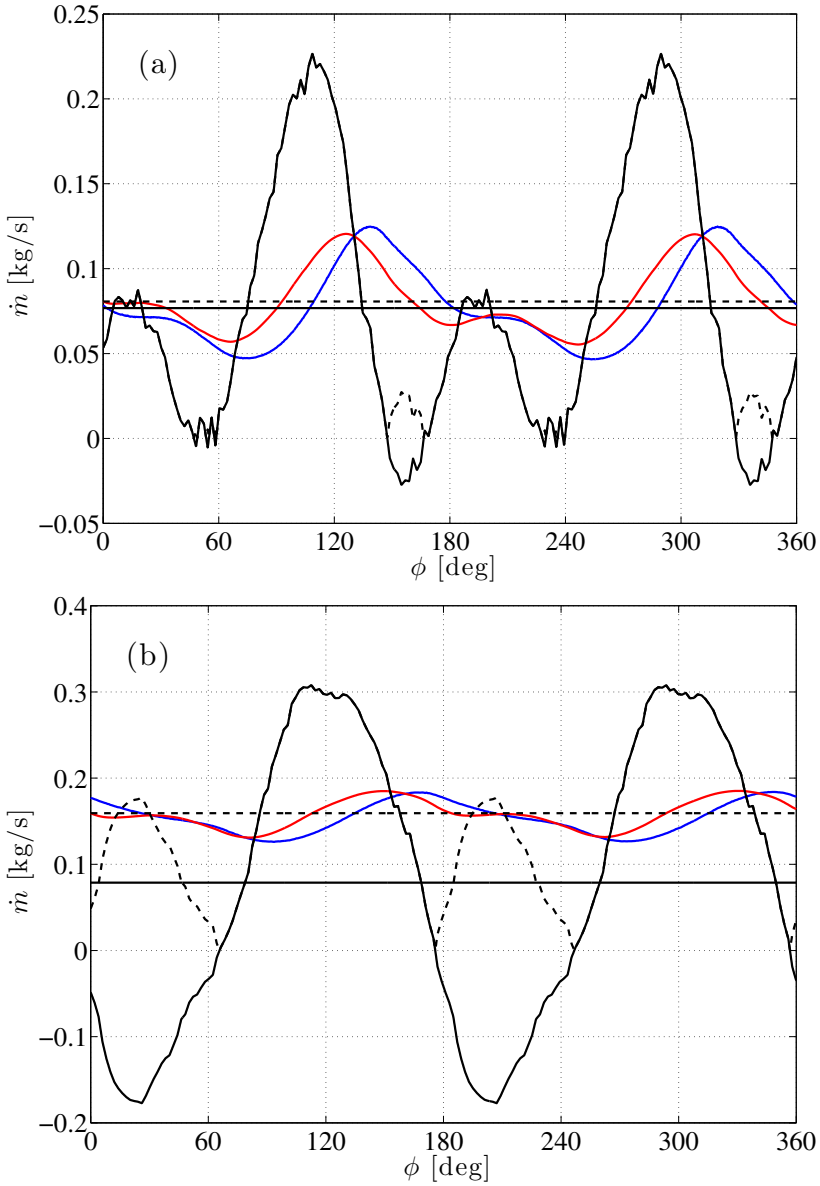

FIGURE 14. Comparison between the LDV and the hot film signals. The true LDV signal (solid black), its mean (horizontal solid black line). The absolute value of the LDV signal (dashed black), its mean (horizontal dashed line). The real hot film output (blue) and the simulated hot film output (red). (a) With negligible back flow f_p 10 Hz. (b) With back flow, f_p 40 Hz.

References

Anderson, J. 2002 *Modern compressible flow: with historical perspective*. McGraw-Hill, New York, USA.

Ardekani, M. & Farhani, F. 2009 Experimental study on response of hot wire and cylindrical hot film anemometers operating under varying fluid temperatures. *Flow Meas. Instrum.* **20**, 174–179.

Atkinson, K. 1992 A software tool to calculate the over-registration error of a turbine meter in pulsating flow. *Flow Meas. Instrum.* **3**, 167–172.

Benedict, R. 1980 *Fundamentals of pipe flow*. Wiley, New York, USA.

Berson, A., Blanc-Benon, P. & Comte-Bellot, G. 2010 On the use of hot-wire anemometry in pulsating flows. A comment on'A critical review on advanced velocity measurement techniques in pulsating flows'. *Meas. Sci. Technol.* **21**, 128001.

Blodgett, L. 1992 Theoretical and practical design of pulsation damping systems. *Flow Meas. Instrum.* **3**, 203–208.

Doblhoff-Dier, K., Kudlaty, K. & Wiesinger, M. 2010 Time resolved measurement of pulsating flow using orifices. *Flow Meas. Instrum.* **22**, 97–103.

Gajan, P., Mottram, R., Hebrard, P., Andriamihafy, H. & Platet, B. 1992 The influence of pulsating flows on orifice plate flowmeters. *Flow Meas. Instrum.* **3**, 118–129.

Grenier, P. 1991 Effects of unsteady phenomena on flow metering. *Flow Meas. Instrum.* **2**, 74–80.

Hebrard, P., Malard, L. & Strzelecki, A. 1992 Experimental study of a vortex flowmeter in pulsatile flow conditions. *Flow Meas. Instrum.* **3**, 173–185.

ISO-5167 2003 *Measurement of Fluid Flow by Means of Pressure Differential Devices Inserted in Circular Cross-section Conduits Running Full*. ISO.

Laurantzon, F. 2009 A pulsating flow rig for analyzing turbocharger performance. *9th International Conference on Turbochargers and Turbocharging* pp. 363–372. IMechE, London, UK.

Laurantzon, F. 2010 Flow Measuring Techniques in Steady and Pulsating Compressible Flows. *Lic. Thesis KTH Mechanics*, Stockholm, Sweden.

Laurantzon, F., Örlü, R., Segalini, A. & Alfredsson, P. 2010 Time-resolved

measurements with a vortex flowmeter in a pulsating turbulent flow using wavelet analysis. *Meas. Sci. Technol.* **21**, 123001.

Li, Y. & Naguib, A. 2003 An oscillating hot-wire technique for resolving the magnitude and direction of velocity measurements using single hot-wire sensors. *Exp. Fluids* **34** (5), 597–606.

McKee, R. 1992 Pulsation effects on single-and two-rotor turbine meters. *Flow Meas. Instrum.* **3**, 151–166.

Mottram, R. 1992 Introduction: An overview of pulsating flow measurement. *Flow Meas. Instrum.* **3**, 114–117.

Nakamura, H., Asano, I., Adachi, M. & Senda, J. 2005 Analysis of pulsating Flow measurement of engine exhaust by a Pitot tube flowmeter. *Int. J. Engine Res.* **6** (1), 85–93.

Persoons, T., Van den Bulck, E. & Fausto, S. 2004 Study of pulsating flow in close-coupled catalyst manifolds using phase-locked hot-wire anemometry. *Exp. Fluids* **36**, 217–232.

Persoons, T., Hoefnagels, A. & Van den Bulck, E. 2006 Calibration of an oscillating hot-wire anemometer for bidirectional velocity measurements. *Exp. Fluids* **40**, 555–567.

Rossberg, A., Bartholomé, K. & Timmer, J. 2004 Data-driven optimal filtering for phase and frequency of noisy oscillations: Application to vortex flow metering. *Phys. Rev. E.* **69**, 16216.

Sieverding, C., Arts, T., Denos, R. & Brouckaert, J. 2000 Measurement techniques for unsteady flows in turbomachines. *Exp. Fluids* **28**, 285–321.

Sokolov, M. & Ginat, Z. 1992 The ladder probe: reverse flow measurements with a hot-wire rake. *Exp. Fluids* **12**, 307–318.

Timité, B., Castelain, C. & Peerhossaini, H. 2010 Pulsatile viscous flow in a curved pipe: Effects of pulsation on the development of secondary flow. *Int. J. Heat Fluid Fl.* **31**, 879–896.

Paper 6

6

Review on the sensed temperature in cold-wire and hot-wire anemometry

By F. Laurantzon, A. Kalpakli, R. Örlü and P. H. Alfredsson

KTH CICERO, Royal Institute of Technology, SE-100 44 Stockholm, Sweden

Technical Report

Instantaneous velocity and temperature measurements by means of hot-wire and cold-wires have become a standard technique used in almost every fluid dynamic research laboratory. Nonetheless, when it comes to compressible flows in applied fields, there seems to remain a need for clarification on which temperature is actually measured by a cold-wire and which temperature a hot-wire senses as its fluid temperature. The present paper reviews the view present in the literature and presents additional experimental evidence, that it is indeed the recovery temperature that is measured by a cold-wire and that this is also the temperature needed to compensate hot-wire readings in non-isothermal compressible flows.

1. Introduction

1.1. *Historical background*

In spite of the fact that hot-wire anemometry is mainly dated back to King (1914), many scientists before him were familiar with the fact that a heated wire with temperature dependent resistance exposed to an air flow can be exploited to measure the fluid velocity (Oberbeck 1895). Also the influence of temperature and humidity on hot-wire readings were known from the very beginning and could be measured (Paeschke 1935; Schubauer 1935). Especially the research on cooling methods for conductors having high temperatures due to the induced heating (Oberbeck 1895) may have given the clue for the practical application of a conductor as a measurement instrument. The detecting element of a hot-wire anemometer consists usually of a tiny tungsten or platinum wire acting as the fourth arm of a Wheatstone bridge, heated by an electrical current, which responds to changes in velocity and temperature of the fluid around the wire. The first practically functioning hot-wire anemometers consisted of about 10 cm long wires with diameters of a few tenths of a millimeter (Oberbeck 1895; Huguenad *et al.* 1924), whereas today platinum wires with diameters less than a micron obtained in form of Wollaston wires

are employed (Ligrani & Bradshaw 1987). However due to robustness issues standard probe sizes around 1 mm in length and 5 micron in diameter are common for laboratory measurements.

The first method and simplest way to measure by means of hot-wire anemometry is by feeding the hot-wire with a constant electrical current and then measuring the decreasing voltage with increasing effective cooling velocity. This is commonly referred to as constant current anemometry (CCA) and is restricted to low turbulence levels due to the sensors inherent thermal inertia. The relatively poor frequency response restricts its use nowadays mainly to temperature measurements by means of so called cold-wires. The first integrated feedback amplifier in an anemometer circuit was probably due to Ziegler (1934) and served to keep the resistance of the sensing element constant, although others had described the concepts already before King (see e.g. references in Huguenad *et al.* 1924; Burgers 1931; Comte-Bellot 1976). The thereby obtained constant temperature anemometer (CTA) is the most common mode of operation, since it circumvents the problem of thermal inertia and is thereby capable of reaching a frequency response of up to hundred kilohertz.

Our advances in the understanding of flow turbulence is directly linked to the advances in hot-wire anemometry which have been made, in particular, in the first half of the last century. A large body of literature has accumulated over the decades devoted to their development, limitations and various correction methods for complex flow situations, e.g. Fingerson (1994) mentions in his review article that over 2500 publications up to 1992 deal with thermal anemometry techniques. Furthermore, their state-of-the-art has been documented in classical textbooks such as those by Sandborn (1972), Strickert (1974), Hinze (1975), Perry (1982), Lomas (1986) and Bruun (1995) as well as very recently in Tropea *et al.* (2007).

While hot-wire anemometry itself has been the focus of research for almost one century, it has for most of this time been exploited to deepen our understanding in fundamental fluid mechanical questions, covering problems from low (Lanspeary 1998) to hypersonic speeds (Spina & McGinley 1994). Despite new optical measurement techniques, hot-wire anemometry still remains the most used device in turbulence research due to its high frequency resolution. This, and the fact, that commercialized hot-wire anemometer systems in conjunction with user-friendly operational instructions are available, has also made it attractive to more applied fields of research, where the hot-wire has traditionally not been used or developed.

2. What is a cold-wire actually measuring and which temperature has to be used to compensate a hot-wire against temperature variations?

Applied fields of research in which cold-wire and hot-wire anemometry has become a common technique is, for instance, the field of internal combustion engines or turbomachinery which inherently exhibits unsteady and non-isothermal flow conditions, as well as exposes the probe and wire to extremely harsh environments and aerodynamic loadings (Dénos & Sieverding 1997; Sieverding *et al.* 2000; Nabavi & Siddiqui 2010; Nabavi 2010). In particular the pulsatile nature of both the flow and the thermodynamical properties, caused e.g. by compressors, pumps or valves, raises the question which temperature the sensing element actually measures. Since cold-wire and hot-wire anemometry has mainly been used in subsonic flows, for which incompressibility can be assumed, it has been common practice to speak about *the* temperature, without differentiating between *static*, *recovery* or *total* temperatures. While such an assumption is justified for subsonic flows ("at low and moderate velocities the difference between the static and stagnation temperature is insignificant" (Bruun 1995), "For low velocities [...] the static temperature is approximately equal to the total temperature. Thus, the static temperature can be approximately measured in low velocity flow" (Sandborn 1972)), it has, however, also been adapted to flows in internal combustion engines or turbomachinery. Here, however, compressibility becomes important ("the difference can be substantial in high-speed flows" (Bruun 1995)) and the Mach number can instantaneously exceed the threshold for which this assumption is valid.

A hot-wire running in CTA mode gives as an output a voltage E_w according to the so called King's law, such that

$$E_w^2/R_w = [A + B(\rho U)^n](T_w - T_f) \tag{1}$$

where A, B, and n are probe specific constants and R_w denotes the resistance of the wire. T_w and T_f are the wire and fluid temperatures, respectively. As can be seen the output increases both with ρU and the temperature excess of the wire. Bruun (1995) showed that with increasing velocity (or rather ρU) the velocity and temperature sensitivities in CTA mode decrease and increase, respectively, as deducible from their analytical expressions:

$$S_{\rho U}^{CTA} = \frac{nB(\rho U)^{n-1}}{2}\left[\frac{R_w(T_w - T_f)}{A + B(\rho U)^n}\right]^{1/2} \tag{2}$$

$$S_{\theta}^{CTA} = -\frac{1}{2}\left[\frac{R_w(A + B(\rho U)^n)}{T_w - T_f}\right]^{1/2}. \tag{3}$$

The effect can more easily be comprehended when considering their ratio, as given in figure 1. As apparent, despite a high overheat ratio, the temperature sensitivity dominates at velocities common to internal combustion or turbomachinery applications, which emphasizes the need to know the recovery temperature accurately in order to compensate the hot-wire readings against temperature variations.

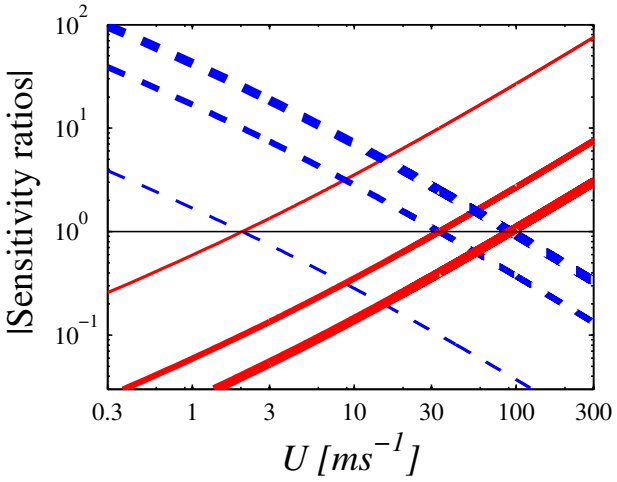

FIGURE 1. Variation of sensitivity ratios under operation of a hot-wire in constant temperature mode with velocity for different temperature overheats ($T_w - T_f$ = 10, 100 and 250 K from thin to thick lines) based on equations (2) and (3). Ratio of velocity ($S_{\rho U}$) to temperature (S_θ) sensitivity (- - -) and temperature to velocity sensitivity (—). The constants A, B and n were taken from a typical calibration curve.

2.1. *Classical literature*

As stated in Sandborn (1972) "an unheated wire placed in a flowing fluid will reach a steady temperature, which depends on the flow conditions. For incompressible continuum flow this temperature is that of the fluid either in motion or at rest. For compressible continuum flow the wire reaches a recovery temperature, which is greater than the static temperature of the flowing fluid but less than the temperature of the fluid if it were brought to rest. [...] For hot-wire anemometer type measurements in compressible flows the term "recovery temperature" is employed to describe the temperature measured by the resistance thermometer." Also Lomas (1986) notes, that "when an unheated sensor is placed in a compressible flow, aerodynamic heating causes the sensor

temperature to rise from ambient to a value called the equilibrium (sometimes referred to as recovery temperature)". Similar formulations can be found in classical text books on hot-wire anemometry. Hence the temperature measured by a cold-wire is the equilibrium or recovery temperature ("It should be noted that, experimentally, when the 'cold-wire' temperature is measured in the flow stream, it is the recovery temperature that is measured" (Fingerson & Freymuth 1996)), and this is also the temperature a hot-wire is exposed to ("[recovery temperature] should be substituted for [the ambient temperature of fluid] in heat transfer equations." (Fingerson & Freymuth 1996)). More explicitly is the literature on supersonic boundary layers, where cold-wires are used "to determine the prevailing recovery temperature" (Lenz *et al.* 2007) and the measured temperature is even termed "cold-wire recovery temperature" (Matlis 2003).

When it comes to the definition of the recovery temperature in conjunction with hot-wires in particular and long cylinders in general, there are two formulations commonly used. For continuum flow the recovery ratio, η, is usually defined as (Sandborn 1972; Hinze 1975; Fingerson & Freymuth 1996)

$$\eta = \frac{T_r}{T_0}\,, \tag{4}$$

where T_r denotes the equilibrium, adiabatic wall or recovery temperature and T_0 the stagnation or total temperature. For free molecular flow on the other hand, where T_r can be greater than T_0, a different relation is taken, see e.g. Dewey (1965); Sandborn (1972); Stainback & Nagabushana (1997). Also definitions involving the static temperature, T_s, adapted from the thermocouple literature, are sometimes used (Stickney 1955; Warren 1994; Szymko *et al.* 2005). In this case the recovery factor, r, (not to be confused with the recovery ratio η) is defined as

$$r = \frac{T_r - T_s}{T_0 - T_s}\,, \tag{5}$$

where r can be related to η through

$$\eta = r\left(1 - \frac{T_s}{T_0}\right) + \frac{T_s}{T_0}\,. \tag{6}$$

Similar relations in which the temperatures are substituted for as well as empirical relations based on this relation can be found in Hirschberg & Muiswinkel (1977). However, the recovery ratio given in relation 4, has often been preferred in the hot-wire literature. In the flows we will consider, $\eta \leqslant 1$ and various correlations as function of the Mach number, M, agree fairly well with each other and indicate that η decreases from 1 at $M = 0$ and asymptotes to 0.94–0.96 towards $M \gtrsim 1.2$ (Lowell 1950; Spangeberg 1955; Laufer & McClellan 1956; Smits *et al.* 1983; Stainback & Nagabushana 1997). So for instance summarises Spina & McGinley (1994) that "In continuum flow, the measured values of η range from 0.95 to 0.97 for a wide range of supersonic Mach numbers". While for

subsonic, but compressible flows, the stagnation temperature and static temperature are not assumed to be equal any longer, the recovery temperature, is often set identical to the stagnation temperature (Johnston & Fleeter 1997), due to the fact that η is very close to unity.

2.2. *More applied literature*

The brief overview given above clearly shows, that the temperature measured by a cold-wire is the equilibrium or recovery temperature and that this is also the temperature a hot-wire is sensing; hence it is the temperature which is needed for temperature compensation of hot-wire readings. Nevertheless, there seems to be a need for clarification, when it comes to more applied literature, in particular, related to internal combustion engines or turbomachinery. To measure in real applications cold-wires are out of the question due to the harsh environment and high temperatures. However many flow investigations are done in special rigs giving a pulsatile flow, where flow components such as turbo-chargers are tested in a low temperature environment (see e.g. Laurantzon *et al.* (2010), Capobianco & Marelli (2010), Karamanis *et al.* (2001)). Despite the fact that fairly clean conditions can be obtained in such rigs, cold-wires are seldom used since they are quite delicate, due to the small diameters needed in order to resolve the pulsations of the flow. The much larger length-to-diameter ratio, compared to hot-wires, needed to minimize the thermal lag (Paranthoen *et al.* 1982; Tsuji *et al.* 1992) is a life shortening circumstance for cold-wires as compared to more robust hot-wires.

As stated in Karamanis *et al.* (2001), one way of circumventing the need to measure the instantaneous temperature has been to obtain "an approximate value for the instantaneous temperature [...] by assuming an isentropic relationship between temperature and pressure". This method has been adopted by various researchers (see e.g. references in Karamanis *et al.* 2001). It can also often be found that the instantaneous temperature obtained in such a way is then in turn employed to compensate the hot-wire readings (i.e. the velocity or more correctly the mass flux in compressible flows) against the instantaneous temperature (i.e. mainly the pulsatile behaviour rather than the turbulence) (Piscaglia *et al.* 2007; Marelli & Capobianco 2009). The habit of hot-wire users in incompressible flows to speak about *the* (instantaneous) temperature, seems to have been adopted to relatively high speed flows and this makes it difficult to conclusively comprehend which of the temperatures are approximated through isentropic relations and how the hot-wire readings were compensated for. Hence, there seems to be some confusion, or at least a need for clarity, in compressible flows regarding *i)* the temperature that is measured by a cold-wire, *ii)* the temperature which is needed to compensate the velocity or mass flux readings from a hot-wire, and *iii)* how the recovery temperature has to be computed.

3. Idea and experimental test case

Instead of directly measuring all three aforementioned temperatures, a procedure common to the determination of the recovery factors for (differently shaped) thermocouple probes (Stickney 1955; Willbanks 1973; Rajoo 2007) has been adapted. Hereby, a convergent nozzle with a large contraction ratio is used, that "circumvents the difficult problem of direct measurement of the fluid temperature" (Willbanks 1973). The temperature of (heated) air within the stagnation chamber of such a nozzle would easily be measurable by means of e.g. a thermocouple, since $T_r = T_0 \approx T_s$. By applying a certain overpressure on the stagnation chamber, the air is accelerated in the nozzle to the desired Mach number at the nozzle exit plane, whereby the total temperature remains unchanged along the nozzle centreline, and the static temperature decreases according to

$$\frac{T_0}{T_s} = 1 + \frac{\gamma - 1}{2} M^2 \,. \tag{7}$$

By traversing a cold-wire along the centreline of the nozzle one would gain certainty on which temperature a cold-wire is actually measuring. By repeating the procedure with a hot-wire one would equivalently gain certainty on the "effective" fluid temperature (T_f) in 1 to be used for the convective heat transfer relation, i.e. the temperature that the overheat is actually applied to.

4. Repetition: Quasi-one dimensional compressible flow relations

Since the flow through the convergent nozzle is quasi one-dimensional and assumed to be isentropic the Mach number-area relation can be employed in order to obtain an estimate of the Mach number distribution throughout the nozzle. Based on this a recovery temperature can be computed for comparison with the cold-wire measurements.

In order to estimate how the recovery temperature theoretically should vary with distance x, the Mach number distribution has been implicitely obtained through

$$\left(\frac{A_e}{A_i}\right)^2 = \left(\frac{M_i}{M_e}\right)^2 \left(\frac{1 + \frac{\gamma - 1}{2} M_e^2}{1 + \frac{\gamma - 1}{2} M_i^2}\right)^{\frac{(\gamma + 1)}{(\gamma - 1)}} \,, \tag{8}$$

where A_e and M_e denote the cross sectional area and Mach number at the nozzle exit, and A_i and M_i denote the cross sectional area and Mach number at a certain x location inside the nozzle at which M is to be evaluated.

The recovery to static temperature ratio has been found to be well approximated by

$$\frac{T_r}{T_s} = 1 + \sqrt{Pr} \frac{\gamma - 1}{2} M^2 \,, \tag{9}$$

where Pr is the Prandtl number and $r = \sqrt{Pr}$ is the previously defined recovery factor (Trenkle & Reinhardt 1973). Since the static temperature is not measured, the recovery to total temperature ratio is preferred and is obtained by substituting the static temperature by means of the adiabatic relation

$$\frac{T_r}{T_0} = \frac{1 + r\dfrac{\gamma - 1}{2}M^2}{1 + \dfrac{\gamma - 1}{2}M^2}\,. \tag{10}$$

5. Experimental setup and measurement technique

The experiments were performed within the Laboratory of KTH CICERO (Centre for Internal Combustion Engine Research Opus) in a newly developed flow rig (Laurantzon *et al.* 2010). For the purpose of the present investigation a hot-wire calibration facility consisting of an electrical heater, a stagnation chamber and a convergent nozzle, was connected to the main pipe system. The set-up, schematically shown in figure 2, shows the nozzle of inlet and exit diameter of 110 and 10 mm, respectively. A digital thermometer (FLUKE) was connected to the stagnation chamber to assess the stagnation temperature.

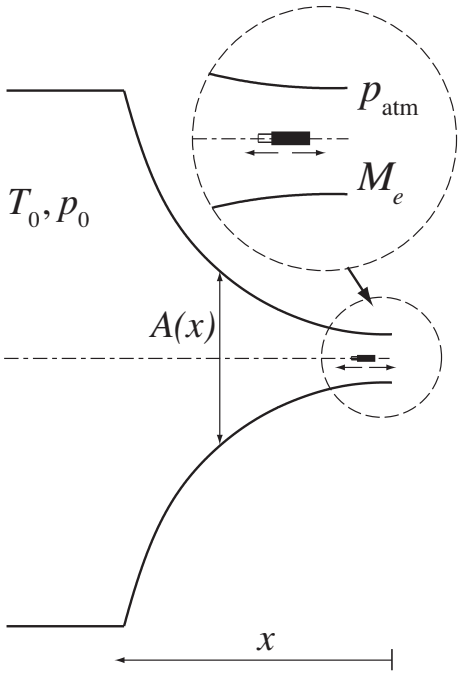

FIGURE 2. Schematic of the convergent nozzle with inlet and exit diameters of 10 and 110 mm.

Both mass flow rate density, ρu, and temperature measurements were performed using a hot-wire and a cold-wire, respectively. The probe consists of a 2.5 micron Platinum (Pt 10%Rh) wire of length, L = 1.5 mm, giving a length-to-diameter ratio of around 600, in order to reduce the thermal lag of the cold-wire measurements (although here we are merely interested in time-averaged quantities). Both the hot-wire and cold-wire were operated by means of an AA-Labs AA-1003 anemometry system in constant temperature (CT) and constant current (CC) mode, respectively. For the measurements of ρU the hot-wire was operated at an overheat ratio of 50%, while for the temperature measurements the cold-wire was operated at a constant current of 0.3 mA. The hot/cold wire probe was mounted on a micrometer screw which could be traversed along the centreline, i.e. the x-axis. The mass flow rate and exit Mach number were measured by the pressure drop across the nozzle and the hot-wire was calibrated at the nozzle exit. The mass flow rate was for the set of experiments presented here adjusted to around 9 $\mathrm{g\,s^{-1}}$ giving an exit Mach number of around 0.3, which is sufficient to yield measurable differences between static, recovery and total temperatures.

6. Results and discussion

As mentioned under Section 3, the total temperature along the nozzle centreline is constant, and the measured temperature profile by means of a cold-wire should directly reveal whether the recovery temperature is measured. Figure 3 depicts the measured temperature from the cold-wire at three different stagnation temperatures. Furthermore the recovery temperature computed through the mass flow rate density obtained from the hot-wire and the utilisation of the isentropic relation is given together with the one from the Mach number-area relation. The qualitative agreement between all three cases indicates—in accordance with the main body of available literature—that the cold-wire indeed measures a recovery temperature.

To assess the obtained recovery temperature along the nozzle centreline quantitatively, the recovery factor, r, is computed based on relation (10) and is shown in figure 4. The agreement between the theoretical estimate of r, i.e. $\sqrt{Pr}$, and the measured and deduced values is remarkable at the nozzle exit, whereas further into the nozzle it starts to deviate from this value. There are two main causes for this, one being the fact that the hot-wire probe, with its diameter of 2.5 mm, represents a blockage when immersed into the nozzle which changes the Mach number distribution. Another cause, mainly responsible for the high scatter, is the fact that both nominator and denominator in Eq. (10) approach zero while traversing into the nozzle and this gives rise to a large scatter.

Having shown, that the measured temperature by means of a cold-wire is the recovery temperature, it remains to ensure that this is also the temperature for the heat transfer relations when using a hot-wire. Therefore the mass flow

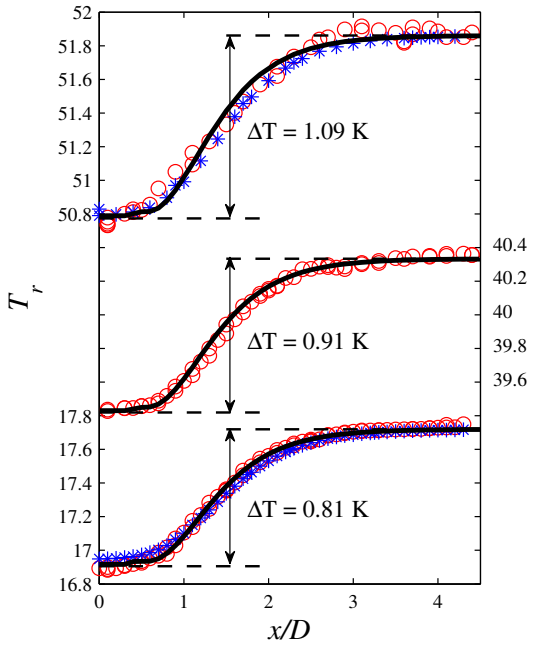

FIGURE 3. Recovery temperature, T_r, along the nozzle centreline for T_0 = 17.7, 40.3, 51.9°. Directly measured T_r by means of the cold-wire: ◯. Indirectly measured T_r through the mass flow rate density, ρu, through utilisation of the isentropic relation using the T_0: ∗. Computed T_r through the Mach number-area relation based on the pressure drop across the nozzle and the isentropic relation using T_0: —. The given temperature differences denote the difference between the recovery temperature at the inlet (x/D = 4.5), which is identical to T_s and T_0 and exit (x/D = 0) of the nozzle.

density ratio profile from a hot-wire at two different fluid temperatures, viz. T_0 = 17.7 and 31.0° is given in figure 5, together with the temperature compensated profile obtained through the recovery temperature. The agreement throughout the nozzle of both the profiles at the reference temperature and the compensated one from the elevated temperature indicates that it is indeed the recovery temperature which is needed for compensating hot-wire readings against temperature variations.

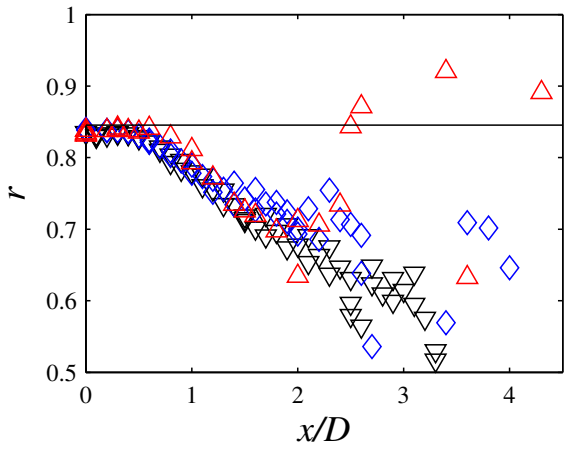

FIGURE 4. Recovery ratio, r, along the nozzle centreline for T_0 = 17.7 (▽), 40.3 (◇), 51.9° (△) computed through relation (10). Solid line indicates $r = \sqrt{Pr}$.

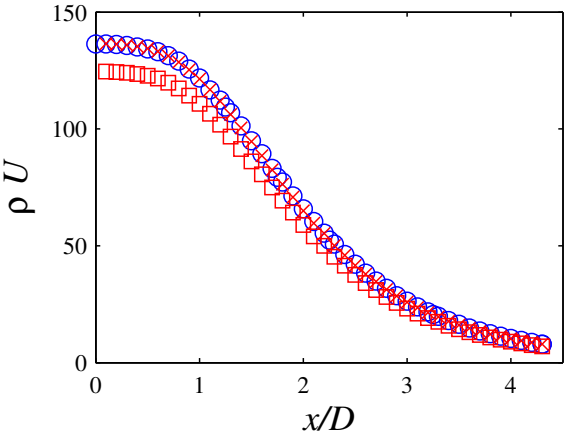

FIGURE 5. Mass flow density rate, ρU, along the nozzle centreline for T_0 = 17.7° ◯ and 31.0° □, whereas both profiles were computed based on a velocity calibration at T_0 =17.7°. Temperature compensated ρU profile for 31.0° by means of the recovery temperature ×.

Acknowledgements

Malte Kjellander, Dr. Antonio Segalini and Dr. Nils Tillmark are acknowledged for discussions on the topic.

References

Bruun, H. H. 1995 Hot-wire anemometry: Principles and signal analysis. *Oxford University Press Inc., New York, USA.*

Burgers, J. M. 1931 Hitzdrahtmessungen. *In: W. Wien and F. Harms (eds.) Handbuch der Experimentalphysik, Band 4 (Leipzig: Akademische Verlagsgesellschaft), pp. 635–667.*

Capobianco, M. & Marelli, S. 2010 Experimental investigation into the pulsating flow performance of a turbocharger turbine in the closed and open waste-gate region. *9th Int. Conf. on Turbocharging and Turbochargers (IMechE)* pp. 373–385.

Comte-Bellot, G. 1976 Hot-wire anemometry. *Annu. Rev. Fluid Mech.* **8**, 209–231.

Dénos, R. & Sieverding, C. 1997 Assessment of the cold-wire resistance thermometer for high-speed turbomachinery applications. *J. Turbomachinery* **119**, 140–148.

Dewey, C. 1965 A correlation of convective heat transfer and recovery temperature data for cylinders in compressible flow. *Int. J. Heat Mass Transfer* **8**, 245–252.

Fingerson, L. 1994 Thermal anemometry, current state, and future directions. *Rev. Sci. Instrum.* **65**, 285–300.

Fingerson, L. & Freymuth, P. 1996 Thermal anemometers. *Fluid Mechanics Measurements, 2nd ed., R. J. Goldstein (Ed.), pp. 115–173, Taylor & Francis, Washington, USA.*

Hinze, J. O. 1975 Turbulence. *McGraw-Hill, 2nd. ed.*

Hirschberg, A. & Muiswinkel, J. V. 1977 A correlation of recovery temperature data for cylinders in a compressible flow at high Reynolds numbers. *Int. J. Heat Mass. Transfer* **20**, 669–674.

Huguenad, E., Magnan, A. & Planiol, A. 1924 A method for the instantaenous determination of the velocity and direction of the wind. *NACA TM 264.*

Johnston, R. & Fleeter, S. 1997 Compressible flow hot-wire calibration. *Exp. Fluids* **22**, 444–446.

Karamanis, N., Martinez-Botas, R. & Su, C. 2001 Mixed flow turbines: Inlet and exit flow under steady and pulsating conditions. *J. Turbomachinery* **123**, 359–371.

King, L. 1914 On the convection of heat from small cylinders in a stream of fluid:

Determination of the convection constants of small platinum wires with applications to hot-wire anemometry. *Phil. Trans. R. Soc. A* **214**, 373–432.

Lanspeary, P. 1998 Establishing very low speed, disturbance-free flow for anemometry in turbulent boundary layers. *Ph. D. Thesis, University of Adelaide, Australia*.

Laufer, J. & McClellan, R. 1956 Measurements of heat transfer from fine wires in supersonic flows. *J. Fluid Mech* **1**, 276–289.

Laurantzon, F., Tillmark, N. & Alfredsson, P. H. 2010 A pulsating flow rig for analyzing turbocharger performance. *9th Int. Conf. on Turbocharging and Turbochargers (IMechE)* pp. 363–372.

Lenz, B., Gaisbauer, U. & Krämer, E. 2007 Fluctuation measurements in the boundary layer of a supersonic flow. *Proc. Appl. Math. Mech.* **7**, 4100035–4100036.

Ligrani, P. & Bradshaw, P. 1987 Subminiature hot-wire sensors: Development and use. *J. Phys. E* **20**, 323–332.

Lomas, C. G. 1986 Fundamentals of hot wire anemometry. *Cambridge University Press*.

Lowell, H. H. 1950 Design and applications of hot-wire anemometers for steady-state measurements at transonic and supersonic airspeeds. *NACA Tech. Note 2117*.

Marelli, S. & Capobianco, M. 2009 Measurement of instantaneous fluid-dynamic parameters in automotive turbocharging circuit. *SAE 2009-24-0124*.

Matlis, E. 2003 Controlled experiments on instabilities and transition to turbulence on a sharp cone at mach 3.5. *Ph. D. Thesis University of Notre Dame, Indiana, USA*.

Nabavi, M. 2010 Invited review article: Unsteady and pulsating pressure and temperature: A review of experimental techniques. *Rev. Sci. Instrum.* **81**, 031101.

Nabavi, M. & Siddiqui, K. 2010 A critical review on advanced velocity measurement techniques in pulsating flows. *Meas. Sci. Technol.* **21**, 042002.

Oberbeck, A. 1895 Ueber die abkühlende Wirkung von Luftströmen. *Ann. Phys.* **292**, 397–411.

Paeschke, W. 1935 Feuchtigkeitseffekt bei Hitzdrahtmessungen. *Phys. Z.* **36**, 564–565.

Paranthoen, P., Petit, C. & Lecordier, J.-C. 1982 The effect of the thermal prong-wire interaction on the response of a cold wire in gaseous flows (air, argon and helium). *J. Fluid Mech* **124**, 457–473.

Perry, A. E. 1982 Hot-wire anemometry. *Clarendon Press*.

Piscaglia, F., Onorati, A., Marelli, S. & Capobianco, M. 2007 Unsteady behavior in turbocharger turbines: Experimental analysis and numerical simulation. *SAE 2007-24-0081*.

Rajoo, S. 2007 Steady and pulsating performance of a variable geometry mixed flow turbocharger turbine. *Ph. D. thesis Imperial College London, UK*.

Sandborn, V. A. 1972 Resistance temperature transducers. *Metrology Press*.

Schubauer, G. B. 1935 Effect of humidity in hot-wire anemometry. *J. Res. Nat. Bur. Stand.* **15**, 575–578.

Sieverding, C., Arts, T., Denos, R. & Brouckaert, J. 2000 Measurement techniques for unsteady flows in turbomachines. *Exp. Fluids* **28**, 285–321.

Smits, A. J., Hayakawa, K. & Muck, K. 1983 Constant temperature hot-wire anemometer practice in supersonic flows. *Exp. Fluids* **1**, 83–92.

Spangeberg, W. G. 1955 Heat-loss characteristics of hot-wire anemometers at various densities in transonic and supersonic flow. *NACA TN 3381*.

Spina, E. & McGinley, C. 1994 Constant-temperature anemometry in hypersonic flow: critical issues and sample results. *Exp. Fluids* **17**, 365–374.

Stainback, P. & Nagabushana, K. 1997 Review: Hot-wire anemometry in transonic and subsonic slip flows. *J. Fluid Eng.* **119**, 1–54.

Stickney, T. 1955 Recovery and time-response characteristics of six thermocouple probes in subsonic flow. *NACA Tech. Note 3455*.

Strickert, H. 1974 Hitzdraht- und Hitzfilmanemometrie. *VEB Verlag Technik*.

Szymko, S., Martinez-Botas, R. & Pullen, K. R. 2005 Experimental evalation of turbocharger turbine performance under pulsating flow conditions. *Proc. GT2005: ASME TURBO EXPO 2005*.

Trenkle, F. & Reinhardt, M. 1973 In-flight temperature measurements. *AGARDograph No. 160, AGARD Flight Test Instrumentation Series, Vol. 2*.

Tropea, C., Yarin, A. & Foss, J. 2007 Springer Handbook of Experimental Fluid Mechanics. *Springer-Verlag Berlin Heidelberg*.

Tsuji, T., Nagano, Y. & Tagawa, M. 1992 Frequency response and instantaneous temperature profile of cold-wire sensors for fluid temperature fluctuation measurements. *Exp. Fluids* **13**, 171–178.

Warren, R. C. 1994 Design of thermocouple probes for measurements of rocket exhaust plume temperatures. *Technical Report DSTO-TR-0006, Aeronautical and Maritime Research Laboratory, Melbourne, Australia*.

Willbanks, C. 1973 Recovery characteristics of a single-shielded self-aspirating thermocouple probe at low pressure levels and subsonic speeds. *J. Phys. E: Sci. Instrum.* **6**, 1140–1144.

Ziegler, M. 1934 The construction of a hot-wire anemometer with linear scale and negligible lag. *Proc. K. Ned. Acad. Wet.* **15**, 3–22.

Paper 7

7

What does the hot-wire measure?

By Fredrik Laurantzon, Nils Tillmark and P. Henrik Alfredsson

CCGEx, KTH Mechanics, SE-100 44 Stockholm, Sweden

Technical Report

This technical note investigates the heat loss characteristics from a hot-wire at high subsonic speeds. Classical works have demonstrated a square-root dependance between the heat loss in terms of the Nusselt number Nu, and the flow rate in terms of the flow Reynolds number Re. The hypothesis for the present work is that in compressible flow Nu is instead dependent of a Reynolds number based on the stagnation density. This hypothesis is then tested by means of experiments.

---

1. Introduction

Hot-wire anemometry is a velocity measurement technique based on forced convective heat transfer from a thin heated wire, immersed in a fluid flow[1]. The wire is made of a material with temperature dependent resistivity. When an electric current is passed through the wire, it heats the wire above the fluid temperature and the heat transfer from the wire depends on the flow rate it is exposed to. Hence if the temperature of the wire varies, so does also its resistance and consequently the Joule heating (Perry 1982).

If the hot-wire is operated in constant temperature anemometry (CTA) mode, the resistance of the wire is kept constant by a feedback loop. The forced convective heat transfer from the wire will then be balanced by the Joule heating (see e.g. Hultmark & Smits 2010), i.e.

$$\frac{E^2}{R_\mathrm{w}} = hA_\mathrm{w}(T_\mathrm{w} - T_\mathrm{a}), \tag{1}$$

where $R_\mathrm{w}, A_\mathrm{w}$ and T_w are the resistance, the projected area and the temperature of the wire respectively, T_a is the ambient fluid temperature, h is the convective heat transfer coefficient and finally, E is the voltage across the wire.

[1] Heat transfer due to radiation is for most applications negligible, and if the wire is sufficiently long, the heat conduction to the prongs are negligible as well.

Eq. (1) can be expressed in terms of the Nusselt number $\mathrm{Nu} = hd/k$, which is the ratio of convective to conductive heat transfer coefficients, as

$$\frac{E^2}{R_\mathrm{w}} = k\mathrm{Nu}\frac{A_\mathrm{w}}{d}(T_\mathrm{w} - T_\mathrm{a}) \tag{2}$$

where k is the thermal conductivity of the fluid and d a characteristic length (here the diameter of the wire). The Nusselt number depends on several parameters, and for a compressible fluid this functional relationship can according to Bruun (1995), be written as

$$\mathrm{Nu} = \mathrm{Nu}(\mathrm{Re}, \mathrm{Pr}, M, \tau, L/d) \tag{3}$$

where the dimensionless numbers are

$$\begin{array}{lll} \mathrm{Re} & = \text{Reynolds number} & = \rho u d/\mu \\ \mathrm{Pr} & = \text{Prandtl number} & = c_p\mu/k \\ M & = \text{Mach number} & = u/a \end{array} \tag{4}$$

The included variables are in turn: velocity u, density ρ, wire length L, dynamic viscosity μ, specific heat at constant pressure c_p and speed of sound a. The so called temperature loading factor or overheat ratio $\tau = (T_\mathrm{w} - T_r)/T_0$, where T_0 is the stagnation temperature, T_r is the recovery temperature. For an unheated wire in a fluid flow, T_r is the temperature of the wire, which is greater than the static temperature but lower than the fluid temperature if it were brought to rest (Sandborn 1972). It can be defined through the the so called recovery factor r, namely

$$\frac{T_r}{T} = (1 + r\frac{\gamma - 1}{2}M^2) \tag{5}$$

where the recovery factor for laminar flow is assumed to be $\sqrt{\mathrm{Pr}}$. A semi-empirical relationship for the Nusselt number (Smits *et al.* 1984) and the flow variables are

$$\mathrm{Nu} = A'(\tau) + B'(\tau)\mathrm{Re}^n \tag{6}$$

where n usually is in the range 0.4-0.55 and the above relation is known as King's Law. For calibration purposes, the above equation can be combined with Eq. (2) to yield

$$E^2 = A(\tau) + B(\tau)\mathrm{Re}^n \tag{7}$$

If the hot-wire is to be used merely to measure flow velocity, one has to compensate for the temperature dependance of the coefficients A and B, since the heat transfer from the wire is due to the ambient temperature as well. Such compensation techniques can be found in e.g. Kostka & Ram (1992), Bruun (1995) and Dijk & Nieuwstadt (2004).

Eq. (7) implies that at a given temperature, the anemometer output voltage $E^2 \sim (\rho u)^n$, which has been confirmed also at lower subsonic speeds, see for instance Durst *et al.* (2008). Hot-wire measurements in high speed flows have been conducted as well, where it has been shown for supersonic flows that the Reynolds number is the predominant parameter that affects the heat

loss in terms of the Nusselt number (Laufer & McClellan 1956). Since a bow shock forms in front of the hot-wire at supersonic speeds, the situation is quite different from subsonic flow and the Reynolds number behind the shock, is the controlling variable. Since the Mach number behind the shock converges slowly to a constant value the higher the upstream Mach number, its impact on the heat transfer is small as compared to Re.

A number of authors (e.g. Kovasznay 1953; Spangenberg 1955; Sandborn 1972; Dewey 2002) have favored to describe the heat transfer loss from the cylinder in terms of

$$\begin{aligned} \mathrm{Nu}_0 &= \frac{hd}{k_0}; \\ \mathrm{Re}_0 &= \frac{\rho u d}{\mu_0} \end{aligned}$$

where the fluid properties, heat conductivity and dynamic viscosity, are evaluated at the stagnation temperature (denoted by subscript 0), whereas the density still is evaluated as the density of the flow. This offers advantages in flows with non-uniform flow fields. With these definitions, the asymptotic trend $\mathrm{Nu}_0 \sim \sqrt{\mathrm{Re}_0}$ has been demonstrated.

The purpose of the present work is to investigate if the hot-wire is sensitive to ρu even at Mach numbers M, approaching unity. A hypothesis for the present work is that the hot-wire is sensitive to $\rho_0 u$ i.e. the product of stagnation density and velocity, rather than ρu. The difference between these variables is given by

$$\rho_0 u = \left(\frac{\rho_0}{\rho}\right) \rho u = \beta(M) \rho u \tag{8}$$

where β is the isentropic relation for the densities

$$\beta = \left(1 + \frac{\gamma - 1}{2} M^2\right)^{1/(\gamma-1)} \tag{9}$$

The Mach numbers in the present study range from $M = 0.3$ to $M = 1$, where the corresponding β from Eq. (9) are 1.045 and 1.58, respectively. Hence, with this difference between ρu and $\rho_0 u$ at Mach number close to unity, the discrimination of the heat loss dependancies would be clearly noticeable. The value of β increases towards $M = 1$ and it starts to decrease for Mach numbers beyond 1, due to the shock in front of the wire.

2. Experimental Set-up

The experiments were performed in the CICERO Laboratory of KTH CCGEx, in a flow rig as described in Laurantzon *et al.* (2012) and the equipment and instrumentation is similar to that employed in Laurantzon *et al.* (2010). For convenience the most important details will be repeated here.

In the present investigation a hot-wire calibration facility consisting of an electrical heater, a stagnation chamber and a convergent nozzle, was connected to the main pipe system of the laboratory. Two compressors can provide up to 0.5 kg/s at 6 bars, however in the present study only a small fraction of the capacity is needed. The pipe system has a high quality mass flow meter (ABB Thermal Mass Flowmeter FMT500-IG) that gives the flow rate. The nozzle, schematically shown in Fig. 1, has an inlet and exit diameter of 110 and 14 mm, respectively. A digital thermometer (FLUKE) was connected to the stagnation chamber to assess the stagnation temperature. The stagnation pressure was measured at the inlet of the nozzle, where the flow is nearly stagnant and the Mach number almost zero. The hot-wire probe used has a long probe body

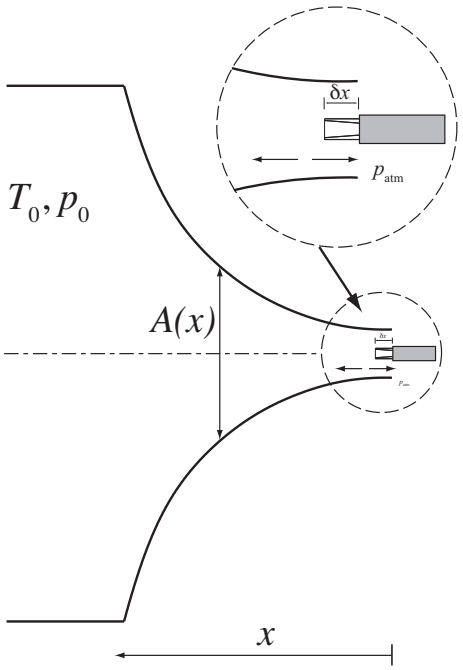

FIGURE 1. The geometry of the nozzle. The probe can be traversed in the x-direction along the centerline. The probe itself causes a blockage of about 8 % of the outlet cross section area.

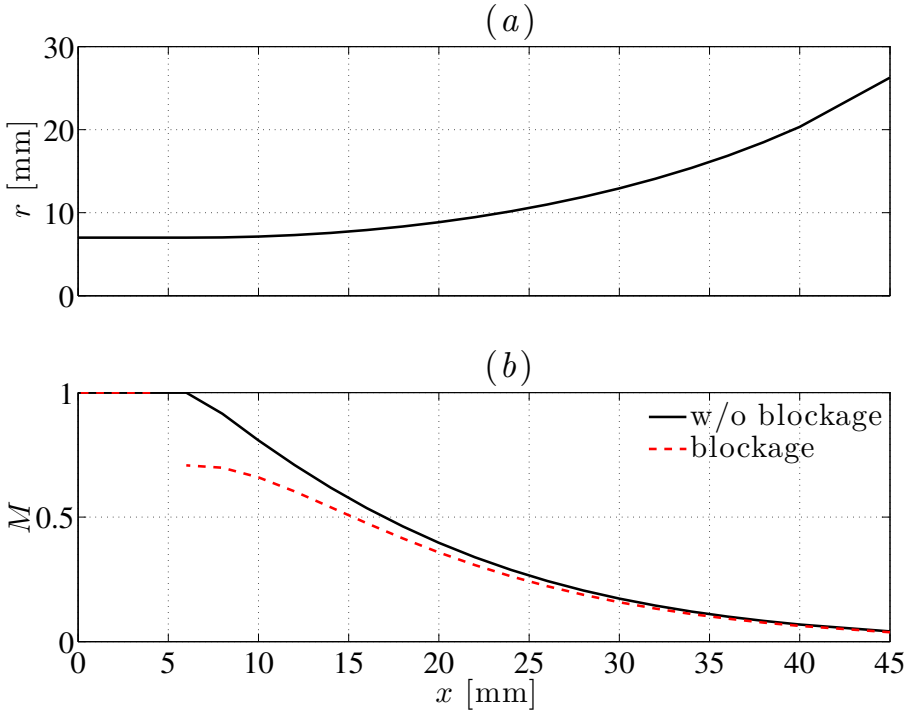

FIGURE 2. (a) The nozzle radius r as function of axial distance x. (b) Theoretical Mach number distribution at choked conditions, with and without the blockage introduced by the hot-wire probe itself, with diameter $D = 4$ mm.

with a diameter of 4 mm. The probe body is always inserted into the nozzle creating the same critical area at the nozzle exit for all different positions of the probe inside the nozzle. The sensing element consists of a 5 micron Tungsten wire of length, $L = 1$ mm, giving a length-to-diameter ratio of around 200. The hot-wire was operated by means of an AA-Labs AA-1003 anemometry system in CTA mode. The hot-wire was operated at an overheat ratio of 60%. The hot-wire probe was mounted on a micrometer screw which could be manually traversed along the centerline, i.e. the x-axis.

In Fig 2(a) the radius $r(x)$, of the nozzle is shown and in Fig 2(b) the corresponding theoretical Mach number distribution based on choked conditions (i.e. the exit Mach number $M_e = 1$), is shown.

3. Experimental results

3.1. *Calibration procedures*

The hot-wire response can be obtained in two principally different ways. One is to place the hot-wire at a specific position inside the nozzle and then change the mass flow rate from zero up to the point when the flow is choked. In this way both ρu and the Mach number change simultaneously. A second possibility is to run the nozzle under choked conditions and varying the stagnation pressure thereby changing the density at the sensor but not the velocity and Mach number.

An example of the former is shown in Fig. 3. Here the hot-wire was placed at $x = 8$ mm, which is the position where $M = 0.7$ at choked conditions. The facility reference mass flow meter, was used to obtain $\dot{m}_{\mathrm{ref}}$, i.e. the total mass flow through the nozzle. Since the cross sectional variation with x is known, the mass flux ρu is obtained from

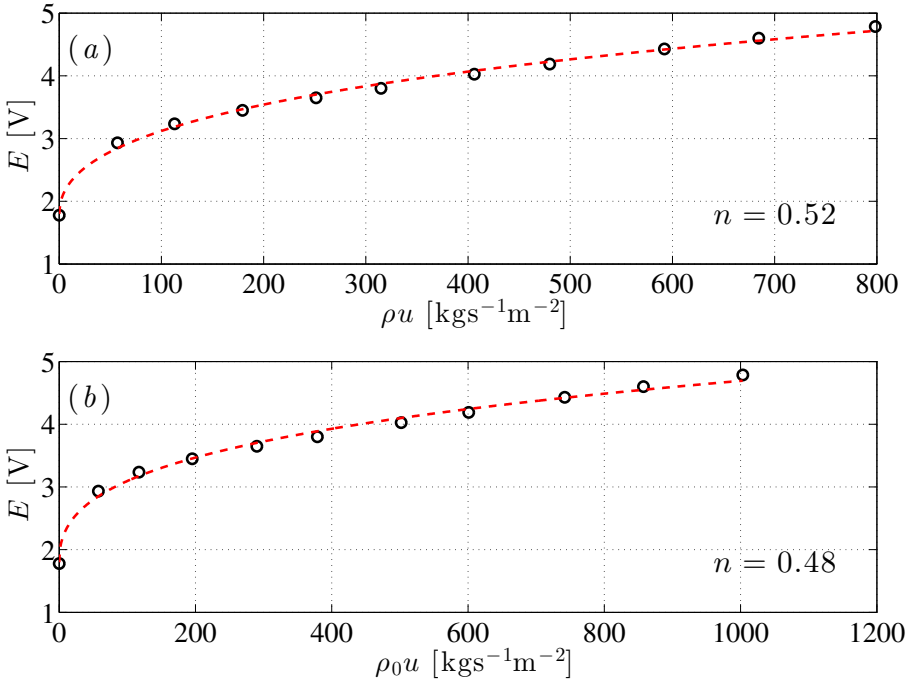

FIGURE 3. Calibration curves for the hot-wire sensor with least square fits to the measured points. (*a*) $E^2 = A + B(\rho u)^n$. (*b*) $E^2 = A + B(\rho_0 u)^n$.

$$\dot{m}_{\text{ref}} = (\rho u)A|_{x=8\text{mm}} \tag{10}$$

and $\rho_0 u$ is obtained from Eq. (8), where M is obtained from the so called Area-Mach (A-M) number relationship (Anderson 2004). The exit Mach number M_e is based on p_0 and p_{atm}. The anemometer output is plotted vs. both ρu and $\rho_0 u$ in Fig. 3(a) and (b) respectively. Least square fits to the calibration points are also provided where A, B and n all are fitted. As can be seen from the figures the least square fit of the calibration data gives values of the exponent n in King's law close to the theoretical value of 0.5 in both cases and also that A becomes close to the measured voltage squared at no flow.

The Mach number distribution can also be obtained in the following way

$$\rho u = \frac{\rho}{\rho_0}\rho_0 M\sqrt{\gamma R\frac{T}{T_0}T_0} \tag{11}$$

After some algebra (using $\gamma = 1.4$) we get the following equation for M

$$\frac{\gamma-1}{2}M^2 - \left(\frac{\gamma}{RT_0}\right)^{1/6}\left(\frac{p_0}{\rho u}\right)^{1/3} M^{1/3} + 1 = 0 \tag{12}$$

where all other quantities are known for a given measurement point. Both methods gave similar results, which gives confidence that the procedures are correct: The former method is based on the area distribution and pressure measurements and the latter on the mass flow rate. When $\rho_0 u$ is known the following equation can be used to find M:

$$\frac{\gamma-1}{2}M^2 - \frac{\gamma}{RT_0}\left(\frac{p_0}{\rho_0 u}\right)^2 M^2 + 1 = 0 \tag{13}$$

The second approach, keeping M constant and varying the stagnation pressure p_0 is illustrated in Fig. 4. Here M and hence u are fix for a given measurement point (each specific line in Fig. 4) and M, p_0 and T_0 are known, therefore ρu and $\rho_0 u$ can readily be determined. The squared output voltage, plotted vs. the square root of the mass flux, shows the approximately linear relation as expected ($E^2 - E_0^2 \sim (\rho u)^{0.48}$ and $E^2 - E_0^2 \sim (\rho_0 u)^{0.52}$). However it is clear from Fig. 4 that the heat transfer from the sensor decreases with increasing Mach number for a given value of ρu (or equivalently $\rho_0 u$).

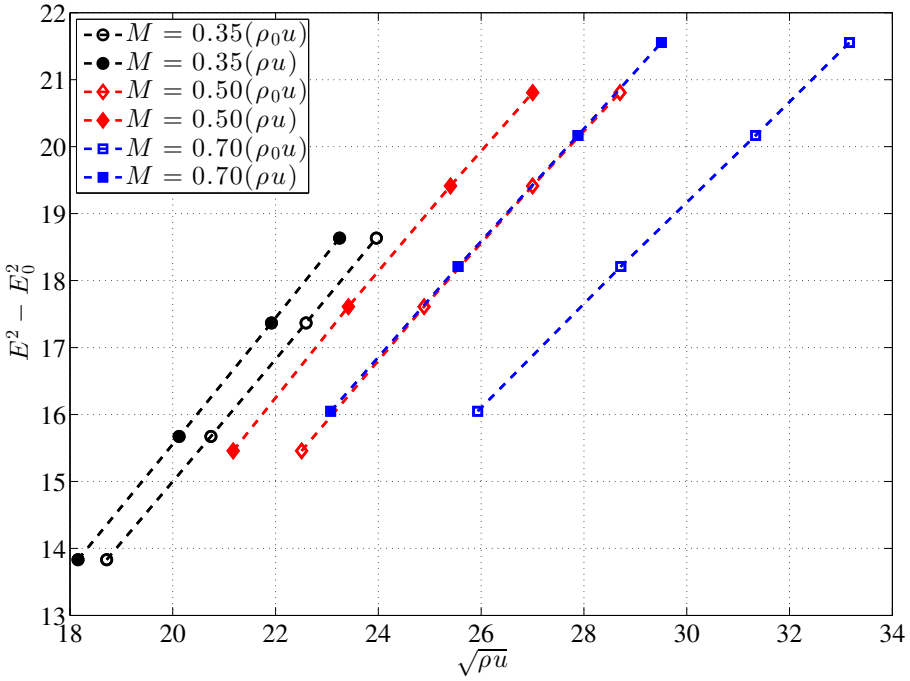

FIGURE 4. E^2 as function of $\sqrt{\rho u}$ and $\sqrt{\rho_0 u}$. The hot-wire is at a fix position for a given M, but the stagnation pressure is changed and hence also the density. Numbers are in SI-units.

3.2. *Nozzle measurements*

This section shows data from the hot-wire sensor where the sensor is traversed through the nozzle. The stagnation pressure p_0 is kept constant and the flow is choked. In this case the sensor is exposed to both a varying mass flux (ρu) and a varying Mach number. In Fig. 5 the anemometer output (voltage) is shown and the corresponding mass fluxes when M is varied by means of traversing the probe along the nozzle.

Now we can calculate the Mach number distribution along the nozzle obtained by the hot-wire and the calibration function given in Fig. 5 and compare it with the distribution obtained from the area distribution. For the latter case two possibillities exist:

- From the A-M relation, see Fig. 1.
- From the reference flow rate $\dot{m}_{\text{ref}}$ and the cross section area $A(x)$ where the measurement is performed, which gives ρu, and M is obtained from Eq. (12).

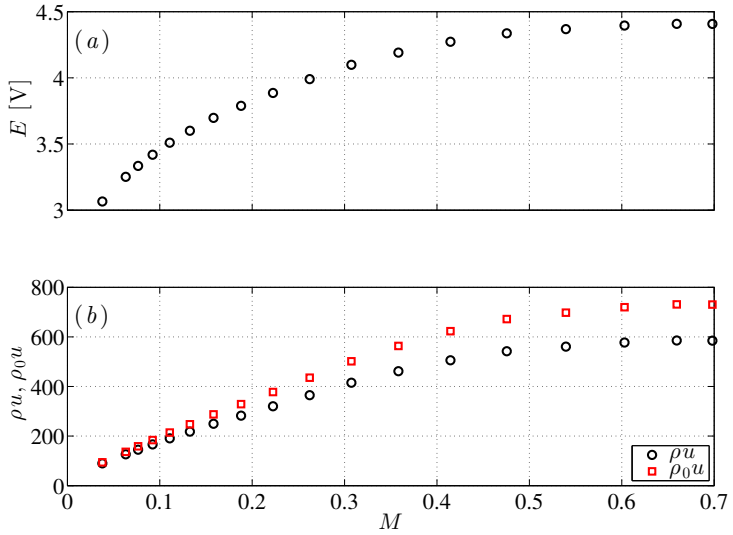

FIGURE 5. Traversing with hot-wire along the nozzle with p_0 kept constant. (a) Anemometer output. (b) The mass fluxes obtained from the calibration, Fig. 3.

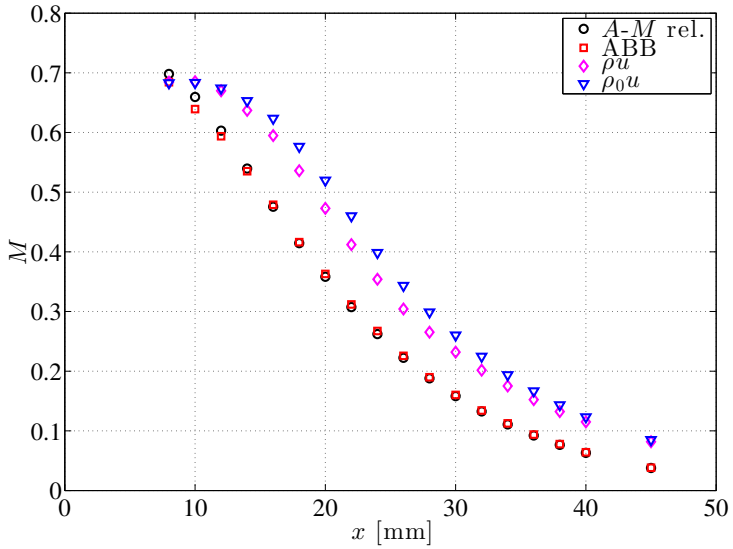

FIGURE 6. M distribution in the nozzle obtained in four independent ways.

These two methods give similar results as is shown in Fig. 6. However if the Mach number is determined from from the hot-wire measurements using Eq. (12) or Eq. (13) it is clear that for both ρu and $\rho_0 u$ the Mach number is overestimated. This is however no surprise when reviewing Fig. 4, for a given ρu the anemometer output voltage depends on the Mach number, and hence it will no be possible to obtain a perfect match with the real Mach number distribution in this way. However as expected the agreement is good at $x = 8$ mm, since this was the position where the hot-wire was calibrated.

3.3. *Measurements with constant ρu*

As a final investigation to determine what the hot-wire is sensitive to, M and p_0 are adjusted in such a way that ρu remains constant and such that $\rho_0 u$ increases with increasing Mach number (see Fig. 7). The hypothesis that the hot-wire is sensitive to $\rho_0 u$ would then imply that the output voltage should also increase with increasing M, but if it instead is sensitive to ρu, then the output voltage should be unaltered. However, in Fig. 7 one can note that the

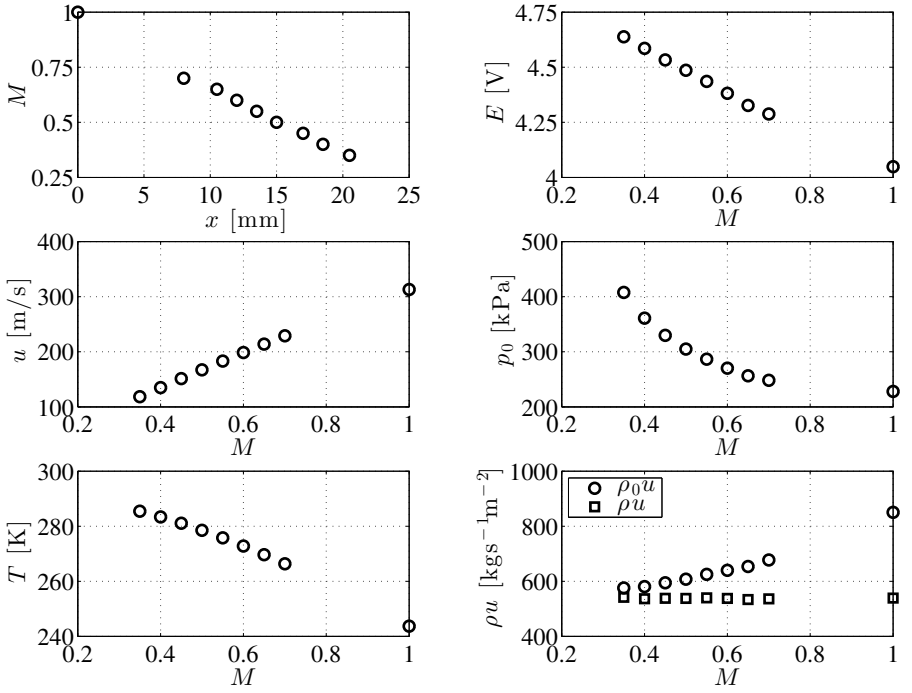

FIGURE 7. For all these measurement points M and p_0 are adjusted such that ρu is constant. T_0 is constant throughout the measurement series.

signal from the anemometer decreases despite that ρu is constant and that $\rho_0 u$ increases.

4. Summary and conclusions

In the present work we have tried to establish how the various flow variables affect the heat transfer and thereby hot-wire anemometer output in compressible flows. In all experiments we keep the stagnation temperature constant, but both the Mach number and the mass flux will affect the anemometer output. The experiments show clearly that for a given mass flux the anemometer output, i.e. heat transfer, decreases with increasing Mach number. This behaviour was not unexpected and have been observed earlier (Sigfrids 2003).

We propose the following hypothesis for this behaviour. In compressible subsonic flow the streamlines are moving away from the body with increasing Mach number, according to the so called Prandtl-Glauert rule. It can be shown that this effect is proportional to

$$s \sim \frac{s_0}{\sqrt{1 - M_\infty^2}} \tag{14}$$

where s is the distance normal to the flow direction and s_0 is the distance at zero Mach number. This will also mean that velocity gradients become smaller normal to the surface of the body (a well-known phenomenon in transonic flow) and our hypothesis is based on the idea that a similar scaling would affect the temperature field as well and hence result in a lower heat transfer. In Fig. 8 we have plotted the same data as in Fig. 7b, using the Prandtl-Glauert transformation directly on the heat transfer term in order to account for smaller gradients. As can be seen the resulting transformed heat transfer now increase with Mach number instead of decreasing. In addition we have normalized these values with $\sqrt{\rho_0 u}$, that is the square root of the stagnation density and flow velocity (also plotted separately in Fig. 7f). Doing so the variation of the anemometer output is ±2% over the Mach number range 0.35-0.7. It is also shown that the anemometer output is a function of the stagnation density of the gas rather than the gas density *per se*.

The results in this study shows that to use hot-wire anemometry in compressible flows it is important not only calibrate the hot wire against the mass flux, but also to have a knowledge of the Mach number. This makes the use of hot-wire anemometry complicated at high subsonic Mach numbers and this will studied in more detail in the future.

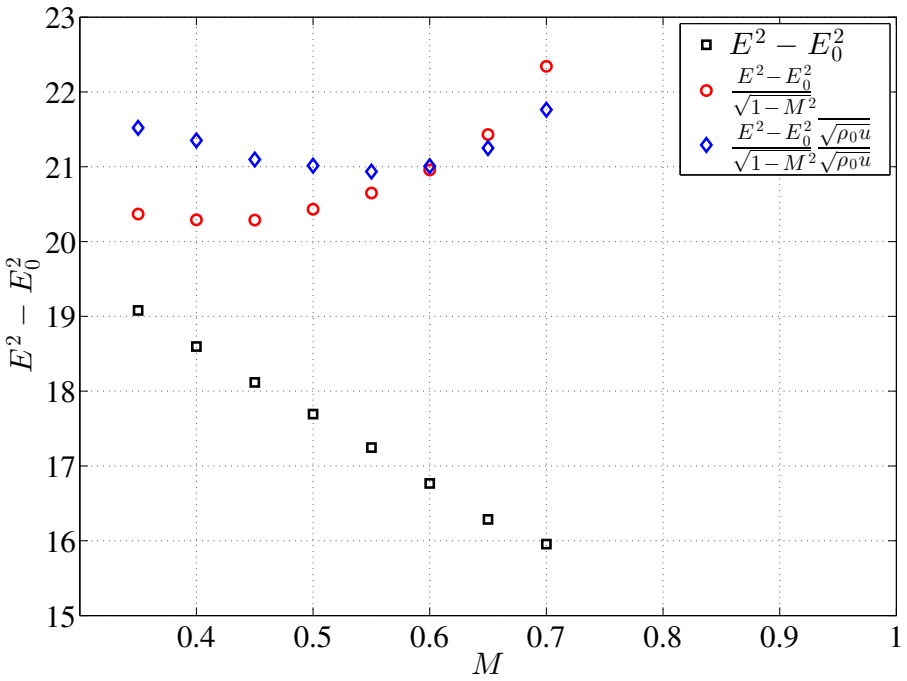

FIGURE 8. $E^2-E_0^2$ as well as the Prandtl-Glauert transformed value, as function of Mach number. Same data as in Fig. 7b. Furthermore the Prandtl-Glauert transformed values are normalized with $\sqrt{\rho_o u}$ giving an almost constant value.

Acknowledgement

This research was done within KTH CCGEx, a centre supported by the Swedish Energy Agency (STEM), Swedish Vehicle Industry and KTH.

References

Anderson, J. D. 2004 Modern compressible flow: with historical perspective. McGraw-Hill.

Bruun, H. H. 1995 Hot-wire anemometry: principles and signal analysis. Oxford University Press Inc.

Dewey, C. 2002 A correlation of convective heat transfer and recovery temperature data for cylinders in compressible flow. *Int. J. Heat Mass Tran.* **8**, 245–252.

Dijk, A. & Nieuwstadt, F. 2004 The calibration of (multi-) hot-wire probes. 1. Temperature calibration. *Exp. Fluids* **36**, 540–549.

Durst, F., Haddad, K., Al-Salaymeh, A., Eid, S. & Ünsal, B. 2008 Mass flow-rate control unit to calibrate hot-wire sensors. *Exp. Fluids* **44**, 189–197.

Hultmark, M. & Smits, A. 2010 Temperature corrections for constant temperature and constant current hot-wire anemometers. *Meas. Sci. Technol.* **21**, 105404.

Kostka, M. & Vasanta Ram, V. 1992 On the effects of fluid temperature on hot wire characteristics. *Exp. Fluids* **13**, 155–162.

Kovasznay, L. S. 1953 Development of turbulence-measuring equipment. *NACA-TR-1209* pp. 1187–1216.

Laufer, J. & McClellan, R. 1956 Measurements of heat transfer from fine wires in supersonic flows. *J. Fluid Mech* **1**, 276–289.

Laurantzon, F., Kalpakli, A., Örlü, R. & Alfredsson, P. H. 2010 Review on the sensed temperature in cold-wire and hot-wire anemometry. Tech. Rep. KTH Mechanics, also Paper 6 in the present thesis.

Laurantzon, F., Tillmark, N., Örlü, R. & Alfredsson, P. H. 2012 A flow facility for the characterization of pulsatile flows. *Flow Meas. Instr.* (accepted, also Paper 1 in present thesis).

Perry, A. E. 1982 Hot-wire anemometry. Clarendon Press.

Sandborn, V. 1972 Resistance temperature transducers. Metrology Press.

Sigfrids, T. 2003 Hot-wire and PIV studies of transonic turbulent wall-bounded flows. Licentiate thesis, KTH, TRITA-MEK 03-05.

Smits, A., Hayakawa, K. & Muck, K. 1984 Constant temperature hot-wire anemometer practice in supersonic flows. *Exp. Fluids* **2**, 33–41.

Spangenberg, W. G. 1955 Heat-loss characteristics of hot-wire anemometers at various densities in transonic and supersonic flow. *NACA Tech Note 3381* .